The role of MyD88-dependent signaling pathways in skin mast cells in UVB-induced skin diseases

Dissertation

zur Erlangung des Doktorgrades (Dr. rer. nat.)

eingereicht bei

der Mathematisch-Naturwissenschaftlichen Fakultät

der Rheinischen Friedrich-Wilhelms-Universität Bonn

Yasmin Majlesain

aus Siegen

Bonn, Juni 2021

Angefertigt mit Genehmigung der Mathematisch-Naturwissenschaftlichen Fakultät,
am Life and Medical Science (LIMES) Institut, Abteilung Immunologie und Umwelt
der Rheinischen Friedrich-Wilhelms-Universität Bonn.

Erstgutachterin PD Dr. Heike Weighardt

Zweitgutachterin Prof. Dr. Eva Kiermaier

Tag der Promotion 03.09.2021

Erscheinungsjahr 2022

Eidesstattliche Erklärung

Hiermit erkläre ich an Eides statt, dass…

…die vorgelegte Arbeit - abgesehen von den ausdrücklich bezeichneten Hilfsmitteln - persönlich, selbständig und ohne Benutzung anderer als der angegebenen Hilfsmittel angefertigt wurde.

…die aus anderen Quellen direkt oder indirekt übernommenen Daten und Konzepte unter Angabe der Quelle kenntlich gemacht wurden.

…die vorgelegte Arbeit oder ähnliche Arbeiten nicht bereits anderweitig als Dissertation eingereicht worden sind.

…ich keinen früheren Promotionsversuch unternommen habe.

…für die Erstellung der vorgelegten Arbeit keine fremde Hilfe, insbesondere keine entgeltliche Hilfe von Vermittlungs- oder Beratungsdiensten in Anspruch genommen wurde.

…die vorgelegte Dissertation weder vollständig noch auszugsweise veröffentlicht worden ist.

Bonn, den _____, _____

Yasmin Majlesain

List of contents

List of figures ..... **IV**

List of tables ..... **VI**

Abbreviations ..... **VII**

1. Introduction **1**
1.1. The immune system 1
1.1.1. Innate Immunity 2
1.1.2. Adaptive immunity 5
1.2. Mast cells 6
1.2.1. Mast cell ontogeny 8
1.2.2. Mast cells in immune responses 8
1.3. The Skin 9
1.4. UV-radiation 13
1.4.1. UV-induced effects on the skin 14
1.4.2. UV-induced effects on immune responses in the skin 14
1.4.3. Photocarcinogenesis 17
1.5. Allergies 18
1.5.1. Anaphylaxis 19
1.5.2. Allergic contact dermatitis 19
1.6. Aim of the thesis 22

2. Material **23**
2.1. Equipment 23
2.2. Consumables 25
2.3. Chemical Reagents 26
2.4. Buffers, Media and Solutions 28
2.5. Kits 29
2.6. Primers 29
2.7. Antibodies 30
2.8. Enzymes 32
2.9. Software 32

3. Methods **33**
3.1. Animal Experiments 33
3.1.1. Mouse Genetics 33
3.1.2. Genomic DNA isolation and gel electrophoresis 34

3.1.3. Passive cutaneous anaphylaxis 35
3.1.4. Chronic UVB irradiation with ST2 blocking 36
3.1.5. UVB-induced immune suppression 36
3.1.6. Photocarcinogenesis 37
3.1.7. Blood serum preparation 38
3.2. Histology 38
3.2.1. Paraffin sections 38
3.2.2. Toluidine Blue staining 38
3.2.3. Frozen sections 39
3.2.4. Immunofluorescence staining 39
3.2.5. Whole ear mounts 39
3.2.6. Mast cell granule staining 40
3.2.7. Microscopy 40
3.3. Cell isolation 40
3.3.1. Isolation of skin cells 40
3.3.2. Isolation of lymph node cells 41
3.4. Flow cytometry 41
3.4.1. Cell surface staining 41
3.4.2. Intracellular transcription factor staining 41
3.5. Cell culture and in vitro assays 42
3.5.1. Bone marrow cell isolation 42
3.5.2. Generation of bone marrow-derived dendritic cells (BMDC) 42
3.5.3. Generation of bone marrow-derived mast cells (BMMC) 42
3.5.4. Co-cultivation of BMDC and BMMC 43
3.5.5. Enrichment of peritoneal cell-derived mast cells (PCMC) 43
3.5.6. Apoptosis assay 44
3.5.7. Transwell migration assay 44
3.5.8. Ca^{2+} mobilization assay 45
3.5.9. Degranulation assay 45
3.6. Protein quantification 46
3.6.1. Protein isolation from back skin 46
3.6.2. Enzyme-linked immunosorbent assay (ELISA) 46
3.7. Statistical analysis 47

4. Results 48
4.1. The role of MyD88 in *in vitro* generated mast cells 48

4.1.1. MyD88 deficiency does not majorly affect BMMC differentiation from bone marrow cells 48
4.1.2. BMMC migration is unaltered in the absence of MyD88 50
4.1.3. BMMC release great amounts of IL-6 and IL-13 upon IL-33 treatment 51
4.1.4. IL-33 ameliorates mast cell survival MyD88-dependently 52
4.1.5. Mast cell degranulation 53
4.2. MyD88 contributes to cutaneous anaphylactic reactions 56
4.3. Impacts of IL-33 signaling in chronic UVB irradiation 58
4.4. DC-mast cell crosstalk in the skin 66
4.4.1. DCs and mast cells are located close together in the skin 66
4.4.2. DC activation is mildly affected by mast cell internal MyD88 signaling 68
4.5. Role of MyD88 in UVB-induced immunosuppression 72
4.5.1. UVB-induced immune suppression is established independent of MyD88 72
4.5.2. UVB exposition prior to CHS changes the immune cell composition in skin-draining lymph nodes 79
4.6. Role of MyD88 in Photocarcinogenesis 84
4.6.1. MyD88 KO mice develop more tumors after long-term UVB exposition 84
4.6.2. Long-term UVB irradiation influences adaptive immune cells in skin and lymph nodes 87

5. Discussion 91
5.1. MyD88 signaling influences mast cell survival, activation and degranulation 91
5.2. IL-33 signaling affects keratinocyte proliferation and immune cell recruitment to UVB exposed skin 94
5.3. MyD88 signaling in mast cell-DC interactions 97
5.4. MyD88 signaling in immune suppression and photocarcinogenesis 100
5.4.1. UVB exposure induces immune suppression MyD88-independently 100
5.4.2. MyD88 signalling protects from photocarcinogenesis 104

6. Summary 108

7. References 111

Publications 124

Acknowledgements 125

List of figures

Figure 1 Overview of innate and adaptive immune cells. 2
Figure 2 Overview of MyD88-dependent TLR- and IL-33/ST2 pathways. 4
Figure 3 Overview of the immune cells in healthy murine skin. 12
Figure 4 UV-radiation types and their skin penetration properties. 13
Figure 5 Mechanisms of UV-induced immune suppression. 17
Figure 6 Genetic background of the mouse model. 33
Figure 7 Model for chronic low-dose UVB irradiation with ST2 blocking. 36
Figure 8 Model for UVB-induced immune suppression. 37
Figure 9 Model for UVB-induced Photocarcinogenesis. 37
Figure 10 MCps in the bone marrow are slightly reduced in the absence of MyD88. 49
Figure 11 Differentiation of BMMC is not altered in the absence of MyD88. 50
Figure 12 BMMC transmigration does not depend on MyD88. 51
Figure 13 BMMC secrete considerable amounts of IL-6 and IL-13 upon IL-33 stimulation. 52
Figure 14 BMMC survival takes place MyD88-dependently in IL-33 treated mast cell cultures. 53
Figure 15 MyD88 contributes to PCMC degranulation. 55
Figure 16 MyD88-signaling contributes to the anaphylactic reaction. 57
Figure 17 IL-33 expression in the skin rises after chronic UVB irradiation. 58
Figure 18 IL-33 signaling is involved in the formation of UVB-induced acanthosis of the epidermis, but not in accumulation of dermal mast cells. 59
Figure 19 IL-33 receptor blocking suppresses UVB-induced proliferation of epidermal cells. 60
Figure 20 IL-33 signaling mainly influences DETC, neutrophils and macrophages in the skin. 63
Figure 21 UVB irradiation leads to an increase of Treg in secondary lymphoid organs independent of IL-33 signaling. 64
Figure 22 DCs and mast cells communicate in back and ear skin. 67
Figure 23 DCs and mast cells in the ear skin interact MyD88-independently. 68
Figure 24 Co-cultivation of BMDC with BMMC leads to the exchange of MHCII to the BMMC surface. 69
Figure 25 Co-culturing of BMDC and BMMC slightly increases activation marker expression on BMDC in unstimulated cultures. 71
Figure 26 UVB-treatment prior to the CHS reaction reduces the ear swelling response. 73

Figure 27 Gating strategy of myeloid cell populations in the skin. 74
Figure 28 A larger number of infiltrated immune cells can be detected in DNFB treated ears of MyD88 KO mice. 76
Figure 29 Gating strategy for skin T-cells. 77
Figure 30 T-cell and B-cell populations in the skin reveal changes after DNFB treatment. 79
Figure 31 Gating strategy of T-cells in the aLN. 80
Figure 32 UVB-induced immune suppression regulates B-and T-cell frequencies in the aLN. 82
Figure 33 Global MyD88 deficiency leads to a higher number of skin tumors, but does not affect tumor size. 85
Figure 34 Long-term UVB treatment induces acanthosis, but does not affect mast cell numbers. 86
Figure 35 MyD88 signaling influences TSLP and TNF-α protein levels in the skin. 87
Figure 36 T-cell populations in skin reveal MyD88-dependent differences. 88
Figure 37 Long-term UVB irradiation changes B- and T-cell proportions in the bLN. 90

List of tables

Table 1 TLR ligands, location and adaptor proteins. 3
Table 2 Equipment. 23
Table 3 Consumables. 25
Table 4 Chemical Reagents. 26
Table 5 Buffers, Media and Solutions. 28
Table 6 Kits. 29
Table 7 Genotyping primers. 29
Table 8 Antibodies for flow cytometry. 30
Table 9 Antibodies for histology. 31
Table 10 Antibodies for animal experiments and cell culture assays. 31
Table 11 Enzymes. 32
Table 12 Software. 32
Table 13 PCR reaction for genotyping. 35

Abbreviations

AMP	Anti-microbial peptide
APC	Antigen-presenting cell
BMDC	Bone marrow-derived dendritic cell
BMMC	Bone marrow-derived mast cell
bp	Base pairs
BSA	Bovine serum albumin
CCL	C-C motif ligand
CD	Cluster of differentiation
cDC	Conventional dendritic cell
CHS	Contact hypersensitivity
c-Kit	Tyrosine protein kinase KIT
Cre	Cyclization recombination
d	Day
DAMP	Danger-associated molecular pattern
DC	Dendritic cell
DETC	Dendritic epidermal T-cell
DNA	Deoxyribonucleic acid
DNFB	1-Fluoro-2,4-dinitrobenzene
ELISA	Enzyme-linked immunosorbent assay
eYFP	Enhanced yellow fluorescent protein
FACS	Fluorescent activated cell sorting
Fc	Crystallizable fragment
FcεRIα	High Affinity Immunoglobulin Epsilon Receptor Subunit Alpha
FoxP3	Forkhead box protein P3
GM-CSF	Granulocyte macrophage colony stimulating factor
Ig	Immunoglobulin
IL	Interleukin
KO	Knockout
L/D	Life/Dead

Lin	Lineage
LPS	Lipopolysaccharide
LSL	Lox-stop-lox
MCp	Mast cell progenitor
Mcpt5	Mast cell protease 5
MHC	Major histocompability complex
moDC	Monocyte-derived dendritic cell
MyD88	Myeloid differentiation factor 88
O/N.	Over night
OD	Optical Density
PAMP	Pathogen-associated molecular pattern
PBS	Phosphate buffered saline
PCMC	Peritoneal cell-derived mast cell
PCR	Polymerase chain reaction
PRR	Pattern recognition receptor
rpm	Rounds per minute
RPMI	Rosewell Park Memorial Institute
RT	Room temperature
SCF	Stem cell factor
ST2	Suppression of tumorigenicity 2
Th	T-helper cell
TLR	Toll-like receptor
TNF-α	Tumor necrosis factor α
Treg	Regulatory T-cell
TRIF	TIR-domain-containing adapter-inducing interferon-β
TSLP	Thymic stromal lymphopoietin
UV	Ultraviolet
WT	Wildtype
i. p.	Intraperitoneal
i. d.	Intradermal
i. v.	Intravenous

1. Introduction

1.1. The immune system

The immune system is a network of different cells, soluble mediators and organs, which together have developed a broad range of defense mechanisms against foreign pathogens, toxins or substances in order to protect the host. This system needs to detect infectious substances and then initiate immune effector functions. As a result, an effective immune response should resolve the infection and generate immune memory. Immune responses require tight regulation, since an unbalanced response could result in a too weak or too strong activation of the immune system. This might have detrimental effects and lead to allergies, chronic diseases, autoimmune diseases, organ failure or even to death. The immune system can be divided into two branches, which are the innate and the adaptive immune response. However, these two parts are strongly interconnected and require each other for effective protection of the host (Murphy & Weaver, 2017; Parkin & Cohen, 2001).

Innate immune mechanisms are highly conserved and are present among many different vertebrate species. The innate arm consists of different cells and soluble mediators, which are able to fight foreign pathogens. Physical and chemical structures of the body build the first barrier for intruders (Murphy & Weaver, 2017; Riera Romo et al., 2016). The immunological barrier includes anti-microbial peptides (AMPs), complement proteins, acute-phase proteins, cytokines and chemokines. Granulocytes, mast cells, monocytes, macrophages, dendritic cells, natural killer (NK) cells and innate lymphoid cells (ILC) have innate features and are able to directly sense foreign structures. They then become activated, secrete cytokines and chemokines to recruit other immune cells and initiate inflammation (Figure 1). Broad classes of infectious substances, so called pathogen-associated molecular patterns (PAMPs) can be recognized by germ-line encoded pattern recognition receptors (PRRs). In addition, also self-derived danger associated molecular patterns (DAMPs) that are released upon cell and tissue damage can be recognized by PRRs and induce immune responses (Medzhitov & Janeway, 1997). The specificity of innate responses is rather low as it is limited to the detection of molecular structures. Activation however occurs rapidly after pathogen encounter and is therefore important for immediate initiation of immune responses.

The adaptive branch of immunity consists of B-cells, T-cells and antibodies, which are responsible for the generation of antibody-mediated (humoral) and cell-mediated immunity

(Figure 1). B-and T-cells express variable receptors, which makes them in contrast to innate immune cells, highly specific. A further characteristic is that T-cells require presentation of antigens by antigen presenting cells (APC) to differentiate into effector cells and become activated. B-cells however, are activated either T-cell-dependently or independently and differentiate thereupon to antibody secreting plasma cells to mediate humoral immunity. Some cell types (like NKT-cells and γδ T-cells) have traits of both parts of immunity and can therefore be considered as a link between innate and adaptive (Pasman & Kasper, 2017). In contrast to innate immunity, adaptive immune responses take much longer time to develop, but are highly specific and capable of developing immunological memory to generate rapid responses upon re-infection with the same pathogen. For a long time, it has been considered that only adaptive immunity can build memory. This dogma has been challenged in the past years, as evidence could be gathered, showing that also innate immune cells are able mount certain resistance after infections, a process called trained immunity (Netea et al., 2020).

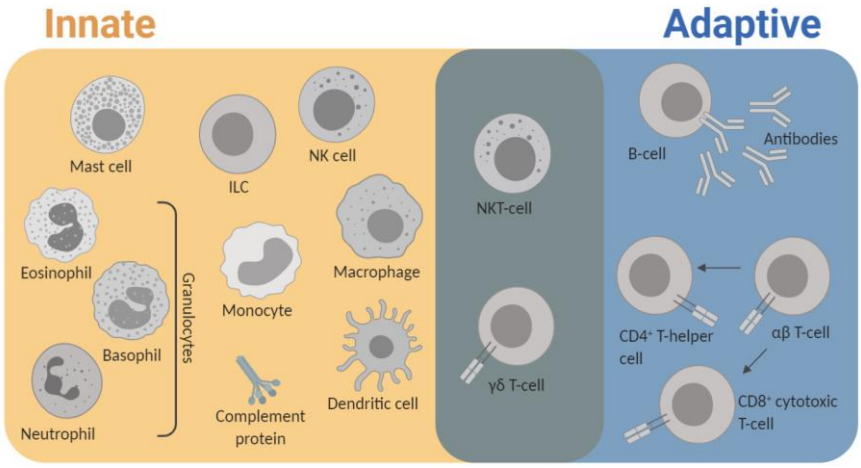

Figure 1 Overview of innate and adaptive immune cells.
Granulocytes, mast cells, monocytes, macrophages dendritic cells, natural killer (NK) cells and innate lymphoid cells (ILC) represent the main cell types of the innate immune response. These cells detect pathogens or damaged tissue rapidly, but are unable to generate an antigen specific response. The adaptive immune response consists of B-cells that produce antibodies and T-cells, which are divided further into $CD4^+$ T-helper cells and $CD8^+$ cytotoxic T-cells. These lymphocytes need more time to become fully activated, but are highly specific due to their variable receptors. NKT-cells and γδ T-cells have characteristics of both, innate and adaptive immune responses, and are therefore located in between the two groups (adapted from Dranoff, 2004).

1.1.1. Innate Immunity

Innate immune cells localize throughout the body and can be both, migratory and tissue-resident. Their main function is to sense irregularities within their environment, such as infection or damage, and to induce an immune response. They do so by expression of a wide

range of cell surface or intracellular receptors that identify viral, bacterial or fungal components (Akira et al., 2006). There are different groups of PRRs: Toll-like receptors (TLRs), NOD-like receptors (NLRs), RIG-I-like receptors (RLRs), C-type lectin receptors (CLRs), cytosolic DNA sensors (CDSs) and scavenger receptors (Takeuchi & Akira, 2010). In the following, the focus will be on the TLRs.

TLRs are integral membrane receptors and all have a common structure that consists of an N-terminal ligand recognition domain comprised of leucine-rich repeats (LRR) and a C-terminal Toll/IL-1R (TIR) domain necessary for downstream signaling. The main differences between TLRs are the cellular location (cell surface or endosomal) and ligand recognition (Table 1). While cell surface TLRs rather sense bacterial proteins, lipopeptides, peptidoglycans, lipoglycans and lipopolysaccharides (LPS), endosomal TLRs identify viral and intracellular pathogen-derived DNA and RNA (reviewed in Kawai & Akira, 2011).

Table 1 TLR ligands, location and adaptor proteins.

Ligand	Receptor	Cellular location	Adaptor protein
Triacylated Lipoproteins	TLR1/2	Cell membrane	MyD88
Diacylated Lipoproteins	TLR2/6	Cell membrane	MyD88
dsRNA	TLR3	Endosomal membrane	TRIF
Lipopolysaccharide	TLR4	Cell and endosomal membrane	MyD88 and TRIF
Flagellin	TLR5	Cell membrane	MyD88
ssRNA	TLR7	Endosomal membrane	MyD88
CpG Oligonucleotide	TLR9	Endosomal membrane	MyD88
Lipoglycans	TLR2/10	Cell membrane	MyD88
Profilin	TLR11*, 12*	Cell membrane	MyD88
rRNA	TLR13*	Endosomal membrane	MyD88

* Expressed only in mice

Yet, a further difference between TLRs is the adaptor protein used for signal transduction. Myeloid differentiation primary response 88 (MyD88) is a central signaling adaptor protein of most TLRs, only TLR3 utilizes TIR-domain containing adaptor protein inducing interferon-β (TRIF). TLR4 has a special role, since it can use both, MyD88 and TRIF, for downstream signaling. The differential utilization of the adaptor molecules leads to induction of different transcriptional programs. MyD88-dependent signaling pathways lead to the production of inflammatory cytokines, type I interferons and genes involved in immune regulation and cell survival. MyD88 is organized in different domains: the death domain (DD), the intermediate

domain (INT) and the toll-interleukin-1 receptor domain (TIR). The TIR domain is required for interaction of MyD88 with the TLR's TIR domain or with TIR Domain Containing Adaptor Protein (TIRAP). TLRs form either homodimers (like TLR4) or heterodimers (like TLR1/2). Upon TLR engagement the Myddosome assembles, which consists of MyD88 and IL-1 receptor-associated kinase (IRAK) proteins that are recruited via the DD of MyD88 (Figure 2). Thereby, IRAK1 is phosphorylated by IRAK4 and associates with TNF-α receptor-associated factor (TRAF6). TRAF6 then dissociates from the receptor complex, interacts with TGF-β-activated kinase 1 (TAK1) and TAK1-binding proteins, which results in a larger complex formation and TAK1 activation. This event is followed by subsequent phosphorylation of the IKK complex and (mitogen-activated protein kinase) MAPK members, eventually inducing translocation of the transcription factors factor nuclear factor 'kappa-light-chain-enhancer' of activated B-cells (NF-κB) and activator protein 1 (AP-1), respectively. Furthermore, endosomal TLRs utilizing MyD88, like TLR 7/8 and TLR9, can recruit TRAF3 in addition to TRAF6, which results in the activation of interferon regulatory factor 7 (IRF7) and induces expression of type I IFN (Kawai & Akira, 2007).

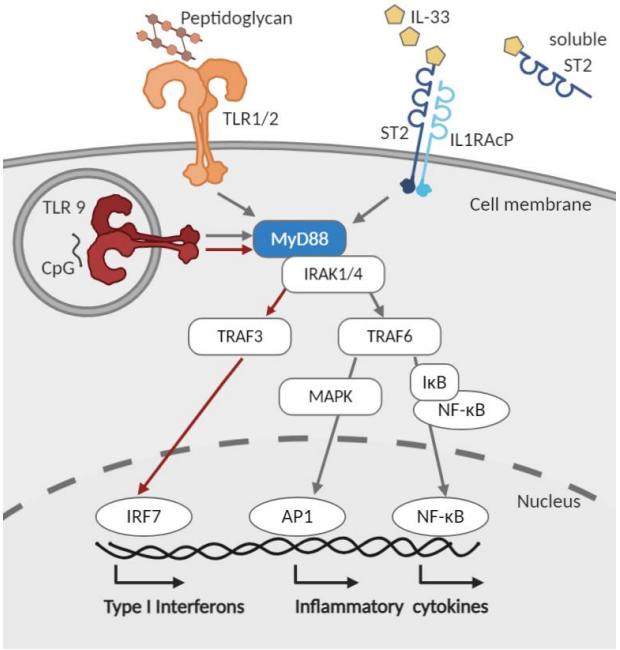

Figure 2 Overview of MyD88-dependent TLR- and IL-33/ST2 pathways.
MyD88 is a central adaptor protein of many TLRs and IL-1 cytokine receptors (here TLR1/2, TLR9 and ST2). After ligand binding, MyD88, IRAK1 and IRAK4 are recruited to the receptor and together form the Myddosome. IRAK4 phosphorylates IRAK1 which leads to the recruitment of TRAF6. For TLR9 signaling, in addition to TRAF6 also TRAF3 can be recruited that causes IRF7 activation, provoking Type I IFN production. TRAF6 activation leads to further downstream translocation of AP-1 and NF-κB to the nucleus, which act as transcriptional regulators in the production of inflammatory cytokines and other inflammation-related genes (adapted from Jain et al., 2014).

In addition to TLR signaling, MyD88 is involved in signal transduction of IL-1 receptor signaling. The IL-1 cytokine family contains different members (e.g., IL-1α, IL-1β, IL-18, IL-33), of which especially IL-1α and IL-33 act as DAMPs and provoke a sterile inflammation (Dinarello, 2018). In the following, the focus will stay on the IL-1 cytokine IL-33 that plays a role in both, innate and adaptive immunity. It is expressed constitutively in barrier lining cells such as epithelial and endothelial cells and fibroblasts of the skin, gastrointestinal tract or the lung (Liew et al., 2016). Studies also demonstrated that hematopoietic cells such as macrophages and DCs can be producers of IL-33. Unlike IL-1β or IL-18, IL-33 is biologically active in its nuclear full-length form, but further processing by caspases is able to potentiate the signaling efficiency. IL-33 was shown to bind chromatin and act as a transcriptional regulator (Choi et al., 2012), but the role for this alarmin was mainly studied in its release upon cell damage or cell stress. IL-33 binds to its specific heterodimeric receptor ST2/IL-1 receptor accessory protein (IL-1RAcP) and induces MyD88 downstream signaling, similar to TLRs (Figure 2, Liew et al., 2016). Further, there are soluble ST2 receptors that act as decoy receptors to regulate IL-33 signaling. The surface receptor ST2 is expressed by a broad range of innate and adaptive immune cells including mast cells, DCs, basophils, NK cells, ILC2, type 2 T-helper (Th) cells and regulatory T-cells (Treg). IL-33 release is associated with many different diseases; especially the role in allergic diseases has been extensively studied (reviewed in Liew et al., 2016; Takatori et al., 2018).

1.1.2. Adaptive immunity

Common lymphoid progenitors (CLP) in the bone marrow can give rise to B-and T-cells that bear antigen receptors produced by somatic recombination. Each of these naïve lymphocytes therefore carries a unique antigen receptor, leading to a highly diverse pool of receptors within the body (Murphy & Weaver, 2017).

T-cell development takes place in the thymus, where the T-cell receptor (TCR) is rearranged. Most of the T-cells carry an αβ TCR, while only around 5 % express the γδ TCR. Following the rearrangement, αβ T-cells, also called conventional T-cells, undergo the positive and negative selection process, where in the end either $CD4^+$ or $CD8^+$ T-cells are generated that will recirculate mainly between secondary lymphoid organs, awaiting activation (Murphy & Weaver, 2017). γδ T-cells are rather tissue-associated and their numbers are enriched in many peripheral tissues. Activation of conventional T-cells requires APCs that present processed

pathogen-derived peptides (antigens) on their surface major histocompatibility complex (MHC) molecules to T-cells. Here, MHCI molecules present viral or tumor-derived peptides to $CD8^+$ T-cells, which then acquire cytotoxic properties after activation and eradicate virus-infected cells and tumor cells (reviewed in Murphy & Weaver, 2017). On the other hand, $CD4^+$ T-cells recognize peptides on MHCII molecules, which leads to the differentiation and expansion of naïve T-cells into different effector T-helper (Th) cell subtypes such as Th1, Th2, Th17 cells, T-follicular helper (Tfh) and regulatory T-cells (Treg). These subtypes are distinguished by expression of different master transcription factors and secretion of a distinct pattern of cytokines. The Th cell subtypes have different effector functions that provide help to other immune cells during pathogen defense, or dampen immune reactions as for the case of Tregs (reviewed in Zhou et al., 2009). A fraction of the activated $CD4^+$ and $CD8^+$ T-cells can develop into long-lived memory T-cells, which home either central lymphoid organs or peripheral regions of the body and can rapidly give rise to potent effector cells upon re-infection (Jameson & Masopust, 2018).

The major task of B-cells is the production and secretion of antibodies to mediate humoral immunity by neutralization of pathogens and subsequent elimination by phagocytes. They develop within the bone marrow where they undergo immunoglobulin rearrangement to produce a unique B-cell receptor (BCR). B-cells then enter the blood circulation and localize in B-cell follicles of secondary lymphoid organs. They are capable of directly binding to antigens; however, some B-cell responses require assistance from Th/Tfh cells for activation and class switch recombination of immunoglobulins. Upon activation, most B-cells develop into plasma cells that secrete large amounts of antibodies to generate humoral immunity (reviewed in Murphy & Weaver, 2017). Similar to T-cells, some activated, antigen-specific B-cells can give rise to long-lived plasma cells or memory cells to provide long-term immunity (Tarlinton & Good-Jacobson, 2013).

1.2. Mast cells

In 1878, Paul Ehrlich described mast cells for the first time based on their special histological staining properties (Ehrlich, 1878); these granular cells are today very well known for their contribution to parasitic infections and allergic reactions. In the past years however, apart from their contribution to immune responses many other important roles have been

attributed to mast cells, such as in tissue remodeling, angiogenesis, cancer and neurological disorders (Coussens et al., 1999; Hendrix et al., 2013; Soucek et al., 2007). They are tissue-resident cells that predominantly live in connective or mucosal tissues of barrier organs, such as the skin, gastrointestinal and respiratory tract. A special property of these cells is that they are packed with secretory granules that are released within seconds to minutes upon stimulation via the high-affinity IgE receptor (FcεRI) (Galli & Tsai, 2012). This process is called degranulation, and leads to the release of biologically active cell mediators like histamine, heparin, proteases, cytokines, chemokines and lipid mediators into the cell environment. This event is accompanied by the release of *de novo* synthesized mediators such as eicosanoids, cytokines and chemokines (Moon et al., 2014). The released granule content affects a wide array of neighboring cells and tissues and modulates their functional properties. Since degranulation occurs quickly after stimulation, local mast cells are one of the first cells to respond in allergy or infection. In humans, mast cells are allocated in two different subtypes based on the expression of the two serine proteases tryptase and chymase. In rodents however, these two groups are distinguished by the tissue localization and expression pattern of different mast cell proteases. Connective tissue mast cells (CTMC) are present in the skin and peritoneal cavity and the granules contain heparin whereas mucosal mast cells (MMC) are located in the intestinal mucosa and have chondroitin sulfate containing granules (reviewed in Moon et al., 2010). One of the first mouse models to study mast cell functions *in vivo* were KIT deficient mice (WBB6F1-Kit^{W}/$Kit^{W\text{-}v}$ and C57BL/6-$Kit^{W\text{-}sh}$/$Kit^{W\text{-}sh}$) that completely lack mast cells. But apart from being mast cell deficient, due to the importance of stem cell factor (SCF)/c-Kit signaling in other cells than mast cells, these mouse models show additional abnormalities. As a few examples, C57BL/6-$Kit^{W\text{-}sh}$/$Kit^{W\text{-}sh}$ do not only lack mast cells, but also are deficient for melanocytes and interstitial cells of Cajal, exhibit bile reflux and show defects in myelopoiesis (Grimbaldeston et al., 2005; Michel et al., 2013). Therefore, observations that were made in these mouse models should be regarded cautiously since they often cannot solely be traced back to mast cell deficiency (Michel et al., 2013; Nigrovic et al., 2008). The generation of genetically defined mouse models was an important step to analyze mast cell functions without confounding effects of Kit deficiency. Among these, mast cell protease 5 (Mcpt5) Cre recombinase expressing mice are a valuable model for research as it allows mast cell-specific recombination of floxed genes (Scholten et al., 2008).

1.2.1. Mast cell ontogeny

Mast cells were long considered to originate from the hematopoietic system of the bone marrow (Kitamura et al., 1977). Immature committed mast cell progenitors (MCp) were thought to continuously be released into the blood circulation and from there home tissues, where they continue maturation. These conclusions were supported by findings showing, that MCps exist within the bone marrow and can re-populate tissues of mast cell deficient mice (Chen et al., 2005; Kitamura et al., 1978). These observations however were made in mouse models that have empty mast cell niches within the tissues and therefore do not represent physiologic conditions. The use of novel fate mapping techniques shed a new light on the ontogeny of mast cells (Gentek et al., 2018; Z. Li et al., 2018). In the skin for example, mast cells seed in several waves, first yolk-sac derived mast cells seed the embryo followed by the replacement by definitive mast cells that maintain themselves without major contribution of bone marrow. This homeostatic maintenance of these cells is mediated by locally expanding MCps in the skin, which form so called 'stable territories' (Weitzmann et al., 2020). Nevertheless, current evidence shows that in inflamed skin MCps are recruited from the bone marrow and together with tissue-resident progenitors, these cells proliferate and expand within the skin, revealing the mast cells' dual origin (Weitzmann et al., 2020).

1.2.2. Mast cells in immune responses

Beside their physiological functions, mast cells play in important role in innate and adaptive immunity. Mast cells essentially contribute IgE-dependent immune reactions, which are classically associated with parasitic infections and allergic reactions (Galli & Tsai, 2010; Mukai et al., 2016). But in the past years, mast cells were also shown to be important in the defense against different bacterial and viral pathogens, revealing other important IgE-independent mechanisms of mast cell activation (Yu et al., 2015). Mast cells express a high variety of PRRs enabling the recognition of pathogens and subsequently followed by activation (Agier et al., 2018). Among these PRRs, most of the TLRs have been identified on human and murine mast cells. After engagement of different TLRs, a differential cytokine and chemokine secretion profile was observed (Sandig & Bulfone-Paus, 2012). In addition, degranulation was shown take place TLR-dependently, while TLR2 ligation potently induces granule release, TLR4 stimulation is not able to induce degranulation (Supajatura et al., 2002). An *in vitro* study

displayed that mast cells could potentially act as APCs since they express MHCII and co-stimulatory molecules under certain circumstances (Kambayashi et al., 2009). *In vivo*, mast cells were shown to have the capacity to migrate into draining lymph nodes, however, there is only little evidence that mast cells contribute to priming of naïve T-cells in the lymph node (Byrne et al., 2008). Nevertheless, mast cells still might have an important role in the peripheral expansion of antigen-specific T-cells (Katsoulis-Dimitriou et al. 2020; Mantri and St. John 2019). The mast cell's immune-regulatory functions on T-cell responses are rather indirect through the influence of mast cell-derived mediators on other immune cells and through direct cell-cell interaction with APCs and modification of their T-cell priming capacities. Current studies show that mast cells and DCs closely interact and boost immune reactions in the skin (Sumpter et al., 2019). This cellular interaction was shown to be a key mechanism in the sensitization phase of a contact hypersensitivity reaction, where mast cells elevate DC activation in a TNF-α-dependent fashion (Otsuka et al., 2011). In addition, this interaction led to mast cell polarization and to the formation of immune synapses with DCs in the skin. As a consequence, intracellular organelles relocate within the cell and mast cells release their granules and cytokines in the direction of the DCs (Carroll-Portillo et al., 2015; A. Dudeck et al., 2011). The secreted mediators can stimulate DCs, but also whole secretory mast cell granules can be engulfed by DCs, inducing DC maturation, antigen-processing and migration (Dudeck et al., 2019). In this manner, priming and Th polarization of T-cells in the lymph node by DCs is modulated in a mast cell-dependent way. A direct mast cell-DC communication furthermore drives the exchange of surface molecules between cells. Here, the transfer of peptide-loaded MHCII molecules from DC to mast cells and of antigen/IgE/FcεRI complexes from mast cells to DCs was observed (Carroll-Portillo et al., 2015; Dudeck et al., 2017). Thereby, Th cell polarization by DCs is fine-tuned, and in addition, mast cells exploit the surface expression of peptide-decorated MHCII molecules to activate effector T-cells in the periphery.

1.3. The Skin

With a surface area of about 2 m^2, the skin is one of the largest organs of the human body (Mosteller, 1987). As a barrier organ, the skin is permanently exposed to the environment and has therefore developed several defense strategies for protection from external danger. In

addition to the protective functions, the skin mediates the regulation of body temperature, vitamin D synthesis, and sensory input. The skin is organized into three different layers, the environment facing epidermis, the dermis underneath and the subcutaneous adipose tissue below the dermal layer (Figure 3). All of these layers contain different types of cells and structural elements, which altogether ensure efficient protection against environmental threats. The skin surface is home to commensal skin microbiota, consisting of millions of bacteria, viruses and fungi that play an important role in host defense as well (Sanford & Gallo, 2013). The normal skin flora impedes colonization of pathogenic microbes on the skin and is essential for education of the body's immune system (Belkaid & Hand, 2014).

The epidermis is composed of many layers of keratinocytes, which is the most abundant cell type there. Keratinocytes derive from the continuously proliferating cells in the basal layer of the epidermis and migrate towards the surface. On their way to the surface, these cells gradually loose water and die to build a cornified top layer on the skin. The epithelial cells are interconnected via tight junctions and are enclosed by lipids that together prevent water loss and provide a compact barrier against pathogens (reviewed in Simpson et al., 2011). Furthermore, keratinocytes express TLRs and can produce AMPs in response to pathogens (Nestle et al., 2009). Through disruption of the invading bacteria's membrane on the one hand and by immune modulation on the other hand, AMPs mediate protection (Lee et al., 2019). Along with keratinocytes, melanocytes are present in the epidermis, they reside in the basal layer and contribute to photo-protection by producing melanin. Langerhans cells (LC) are specialized APCs of the epidermis and are one of the first cells responding to pathogens. Although these cells seed the skin during embryogenesis, similar to tissue macrophages, they behave like DCs and migrate to lymph nodes upon antigen-uptake to prime naïve T-cells (Hoeffel et al., 2012; Merad et al., 2008). Studies showed that under homeostatic conditions, LCs are able to maintain themselves without bone-marrow contribution, but in inflammation, bone marrow-derived monocytes certainly might give rise to LCs (Ferrer et al., 2019). A unique γδ T-cell population called dendritic epidermal T-cells (DETC), which is absent in human epidermis, can be found in the murine epidermal layer, which together with dermal γδ T-cells play an important role in skin injury, wound repair and immune surveillance (Li et al., 2018; Ribot et al., 2021). They can rapidly react to damaged keratinocytes by secretion of IL-17A and AMPs to stimulate keratinocyte proliferation and differentiation (MacLeod et al., 2013). A further immune cell type are the tissue-resident memory T-cells (T_{RM}) which can be found in

both, the epidermis and the dermis, where they equip the host with prompt adaptive immune defense upon re-infection and provide immunosurveillance (Mueller & Mackay, 2016). While mainly $CD8^+$ T_{RM} reside in the epidermis, $CD4^+$ T_{RM} can predominantly be found in the dermis and have a more migratory behavior (Gebhardt et al., 2011).

Below the epidermis, fibroblasts build the dermal structure and are producers of extracellular matrix proteins. In addition, these cells are critical for the detection of pathogens via TLRs (Yao et al., 2015). Moreover, many other structures are located in the dermis, such as sensory nerves, hair follicles, blood and lymphatic vessels, sweat and sebaceous glands. Unlike the epidermis, the diversity of immune cells in the dermis is much greater (Figure 3). Mast cells contribute to local inflammation and are important during allergic reactions (see 1.2 for a more detailed review). Moreover, dermal DCs and macrophages are present in the dermis. The DC compartment comprises of a DC network whose members differ in cell ontogeny, gene expression profiles and functional properties (Malissen et al., 2014). By secretion of high levels of type I IFNs, plasmacytoid DC (pDC) are specialized cells in anti-viral immunity, but these cells also support wound healing in the skin (Conrad et al., 2009). The migratory dermal DCs are the conventional DCs (cDC) that develop from blood-derived pre-cDCs Fms-related tyrosine kinase ligand (Flt3L)-dependently and in contrast to the slow turnover of LCs, cDCs are replaced continuously in healthy skin (Henri et al., 2010; Waskow et al., 2008). In general, these cells function as sentinels in the peripheral tissues and transport captured antigens to lymph nodes to instruct T-cell activation and differentiation. In the dermis there are four different types of cDCs, all of them express CD11c and MHCII and can be further distinguished, based on different transcription factors and surface markers (Clausen & Stoitzner, 2015). The most abundant cDC type are $CD11b^+$ cDC2 (IRF4-dependent), followed by $XCR1^+$ $CD11b^-$ cDC1 (IRF8-dependent) that can be further divided into two populations by CD103 expression (Malissen et al., 2014). cDC1 are experts in cross-presentation of tumor and other exogenous antigens, and therefore are potent initiators of cytotoxic immune responses by $CD8^+$ T-cells and important in Th1 immunity to infection (Bachem et al., 2010; Haniffa et al., 2012; Soares et al., 2007). On the other hand, cDC2 rather present antigens to $CD4^+$ T-cells and initiate priming of Th-cells like Th2 and Th17 cells (Gao et al., 2013; Schlitzer et al., 2013). The fourth dermal cDC population are $CD11b^-$ $XCR1^-$ double-negative (DN) cDC that similarly to cDC2 are responsible for Th2 immunity (Tussiwand et al., 2015). Apart from these cDC populations, upon inflammation monocyte-derived DCs (moDC) or inflammatory DCs differentiate from

infiltrating monocytes, which are recruited to the skin CCR2-dependently (Tamoutounour et al., 2013). In comparison to dermal DCs, dermal macrophages are rather resident and phagocytic, thereby contributing to pathogen resistance, local tissue homeostasis and repair, but also to regeneration of local nerves (Kolter et al., 2019). Dermal macrophages have a dual origin; monocyte-derived macrophages co-exist together with embryonically seeded macrophages within the skin (Mass et al., 2016; Tamoutounour et al., 2013). Next to γδ T-cells and T_{RM} cells in epidermis and dermis, other conventional αβ T-cells exist in healthy skin. Especially Tregs are crucial cell types of the skin. Apart from their role in hair follicle regeneration and wound healing, they are detrimental cells in the suppression of immune responses and are localized in close proximity to hair follicles within the dermis (Ali et al., 2017; Whibley et al., 2019).

The subcutaneous adipose tissue is mainly populated by adipocytes. Aside from insulation and energy reservoirs, these cells provide AMPs to protect against skin infections (Wong et al., 2019). Under inflammatory conditions, studies could show that dermal fibroblasts undergo adipogenesis, thereby promoting AMP production (Zhang et al., 2015). Interestingly, in aged skin this capacity of dermal fibroblasts is gradually lost (Zhang et al., 2019).

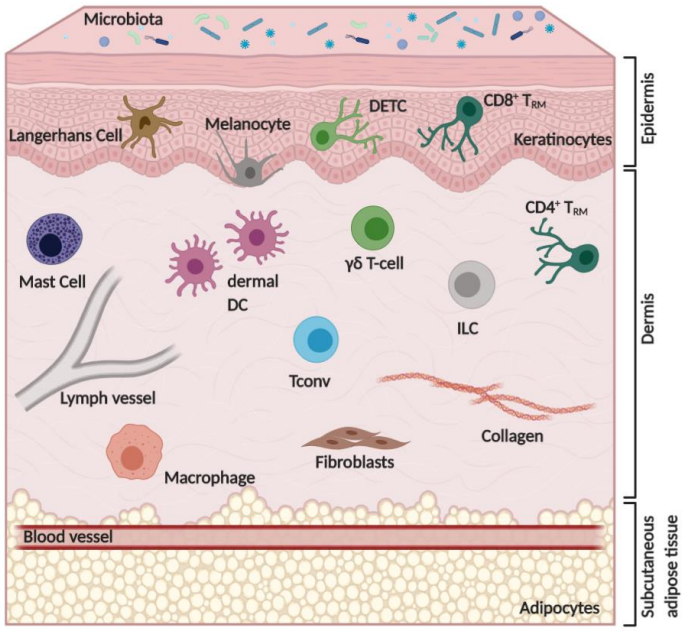

Figure 3 Overview of the immune cells in healthy murine skin.
The skin is divided into three different layers, which are the epidermis, the dermis and the subcutaneous tissue. The epidermis faces the environment and is colonized with commensal microbes. Epidermal immune cells are Langerhans cells, $CD8^+T_{RM}$ and DETC, the dermal pool of immune cells consist of mast cells, dermal DC and macrophages, ILC, $CD4^+T_{RM}$, conventional T-cells (Tconv) and dermal γδ T-cells.

1.4. UV-radiation

Solar UV-radiation is an environmental factor that has an impact on a wide range of biological processes. It is electromagnetic and can be divided into three types of radiation based on the wavelength. There are UVA (315-380 nm), UVB (280-315 nm) and UVC (100-280 nm) radiation, the radiation type with the shortest wavelength is the highest in energy, and vice versa. Highly energetic UVC radiation and parts of UVB radiation are absorbed and scattered by the stratospheric ozone layer, while the less energetic UVA and parts of UVB radiation reach the earth's surface (Figure 4). UVA and UVB are able to pass through the upper skin layers of the human body, UVA radiation can penetrate the skin and reach deeper areas in the dermis, while UVB is mainly absorbed by the human epidermis. In murine skin, UVB however reaches until the upper dermal layers. Both UVA and UVB radiation can be harmful for the human body, UVB radiation however can cause more damage due to its higher energy (reviewed in D'Orazio et al., 2013).

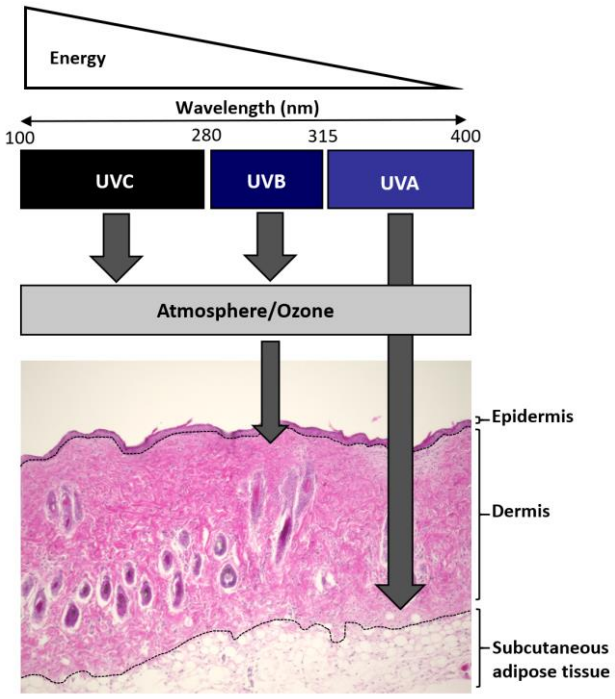

Figure 4 UV-radiation types and their skin penetration properties in murine skin.
UV radiation can be classified in UVA, UVB and UVC radiation. They differ from each other based on the wavelength and energy. UVC is completely absorbed by the atmosphere, while UVB and UVA can enter the skin and reach different layers in the dermis (exemplary image of murine skin, hematoxylin & eosin staining).

1.4.1. UV-induced effects on the skin

When UV irradiation reaches and penetrates the skin, the electromagnetic radiation is absorbed by chromophores, which become energetically excited. Melanin, DNA, urocanic acid, 7-dehydrocholesterol, tryptophan and proteins that are in the absorbance range of UV light are a few examples of such chromophores (Bernard et al., 2019). The absorbance of UV light by 7-dehydrocholesterol for vitamin D synthesis and by melanin are beneficial, while the absorbance by DNA or urocanic acid is considered as harmful. Different factors, including the skin type, age, genetic predispositions and the UV dose can determine the susceptibility to UV-induced diseases (D'Orazio et al., 2013).

Acute UV irradiation leads to tissue damage, inflammation and manifests itself in a sunburn. Such a sunburn is characterized by formation of erythema and edema, in severe cases the skin might blister. However, not only acute UV exposure can be harmful, chronic exposure to low doses without acute symptoms can also have adverse effects (Matsumura & Ananthaswamy, 2004). Long-term consequences for acute and chronic exposure are premature skin ageing, suppression of adaptive immune responses and eventually skin tumor formation (Hart & Norval, 2018; Norval & Halliday, 2011; Rittié & Fisher, 2015). The skin provides its own strategies for protection from UV-light, but these mechanisms are limited. For example, the epidermis of UV-irradiated skin is thickened due to enhanced proliferation of keratinocytes, a phenomenon referred to as acanthosis. This epidermal thickening protects underlying skin layers by decreasing the penetration depth of irradiation (Bech-Thomsen & Wulf, 1995). Moreover, epidermal melanocytes produce increased amounts of melanin, which is transferred in melanosomes to neighbouring keratinocytes within the epidermis to shield DNA from UV-induced damage (Stanojević et al., 2004).

1.4.2. UV-induced effects on immune responses in the skin

In a more detailed perspective, some of the main UV-induced mechanisms and molecules that interfere with cellular processes and influence innate and adaptive immunity will be introduced. Figure 5 illustrates and summarizes some of these mechanisms.

Innate immune activation through the release of DAMPs

UV-injured and stressed cells release damaged DNA, proteins and reactive oxygen species (ROS). These compounds might act as DAMPs and activate the immune system via TLRs and other PRRs, resulting in inflammation (Gallo & Bernard, 2014). Pro-inflammatory cytokines are

secreted in this process by skin-resident immune cells and keratinocytes, thereby recruiting neutrophils and monocytes (Noske, 2018; Piskin et al., 2005). LCs, dermal DCs and mast cells become activated when sensing these DAMPs and initiate adaptive immune responses that are strongly modulated by UV irradiation (Bernard et al., 2019). The alarmin IL-33 was shown to be secreted by epithelial cells upon UVB irradiation and to promote tumor development (Amôr et al., 2018; Byrne et al., 2011; Suhng et al., 2018). IL-33 expressing cells were also described to interact with mast cells and neutrophils in the skin (Byrne et al., 2011). Moreover, extracellular matrix proteins might experience oxidative damage after UV irradiation. Fragmented parts of these proteins can then be recognized by immune cells, which not only contributes to innate inflammation, but also leads to skin ageing since collagen fibers and other matrix proteins are degraded prematurely (Amano, 2016; Gariboldi et al., 2008).

DNA damage

Further effects of UV irradiation are DNA lesions, the most frequent modification are cyclobutane pyrimidine dimers (CPDs) and pyrimidine-pyrimidone (6-4) photoproducts (6-4PP) (Cadet & Douki, 2018). These modifications are formed either directly by irradiation or indirectly through oxidative damage and are highly mutagenic (Ravanat et al., 2001). Cells have evolved a whole DNA repair machinery, enabling the repair of these mutations. The nucleotide excision repair (NER) is most common repair mechanism for UV-induced DNA modifications. Here, the damaged DNA strand is enzymatically excised, followed by a refill of the gap using the remaining strand as a template (Rastogi et al., 2010). However, some mutations remain irreparable and cause skin cancers if they occur in oncogenes or tumor suppressor genes. In addition, DNA damage in keratinocytes and LCs was associated with immunosuppression (Kripke et al., 1992). Especially LCs are important in instructing Tregs to mediate immunosuppression (Schwarz et al., 2010). The importance of DNA repair mechanisms and the contribution of DNA damage to immunosuppression becomes apparent in xeroderma pigmentosum patients, these patients lack DNA repair enzymes and show very high numbers of skin tumors in UV-exposed skin regions (Digiovanna & Kraemer, 2012).

Molecules involved in immunosuppression

UVB irradiation is necessary in the first step of vitamin D synthesis, since it is required for the conversion of 7-dehydrocholesterol to pre-vitamin D_3 in the skin. Besides the function in calcium absorption, vitamin D_3 contributes to immunosuppression by modulating

macrophages and DCs (Penna et al., 2007; Y. Zhang et al., 2012). In consequence, these cells acquire tolerogenic phenotypes and promote immunosuppression through the generation of Tregs (Schwarz et al., 2012; Van Der Aar et al., 2011).

Urocanic acid (UCA) is a chromophore that is present in the stratum corneum of the epidermis. It derives from filaggrin catabolism and upon UVB light exposure, the naturally existent trans-UCA is converted to cis-UCA (Gibbs et al., 2008). Cis-UCA was shown to further increase levels of DNA damage, thus possibly regulating immunosuppression and photocarcinogenesis (Sreevidya et al., 2010). Furthermore, studies show that cis-UCA on the one hand activates mast cells and induces the release of histamine, and on the other hand stimulates the production of TNF-α by keratinocytes which supports emigration of LCs from the skin (Cumberbatch & Kimber, 1992; Hart et al., 2000; Kurimoto & Streilein, 1992). Both events together facilitate the induction of immunosuppression. Supporting evidence shows that mice with LC-depleted skin failed to develop UV-induced immunosuppression (Schwarz et al., 2010).

Moreover, UV-induced ROS generation triggers the oxidization of keratinocyte lipids, resulting in the release of platelet-activating-factors (PAF). PAF activates many different immune cells such as mast cells, neutrophils, macrophages, but also keratinocytes via the PAF receptor (PAFR) (reviewed in Damiani & Ullrich, 2016). PAFR deficient mice failed to generate immunosuppressive effects due to impaired mast cell migration, therefore indicating a highly significant role for PAF signaling in this mechanism (Chacon-Salinas et al., 2014). The responsible cell type for the induction of immune suppression are mast cells, which migrate along the CXCR4-CXCL12 axis to draining lymph nodes and suppress antibody formation in an IL-10 dependent manner (Byrne et al., 2008).

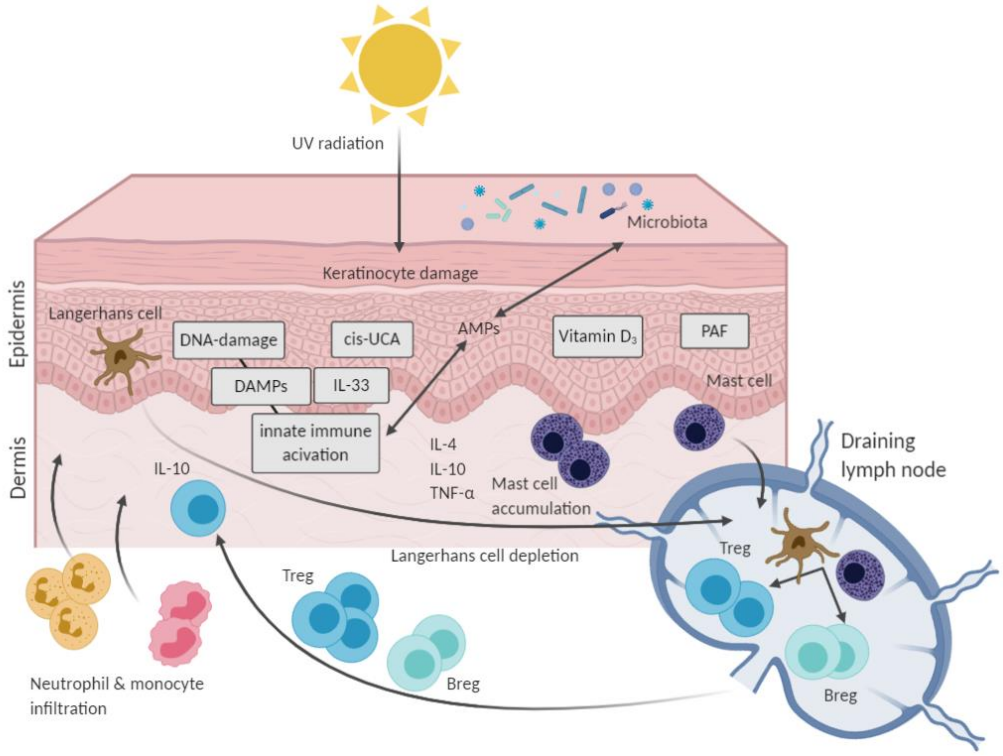

Figure 5 Mechanisms of UV-induced immune suppression.
UV irradiation is absorbed by different chromophores in the skin. DNA damage and the release of DAMPS and IL-33 from dying cells can lead to innate immune activation, resulting in the secretion of AMPs and inflammatory cytokines. This process is accompanied by the recruitment of other innate immune cells like monocytes and neutrophils. The dermal cytokine milieu of UV-irradiated skin is characterized by IL-4, IL-10 and TNF-α. Moreover, vitamin D_3, cis-UCA and PAF affect Langerhans cells and mast cell functions. In consequence, these cells acquire tolerogenic functions and migrate to skin-draining lymph nodes where they induce the differentiation of Treg and Breg. These regulatory lymphocytes then home tissues and suppress immune responses by secretion of IL-10 (adapted from Bernard et al., 2019).

1.4.3. Photocarcinogenesis

UV light is one of the main risk factors for the development of melanomas and non-melanoma skin cancers in humans. In mice, only non-melanoma skin cancers emerge after UV exposure, the formation of melanomas requires additional mutations in genes like tumor suppressor genes for example (Day et al., 2017). DNA mutations and the suppressive immune environment collectively facilitate formation of UV-induced tumors and their pre-cancerous forms such as solar keratosis (Hart & Norval, 2018). The two most frequent non-melanoma cancer types are basal cell carcinomas and squamous cell carcinomas. Principally, they form in sun-exposed areas of the skin, since the main cause for these types is the long-term impact of UV irradiation. Basal cell carcinomas originate from basal keratinocytes of the epidermis, while squamous cell carcinomas derive from keratinocytes in the epidermal stratum spinosum. In contrast to non-melanoma cancers that are rather non-metastatic, melanomas

are more fatal and highly metastatic. Besides genetic factors, recurrent and intensive UV exposure in childhood and adolescence are the main risk factor for melanomas in humans (reviewed in Mengoni et al., 2021). The disease incidence for melanoma and non-melanoma skin cancers increased within the past years due to ageing populations, high disease rates in elder individuals and changed lifestyles (*Krebs in Deutschland Für 2015/2016*, 2019). Since 2015, some non-melanoma skin cancer types are recognized as occupational diseases in Germany (Strom et al., 2015). This is one of the many reasons, why the identification of immunosuppressive mechanisms and the influence of innate signaling pathways in disease emergence are of high interest.

1.5. Allergies

The immune system requires a tight regulation and fine-tuning in order to initiate a specific immune response against dangerous substances or pathogens and to shut down immune responses once an infection is resolved. However, when the immune system is dysregulated, it might react to innocuous antigens and lead to disease. Autoimmune diseases can develop when the immune response is directed towards self-derived antigens, while in allergic reactions the immune system responds to environment-derived allergens that and can be found in certain food, drugs, pollen, insect venoms, chemicals, metals or UV-light induced self-antigens (Murphy & Weaver, 2017). The prevalence of allergies has been steadily increasing over the past decades and seem to predominantly appear in industrialized countries, revealing a correlation between increased hygienic standards to allergy occurrence (Lambrecht & Hammad, 2017).

Classically, Gell and Coombs categorized immune reactions towards allergens into four groups (Gell & Coombs, 1963). Type I hypersensitivity reactions are IgE-mediated and occur within a very short time frame after allergen exposure. The underlying reaction is that allergens bind to antigen-specific IgE antibodies on the mast cell and basophil cell surface. This recognition will result in cross-linking of the IgE receptor, followed by degranulation. The released granule compounds like histamine, prostaglandin and tryptase may cause inflammation and tissue swelling, in the worst case leading to anaphylaxis. Type II allergic reactions are mediated by IgG antibodies towards cell surface antigens and induce cell-mediated or complement mediated cytotoxicity. Type III reactions are characterized by complement activation by free

floating antigen/antibody immune complexes, inducing leukocyte activation. In contrast to the first three described hypersensitivity reactions, type IV reactions happen in a cell-mediated manner. Here, APCs recognize foreign soluble or cell-associated antigens, internalize these and present the antigenic peptide to T-cells. CD8+ T-cells are activated and mediate cytotoxicity or Th1 cells can differentiate and might in turn activate tissue macrophages via cytokines to mediate cellular damage (reviewed in Descotes & Choquet-Kastylevsky, 2001; Murphy & Weaver, 2017).

1.5.1. Anaphylaxis

The anaphylactic reaction is a sudden, allergic reaction that belongs to the group of type I hypersensitivity reactions. Its effects can range from mild cutaneous signs like erythema or urticaria to life threatening symptoms like hypotension, arrhythmias, cardiac or respiratory arrest (Simons, 2010). Patients with type I allergies tend to have elevated levels of antigen-specific IgE antibodies due to prior sensitization with a certain allergen (Qiu et al., 2020). Mast cells and basophils express the receptor FcεRI that bind these IgE antibodies. One hallmark of a type I reaction is degranulation and thereby the release of vasoactive and pro inflammatory compounds by these two cell types upon binding of the allergen to IgE antibodies on the cell surface (Murphy & Weaver, 2017).

Passive cutaneous anaphylaxis (PCA) is an animal model frequently used to mimic a local type I allergic reaction of the skin. In this model, antigen-specific IgE antibodies are administered to the skin, followed by antigen exposure to induce allergy. Often, an indicator dye is injected together with the antigen to monitor vascular leakage, which is one of the key processes in the course of local anaphylaxis. Thus, the severity of the reaction can be examined by the amount of dye that penetrates the tissue, as well as by the enhanced release of inflammatory mediators and swelling of the tissue (Evans et al., 2014).

1.5.2. Allergic contact dermatitis

Contact dermatitis is an allergic skin disease and belongs to the group of type IV delayed-hypersensitivity reactions. This disease represents the largest group of occupational-related skin diseases, patients often work in sectors with frequent allergen exposure, such as the

healthcare or cosmetic sector, food industry or metal sector. Symptoms of contact dermatitis include a rash accompanied by itch, dryness and skin swelling, and in severe cases even blisters might develop (Sasseville, 2008). Allergic contact dermatitis (ACD) is a subtype of contact dermatitis and occurs when skin is exposed to an allergen during the sensitization phase of the disease. This sensitization can arise either after a single exposure or it can be established after repeated exposures, which is dependent on the type of allergen. After priming of allergen-specific T-cells in the sensitization phase, further allergen exposure initiates elicitation, which is characterized by the recruitment of allergen-specific T-cells to the site of exposure (Kaplan et al., 2012). In ACD, almost all of the contact allergens are haptens. Haptens are small molecules (<500 Da) that are not antigenic per se. However, when they pass through the skin these molecules covalently bind to self-proteins thereby making them antigenic and recognizable to innate immune cells (Eisen et al., 1952; Kaplan et al., 2012). In more detail, skin penetrating haptens form complexes with self-derived proteins and lead to the activation of keratinocytes, LCs, dermal DCs and mast cells. This activation occurs through DAMPs which are released by damaged skin cells, by pro inflammatory cytokines such as IL-1β, TNF-α and mast cell-derived histamine which lead to activation of skin immune cells (Martin et al., 2011). This inflammatory environment induces phagocytosis of hapten-self-protein complexes, activation and migration of dermal DCs and LCs to the skin draining lymph node. Especially mast cells have been shown to enhance DC migratory abilities. In the lymph node, DCs present antigens and prime $CD4^+$ and $CD8^+$ T-cells which will proliferate and differentiate into effector cells which will migrate to the inflamed skin tissue. Further exposure to the same hapten, also on unrelated sites of the skin, will elicit a rapid, antigen-specific allergic reaction since the T-cells were primed before and memory T-cells have been generated. These memory T-cells moreover induce infiltration of monocytes/macrophages and neutrophils to the skin, which contributes to the hypersensitivity reaction in an antigen-unspecific manner (reviewed in Honda et al., 2013).

Allergic contact dermatitis is commonly studied in a mouse model of contact hypersensitivity (CHS). Here, animals are sensitized on the shaved skin with a hapten like 1-Fluoro-2,4-dinitrobenzene (DNFB) and challenged several days later with the same hapten on a different site of the skin, which usually are the ears. This challenge initiates the elicitation phase and the skin rapidly begins to show symptoms of inflammation. One hallmark of inflammation, the swelling response, is monitored during the elicitation phase by measurements of the ear

thickness, which directly correlates with the degree of inflammation. To study UV-induced immunosuppression, the CHS model is performed with additional UV exposure prior to sensitization. Here, the ear swelling response directly correlates with the degree of immunosuppression (Schwarz, 2005). Analysis of immune cell infiltrates in the skin gives further information about the underlying immune reaction.

1.6. Aim of the thesis

Excessive exposure to UVB radiation is as a danger for human health. However, not only acute exposure leading to sunburns and erythema is dangerous, but also chronic exposure with low UVB doses might become harmful. Chronic UVB radiation leads to photoaging of the skin, which is characterized by wrinkle formation and decreased elasticity, but also leads to suppression of adaptive immunity. Moreover, repeated UVB exposure leads to accumulated DNA mutations and along with the immunosuppressive skin environment, the risk for development of tumors rises. As a central protein of innate immunity, MyD88 mediates signaling of infectious substances or self-derived DAMPs through several TLR and IL-1 receptor pathways and thereby induces inflammation. Previous experiments from our group could indeed demonstrate MyD88-dependent effects on the skin after UVB-irradiation concerning inflammation, mast cell accumulation, acanthosis and DNA damage (Opitz, 2016). Most of these UVB-induced effects were restored in mast cell-specific MyD88 knock-in animals in the model of chronic UVB irradiation, revealing a fundamental role for mast cell-specific MyD88 signaling in UVB irradiation. Therefore, this thesis focused on the role of MyD88 signaling in mast cells to investigate the influence of MyD88 on mast cell functionality. Furthermore, the influence of IL-33 in chronic UVB irradiation was studied. Mast cells are not only key effector cells in allergies, but are also involved in the host defense during other diseases and have the capability to induce and guide adaptive immune responses into certain directions. Together with dermal DCs, mast cells can regulate the course of skin disease and alter adaptive effector responses. Especially in UV-induced diseases, dermal mast cells were shown to contribute to immunosuppression and tumor formation. In this project, we therefore wanted to further examine if MyD88 signaling in mast cells affects these processes.

As a summary, we aim to understand the following:

1. What is the role of MyD88 in *in vitro* generated mast cells?
2. How does the alarmin IL-33 signaling affect mast cells during chronic UVB irradiation?
3. Does MyD88 signaling have an impact on mast cell-DC interactions?
4. How does MyD88 signaling in mast cells contribute to the generation of immune suppression and to UV-induced tumor formation?

2. Material

2.1. Equipment

Table 2 Equipment.

Equipment	Product/Company
Automatic tissue processor	Leica TP1020 (Leica Microsystems, Wetzlar, Germany)
Balances	440-35A (Kern & Sohn, Balingen, Germany) ABJ-NM (Kern & Sohn, Balingen, Germany)
Caliper	Oditest (Kroeplin Längenmesstechnik, Schlüchtern, Germany)
Cell counting chamber	Neubauer Improved (BRAND, Wertheim, Germany)
Centrifuges	5415R (Eppendorf, Hamburg, Germany) 5810R (Eppendorf, Hamburg, Germany)
Cryostat	Leica CM3050S (Leica Microsystems, Wetzlar, Germany)
Electrical shaver	ChroMini® Pro (Moser, Unterkirnach, Germany)
ELISA washer	CAPP wash 12 (CAPP, Nordhausen, Germany)
Flow Cytometer	BD FACSSymphony™, BD LSR II, BD FACSCanto™ II (BD Biosciences, Heidelberg, Germany)
Freezer (-20 °C)	Bosch GSD12A20 (Bosch, Gerlingen, Germany)
Freezer (-80 °C)	New Brunswick Ultra-Low Temperature Freezer (Eppendorf, Hamburg, Germany)
Homogenizer	Precellys®24 (Bertin Instruments, Montigny-le-Bretonneux, France)
Hydrophobic barrier pen	ImmEdge™ pen (Vector Lab, Burlingame, USA)
Ice machine	Scotsman Flockeneisbereiter AF200 (Hubbard Systems, Gt. Blakenham, UK)
Incubator	CB 150 (Binder, Tuttlingen, Germany)
Incubator shaker	New Brunswick™ Innova 44 (Eppendorf, Hamburg, Germany)

Isoflurane Vaporizer	Combi-vet® system (Rothacher Medical, Berne, Switzerland)
Laminar flow workbench	BDK Laminar Flow (BDK, Sonnenbühl, Genkingen, Germany)
Light microscope	Eclipse TS100-F (Nikon, Tokyo, Japan)
Magnetic stirrer	IKA RCT basic (IKA-Werke GmbH & Co. KG, Staufen, Germany)
Microliter pipettes (2 µl, 20 µl, 200 µl, 1000 µl)	Finnpipette™ F2 (Thermo Scientific, Waltham, USA)
Microscope	BZ-9000 (Keyence, Neu-Isenburg, Germany) LSM 780 (Carl Zeiss Microscopy, Jena, Germany)
Microtome	Leica RM2255 (Leica Microsystems, Wetzlar, Germany) Leica HI1210 (Leica Microsystems, Wetzlar, Germany)
Microwave	NN-E235M (Panasonic, Osaka, Japan)
Multichannel pipette	DV8-10, DV12-50, DV8-300 (HTL Lab Solutions, Warsaw, Poland)
Pipette controller	Accu-jet® pro (BRAND, Wertheim, Germany)
Power supply	PowerPac Basic (BioRad, Hercules, USA)
Spectrophotometer	NanoDrop™ ND-1000 (Thermo Scientific, Waltham, USA) EL 800 (BioTek, Winooski, USA)
Thermal cycler	T100 (BioRad, Hercules, USA)
Transilluminator	Transilluminator UST-30M-8R (BioView, Rehovot, Israel) Dark Hood DH-40/50 (Biostep, Burkhardtsdorf, Germany)
UVB lamp	TL 20W/12RS (Philips, Amsterdam, Netherlands)
UV-meter	Variocontrol (Waldmann, Villingen-Schwenningen, Germany)
Vortex shaker	Vortex Genie 2 (Scientific Industries, New York, USA)

2.2. Consumables

Table 3 Consumables.

Product	Company
Cell culture plates (6-,12-,24-,48-,96-well)	Greiner, Frickenhausen, Germany
Cell strainer (100 µm, 70 µm)	Corning, Glendale, USA
Corning® Costar® Transwell® cell culture inserts (8 µm)	Corning, New York, USA
Cover slips	Carl Roth, Karlsruhe, Germany
Cryomold	Sakura Finetek, Torrance, USA
Cryotubes	Sarstedt, Nümbrecht, Germany
Disposal Bags	Carl Roth, Karlsruhe, Germany
Embedding cassette	Carl Roth, Karlsruhe, Germany
Flow cytometry tubes	Sarstedt, Nümbrecht, Germany
Glass beads	Carl Roth, Karlsruhe, Germany
Glass slide	Thermo Fisher, Waltham, USA
Gloves	Sentina Ambidextrous Nitrile
Half-area ELISA plates	Greiner, Frickenhausen, Germany
Microtubes (2 ml, 1,5 ml, 0,5 ml)	Sarstedt, Nümbrecht, Germany
Multiply®µStrip Pro mix.colour	Sarstedt, Nümbrecht, Germany
Omnican ® 50 Syringes	B. Braun, Melsungen, Germany
Parafilm®	Bemis, Neenah, USA
Petri dishes	Greiner, Frickenhausen, Germany
Reagent reservoirs	VWR, Darmstadt, Germany
Screw cap microtube	Sarstedt, Nümbrecht, Germany
Serological pipette (5 ml, 10 ml, 25 ml)	Greiner, Frickenhausen, Germany
Sterican® needles	B. Braun, Melsungen, Germany
Surgical Scalpel	B. Braun, Melsungen, Germany
Syringes (1 ml, 5 ml, 10 ml)	B. Braun, Melsungen, Germany
Tubes (15 ml, 50 ml)	Greiner, Frickenhausen, Germany

2.3. Chemical Reagents

Table 4 Chemical Reagents.

Reagent	Company
1,4-Diazabicyclo (2.2.2) octane (DABCO)	Carl Roth, Karlsruhe, Germany
100 bp DNA ladder	New England Biolabs, Ipswich, USA
10x TAE buffer	Invitrogen, Carlsbad, USA
1-Fluoro-2,4,-dinitrobenzene (DNFB)	Sigma-Aldrich, St. Louis, USA
2-Propanol	Carl Roth, Karlsruhe, Germany
4-(2-hydroxyethyl)-1-piperazineethanesulfonic acid (HEPES)	Sigma-Aldrich, St. Louis, USA
4'-6-Diamidino-2-phenylindole (DAPI)	Sigma-Aldrich, St. Louis, USA
Acetone	VWR, Darmstadt, Germany
Agarose	PeqLab, Darmstadt, Germany
Albumin Bovine Fraction V, pH 7	SERVA Electrophoresis, Heidelberg, Germany
AnnexinV APC	Biolegend, Fell, Germany
Brilliant stain buffer	BD Biosciences, Franklin Lakes, USA
Calcium chloride ($CaCl_2$)	Merck, Darmstadt, Germany
Compensation Beads	Thermo Fisher Scientific
cOmplete™ Protease inhibitor tablets	Roche, Basel, Switzerland
Dinitrophenyl human serum albumin (DNP-HSA)	BioCat, Heidelberg, Germany
Dulbeccos phosphate buffered saline (DPBS)	PAN-Biotech, Aidenbach, Germany
Ethanol 70%, 99%	Carl Roth, Karlsruhe, Germany
Ethylenediaminetetraacetic acid (EDTA)	Sigma-Aldrich, St. Louis, USA
Euparal	Carl Roth, Karlsruhe, Germany
Evans Blue	Sigma-Aldrich, St. Louis, USA
Fetal Bovine Serum	PAN-Biotech, Aidenbach, Germany
FITC-Avidin	Biolegend, Fell, Germany
Fixable Viability Dye eFlour™ 780	Thermo Fisher, Waltham, USA
Formamide	Carl Roth, Karlsruhe, Germany
Glycerol	Carl Roth, Karlsruhe, Germany
Hank's Balanced Salt Solution (HBSS, w and w/o Ca^{2+} and Mg^{2+})	PAN-Biotech, Aidenbach, Germany
Indo-1	Invitrogen, Carlsbad, USA

Ionomycin	Sigma-Aldrich, St. Louis, USA
Isoflurane	Zoetis, Parsippany-Troy Hills, USA
L-Glutamine	Life Technologies, Carlsbad, USA
Lipopolysaccharide (LPS) from *Escherichia coli* O111:B4	Sigma-Aldrich, St. Louis, USA
Mowiol® 4-88	Carl Roth, Karlsruhe, Germany
Murine recombinant cytokines (IL,3, IL-33, SCF, CCL5, CCL17, CCL21)	Peprotech, New York, USA
Olive Oil	Sigma-Aldrich, St. Louis, USA
OneComp / UltraComp eBeads™	Thermo Fisher, Waltham, USA
Pam_3CSK_4	EMC Microcollections, Tübingen, Germany
Pantevit® eye drops	WDT, Garbsen, Germany
Paraffin	Leica Biosystems, Nußloch, Germany
Paraformaldehyde (PFA)	Merck, Darmstadt, Germany
Penicillin-Streptomycin	Life Technologies, Carlsbad, USA
Phosphate buffered saline (PBS)	Bio & Sell, Feucht, Germany
Phosphate buffered saline (PBS)	Merck, Darmstadt, Germany
Precision Count beads™	Biolegend, Fell, Germany
Radioimmunoprecipitation Assay (RIPA) buffer	Cell Signaling, Danvers, USA
Roswell Park Memorial Institute (RPMI)1640	PAN-Biotech, Aidenbach, Germany
Serum (goat, mouse, rat)	Sigma-Aldrich, St. Louis, USA
Skim milk powder	Carl Roth, Karlsruhe, Germany
Sodium chloride (NaCl)	Carl Roth, Karlsruhe, Germany
Sodium dodecyl sulfate (SDS)	Carl Roth, Karlsruhe, Germany
Sodium hydroxide (NaOH)	Carl Roth, Karlsruhe, Germany
Sucrose	Sigma-Aldrich, St. Louis, USA
Sulfuric acid (H_2SO_4)	Carl Roth, Karlsruhe, Germany
SYBR® safe DNA gel stain	Invitrogen, Carlsbad, USA
Tissue freezing medium	Leica Biosystems, Nußloch, Germany
Toluidine Blue O	VWR, Darmstadt, Germany
Tris-HCL	Carl Roth, Karlsruhe, Germany
Triton X-100	Sigma-Aldrich, St. Louis, USA
Trypan Blue	Sigma-Aldrich, St. Louis, USA
Tween20	Carl Roth, Karlsruhe, Germany

Xylol	Carl Roth, Karlsruhe, Germany
Zymosan from *Saccharomyces cerevisiae*	Sigma-Aldrich, St. Louis, USA
β-mercaptoethanol	Sigma-Aldrich, St. Louis, USA

2.4. Buffers, Media and Solutions

Table 5 Buffers, Media and Solutions.

Name	Dissolved in	Ingredients
AnnexinV binding buffer	Aqua. Dest.	10 mM HEPES (pH 7.4) 140 mM NaCl 2.5 mM $CaCl_2$
Blocking buffer (ELISA)	PBS	1 % BSA
Blocking buffer (histology sections)	PBS	2.5 % FCS 2.5 % BSA 1 % rat serum 1 % goat serum
Blocking buffer (histology whole mount)	PBS	0.5 % BSA 0.3 % Triton-X-100
Complete medium	RPMI 1640 w/o Glutamine	10 % FCS 1000 U/ml Penicillin 1000 µg/ml Streptomycin 2 mM L-Glutamine 50 µM β-Mercaptoethanol
Digestion buffer	HBSS (with Ca^{2+} and Mg^{2+})	0.8 U/ml Liberase™ 200 U/ml DNase I
EDTA (0.5 M)	Aqua. Dest.	0.5 M EDTA Set to pH 8 with NaOH
Lysis buffer	Aqua. Dest.	100 mM Tris HCl (pH 8.5) 5 mM EDTA (pH 8.0) 0.2 % SDS 200 mM NaCl

Mowiol mounting solution	Aqua. Dest. (6 ml)	2.4 g Mowiol 6 g Glycerol 12 ml Tris (0.2 M, pH 8.5) 2.5 % DABCO
PFA	PBS	4 % PFA
Staining buffer (histology whole mount)	PBS	0.25 % BSA 0.15 % Triton-X-100
Starving medium	RPMI 1640 w/o Glutamine	0.5 % FCS 1000 U/ml Penicillin 1000 µg/ml Streptomycin
Stop solution (ELISA)	Aqua. Dest.	2 N H_2SO_4
TE-buffer	Aqua. Dest.	100 mM Tris HCl (pH 8.0) 1 mM EDTA
Washing buffer (ELISA)	PBS	0.5 % Tween20

2.5. Kits

Table 6 Kits.

Product	Company
DuoSet® ELISA Development Kit (IL-6, TNF-α, IL-10, TSLP)	R&D systems, Minneapolis, USA
IL-13 ELISA Ready-SET-Go!™	eBioscience, San Diego, USA
MyTaq™ HS Red DNA Polymerase	Bioline, London, UK

2.6. Primers

Table 7 Genotyping primers.
All Primers were purchased from IDT (Coralville, USA).

Gene	Sequence	Product size
Mcpt5	TGA GAA GGG CTA TGA GTC C GTC AGT GCG TTC AAA GGC CA ACA GTG GTA TTC CCG GGG AGT GT	300 bp (WT 600 bp (Cre)
MyD88 WT allele	ACA CTG TAG CTG CCT GCA GAC ACA C GGA CTC CTG GTT CTG CTG CTT ACC T	305 bp (WT) 500 bp ($MyD88^{IND}$)
MyD88 LSL allele	CTG AAG AGG AGT TTA CGT CCA G CTA GCC TTG GCA TAT TAA TCT TG	825 bp

2.7. Antibodies

Table 8 Antibodies for flow cytometry.

Antibody	Clone	Dilution	Company
B220	RA3-6B2	1:200	Biolegend, Fell, Germany
CCR2	475301	1:200	R&D systems, Minneapolis, USA
CD103	M290	1:200	Biolegend, Fell, Germany
CD11b	M1/70	1:200	Biolegend, Fell, Germany
CD11c	N418	1:100	Biolegend, Fell, Germany
CD16/32 (TruStain FcX™)	93	1:100	Biolegend, Fell, Germany
CD19	6D5	1:200	Biolegend, Fell, Germany
CD24	M1/69	1:200	Biolegend, Fell, Germany
CD25	PC61	1:200	Biolegend, Fell, Germany
CD3	145-2C11	1:200	Biolegend, Fell, Germany
CD4	RM4-5	1:250	Biolegend, Fell, Germany
CD40	HM40-3	1:200	Biolegend, Fell, Germany
CD44	IM7	1:200	Biolegend, Fell, Germany
CD45	30-F11	1:400	Biolegend, Fell, Germany
CD62L	MEL-14	1:200	Biolegend, Fell, Germany
CD64	X54-5/7.1	1:200	BD Biosciences, Franklin Lakes, USA
CD80	16-10A1	1:200	Biolegend, Fell, Germany
CD86	GL-1	1:200	Biolegend, Fell, Germany
CD8a	53-6.7	1:250	Biolegend, Fell, Germany
c-Kit	2B8	1:200	BD Biosciences, Franklin Lakes, USA
FcεRIα	MAR-1	1:200	Biolegend, Fell, Germany
FoxP3	FJK-16s	1:100	BD Biosciences, Franklin Lakes, USA
Ly6C	HK1.4	1:200	Biolegend, Fell, Germany
Ly6G	1A8	1:200	Biolegend, Fell, Germany
MHCII	M5/114.15.2	1:500	Biolegend, Fell, Germany
Sca-1	D7	1:200	Biolegend, Fell, Germany
ST2	U29-93	1:200	BD Biosciences, Franklin Lakes, USA
TCRβ	H57-597	1:200	BD Biosciences, Franklin Lakes, USA
TCRγδ	GL3	1:200	Biolegend, Fell, Germany
β7 integrin	FIB501	1:200	BD Biosciences, Franklin Lakes, USA

Table 9 Antibodies for histology.

Antibody	Clone	Dilution	Company
Primary antibodies			
CD31 (rat)	MEC13.3	1:200 ear skin	BD Biosciences, Franklin Lakes, USA
GFP (rabbit)	polyclonal	1:200 back and ear skin	Life Technologies, Carlsbad, USA
Ki-67 (rat)	SolA15	1:50 back skin	eBioscience, San Diego, USA
MHCII APC	M5/114.15.2	1:200 back and ear skin	Biolegend, Fell, Germany
Secondary antibodies			
IgG Alexa Flour 488 (goat anti-rabbit)	polyclonal	1:200 back skin 1:400 ear skin	Life Technologies, Carlsbad, USA
IgG Alexa Flour 594 (goat anti-rat)	polyclonal	1:400 ear skin	Life Technologies, Carlsbad, USA
IgG Texas Red (goat anti-rat)	polyclonal	1:100 back skin	Life Technologies, Carlsbad, USA

Table 10 Antibodies for animal experiments and cell culture assays.

Antibody	Clone	Concentration	Company
Dinitrophenyl-IgE (DNP-IgE)	SPE-7	2 µg/ml	Sigma-Aldrich, St. Louis, USA
FcεRIα	MAR-1	1 µg/ml	Biolegend, Fell, Germany
IgG1	RTK2071	1 mg/ml	Biolegend, Fell, Germany
ST2	DIH4	1 mg/ml	Biolegend, Fell, Germany

2.8. Enzymes

Table 11 Enzymes.

Enzyme	Company
DNase I	Roche, Basel, Switzerland
Liberase™	Roche, Basel, Switzerland
MyTaq™ HS DNA polymerase	Bioline, London, UK
Proteinase K	Sigma-Aldrich, St. Louis, USA

2.9. Software

Table 12 Software.

Software	Company
Argus X1	Biostep (Burkhardtsdorf, Germany)
BD FACS Diva	BD Biosciences (Heidelberg, Germany)
BioRender	BioRender (Toronto, Canada)
BZ-II Analyzer & Viewer	Keyence (Neu-Isenburg, Germany)
Fiji	Open-source software
FlowJo 10.7.1	BD Biosciences (Franklin Lakes, USA)
Gen 5	BioTek (Winooski, USA)
GraphPad Prism 6.0	GraphPad Software (San Diego, USA)
Mendeley	Elsevier (Amsterdam, Netherlands)
Microsoft Office 2016	Microsoft Corporation (Redmond, USA)
NanoDrop 1000 V3.8.1	Thermo Fisher (Waltham, USA)

3. Methods

3.1. Animal Experiments

All mice were maintained and bred at the Life and Medical Science Institute (LIMES) Genetic Resources Center (GRC) at the University of Bonn. The animals were kept in individual ventilated cages with up to five mice per cage under specific-pathogen-free (SPF) conditions and had unlimited access to food and water. All animal experiments were approved by the regional authorities of North Rhine-Westphalia (Germany).

3.1.1. Mouse Genetics

To analyze the global and cell-type specific role of the adaptor protein MyD88, genetically modified mouse lines were used. The MyD88 loxP-Stop-loxP (MyD88 LSL) mouse line was generated by insertion of a loxP-flanked stop cassette into intron 1 of the MyD88 locus, which leads to a premature stop in transcription and therefore to global MyD88-deficiency (Gais et al., 2012). Following Cre-mediated recombination, the floxed stop cassette is excised and functional MyD88 expression can be restored (Figure 6). Hence, utilization of Mcpt5 Cre recombinase expressing mice which express Cre in mast cells selectively, enables the analysis of mast cell specific MyD88 re-expression in otherwise MyD88 deficient mice (Scholten et al., 2008).

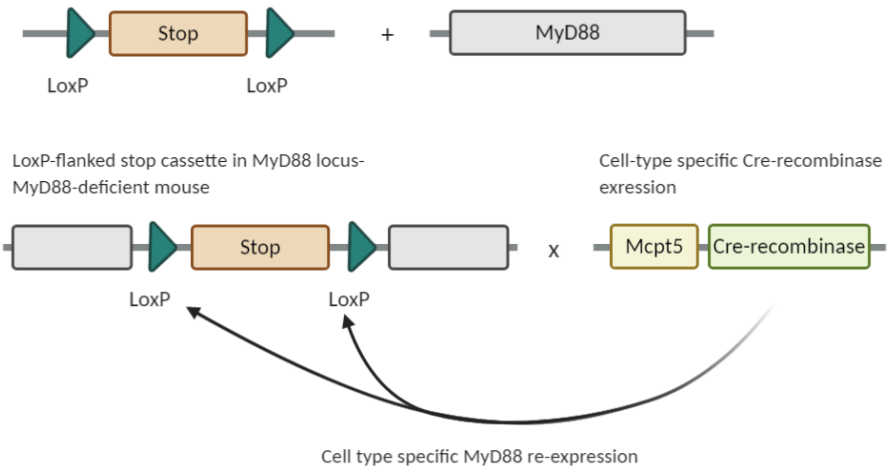

Figure 6 Genetic background of the mouse model.
MyD88 LSL mice contain a floxed stop cassette in intron 1 that prevents transcription, homozygous MyD88 LSL mice therefore are MyD88 deficient. Presence of Cre recombinase leads to excision of the stop cassette and restoration of MyD88 expression. Here, Mcpt5 Cre mice were used to generate mast cell-specific expression of MyD88.

For an overview of the genetic modifications, the following section lists all the mouse lines that were employed. All animals were C57BL/6 mice with a JRcc background.

WT	These mice were Wildtype mice without any further genetic modification.
MyD88 proficient	These mice were heterozygous for the floxed stop cassette. Previous results from AG Weighardt showed that they behave similar to WT mice, therefore they were used as controls.
MyD88 KO	These mice were homozygous, both alleles contained the floxed stop cassette and these mice were therefore MyD88 deficient (Gais et al., 2012).
MyD88^{Mcpt5Ind}	These mice were MyD88 deficient while only Mcpt5 expressing mast cells had MyD88 (Scholten et al., 2008).
R26eYFP^{Mcpt5Ind}	These mice expressed the fluorescent protein eYFP specifically in Mcpt5 expressing mast cells and were therefore used as mast cell reporter mice (Srinivas et al., 2001).

3.1.2. Genomic DNA isolation and gel electrophoresis

In order to determine the genotype of mice, genomic DNA was isolated and the genetically modified locus was amplified via PCR and was visualized on an agarose gel. For this, ear punch biopsies were lysed o. N. at 56 °C with 500 µl lysis buffer and Proteinase K (100 µg/ml). The next day, tubes were inverted and centrifuged at 16000 g 10 min 4 °C. The DNA containing supernatant was transferred to a fresh tube and the DNA was precipitated by addition of 500 µl isopropanol, followed by inversion of the tube and centrifugation at 16000 g 10 min. Then, the precipitated DNA pellet was washed with 500 µl 70 % Ethanol, centrifuged at 16000 g 5 min and the pellet was air-dried. Then, the DNA was dissolved in 100 µl TE-buffer and stored at 4 °C until the PCR was performed. The master mix for each mouse line-specific genotyping PCR was pipetted and the PCR was run in a thermocycler (Table 13). Afterwards, the PCR products were applied together with a 100 bp DNA standard on a 1.5 % agarose gel with SYBR^{TM} Safe (1:20000) to identify mouse genotypes.

Table 13 PCR reaction for genotyping.

Reagent	Volume (per reaction)
H_2O	13.5 µl (12.8 µl for 3 Primers)
4x MyTaq Buffer	4 µl
Primer 1	0.7 µl
Primer 2	0.7 µl
(Primer 3)	(0.7 µ)
MyTaq Polymerase	0.1 µl
Genomic DNA	1.5 µl

3.1.3. Passive cutaneous anaphylaxis

Mast cell and basophil degranulation are one of the main hallmarks of a type I allergic reaction. The passive cutaneous anaphylaxis assay, which is a model for a type I allergic reaction, induces local anaphylaxis. The severity of the anaphylactic reaction correlates with the amount of degranulation by mast cells and basophils. To test whether MyD88 is involved in mast cell degranulation *in vivo*, the passive cutaneous anaphylaxis assay was performed with female 8-10 week old MyD88 proficient, MyD88 KO and MyD88^{Mcpt5IND} mice. Under isoflurane anesthesia, either 10 µl PBS as control or 10 µl anti Dinitrophenyl-IgE (anti DNP-IgE) antibodies (2 µg/ml) were i.d. injected to the ventral side of the ear skin, which bind to FcεRI surface receptors via their Fc portion. After 24 h, mice were restrained and 100 µl DNP-human serum albumin (DNP-HSA; 1 mg/ml) with 0.1 % Evans Blue were i.v. injected to the tail vein and mice were then transferred back to the cage. DNP-HSA serves as an antigen, thus binds to DNP-directed IgE antibodies on the cell surface and thereby crosslinks IgE receptors. This induces a downstream signaling cascade that finally leads to the release of preformed granule content such as histamines and prostaglandins, which increase vascular permeability. The dye Evans Blue has a high binding affinity to serum albumin. Due to the increased vascular permeability, the injected albumin-bound dye can extravasate into the ear tissue and therefore serves as a color indicator for degranulation. 1 h after i.v. injection, mice were sacrificed and ears were excised. The Evans Blue dye was extracted from the tissue by incubation of each ear in 700 µl formamide for 48 h at 60 °C. Then, the formamide solution was filtered through 100 µm filters to remove hair and the optical density (OD) was determined in duplicates in 96-well plates at 630 nm.

3.1.4. Chronic UVB irradiation with ST2 blocking

To analyze the significance of IL-33 signaling in the context of UVB irradiation, a chronic UVB irradiation protocol with additional blocking of the IL-33 pathway was conducted. Therefore, female 8-10 week old WT mice were shaved in the beginning of every experimental week with electrical shavers and irradiated five times a week beginning with low, non-inflammatory doses of UVB (Figure 7). The UVB dose was increased weekly by 10 mJ/cm^2 for adaptation and reached a maximal dose of 100 mJ/cm^2 in week five and six. In addition, from week four onwards 100 µl of antibodies against the IL-33 receptor ST2 or IgG1 control antibodies (both 1 mg/ml) were administered i.p. to block IL-33 signaling. On d40, mice were sacrificed and organs were harvested for further analyses.

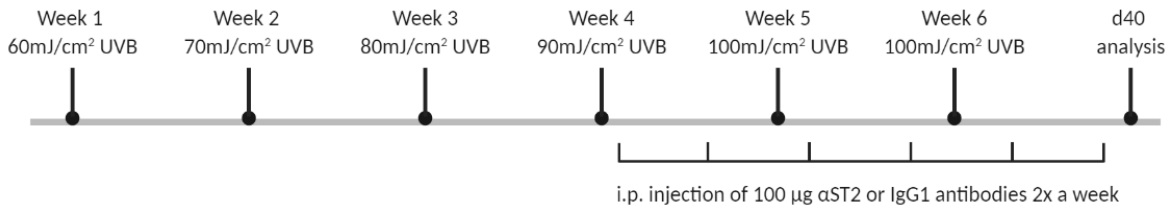

Figure 7 Model for chronic low-dose UVB irradiation with ST2 blocking.
Mice were shaved on the first day of the week and irradiated 5x a week with low, but weekly increasing doses of UVB-light to adapt mice and impede skin inflammation. In week 4, 5 and 6 mice were i.p injected twice a week with 100 µg in 100 µl of αST2 to block IL-33 signaling, control mice received IgG1 antibodies. On d40, the experiment was ended and organs were harvested.

3.1.5. UVB-induced immune suppression

In order to analyze the immunosuppressive effects of UVB irradiation on inflammatory skin diseases and to identify the role of MyD88 signaling in this process, mice were irradiated with UVB, followed by the model of contact hypersensitivity (Figure 8). Male 8-10 week old MyD88 proficient, MyD88 KO and MyD88^{Mcpt5IND} mice were shaved on their back under isoflurane anesthesia on d-9 and irradiated on four consecutive days with 100 mJ/cm^2 UVB light, followed by sensitization of the back skin on d-5 with 25 µl 0.5 % DNFB (w/v) in acetone/olive oil (4:1). On d0, mice were anesthetized and the baseline ear thickness was measured with a caliper. Then, mice were challenged with 20 µl 0.3 % DNFB (w/v) in acetone/olive oil (4:1) on one ear and 20 µl of acetone/olive oil (vehicle) as a control on the other ear (10 µl on the dorsal side, 10 µl on the ventral side for each ear). On d1, d2 and d3 mice were anaesthetized

and the ear swelling was measured with a caliper, on d3 the experiment was ended and organs were harvested for further analyses.

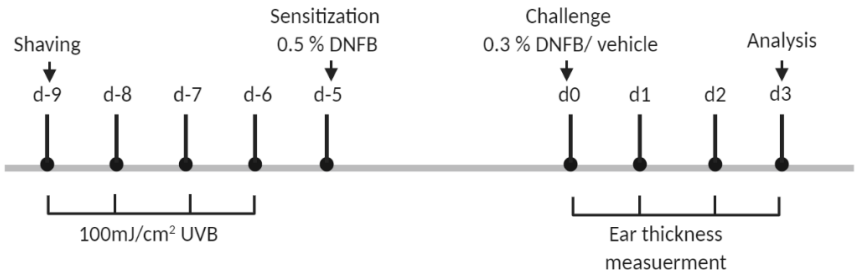

Figure 8 Model for UVB-induced immune suppression.
Mice were shaved on the back and irradiated for four consecutive days with 100 mJ/cm^2 UVB. The following day, mice were sensitized on the back with 0.5 % DNFB and five days after sensitization the challenge took place. For this, the ear thickness was measured and 0.3 % DNFB or vehicle solution were applied on the ears. The ear thickness was determined daily for three days, then the experiment was ended and immune cell populations were analyzed.

3.1.6. Photocarcinogenesis

In order to examine the role of MyD88-signaling on UV-induced skin tumor formation, female 6-10 week old MyD88 proficient, MyD88 KO and MyD88^{Mcpt5IND} mice were shaved on the back with an electrical shaver in the beginning of every experimental week and irradiated with UVB light three times a week, starting with a dose of 100 mJ/cm^2. The UVB dose was increased weekly by 25 or 50 mJ/cm^2 until reaching the final dose of 300 mJ/cm^2 in week six (Figure 9). Mice were then further irradiated with 300 mJ/cm^2 for a total of 32 weeks with this UVB dose. During the entire period of the experiment, tumor sizes and tumor numbers were documented weekly and in week 33 mice were sacrificed and organs were harvested for further analyses.

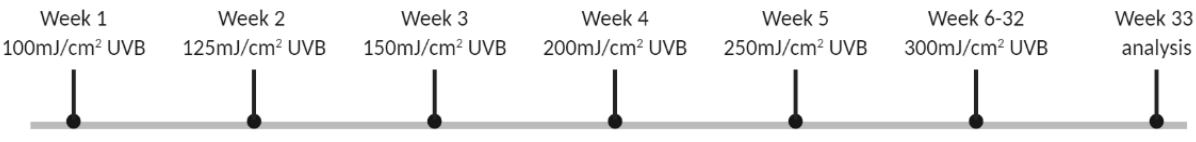

Figure 9 Model for UVB-induced Photocarcinogenesis.
Mice were shaved on the back on the first day of the week and were irradiated with the indicated doses thrice a week. The doses increased weekly from week one to six, reaching the maximal dose of 300 mJ/cm^2. Mice were irradiated for 32 weeks in total before the experiment was ended in week 33 and organs were harvested.

3.1.7. Blood serum preparation

Post mortem, blood was immediately collected in an empty tube by puncturing the inferior vena cava or the submandibular vein. The tube was centrifuged twice at 16000 g 15 min 4 °C to separate coagulated blood components from the serum. The serum was transferred to a fresh tube and then stored at -80 °C.

3.2. Histology

To visualize the architecture and the location of cells within the tissue, the back skin and the ear skin was histologically analyzed. Toluidine Blue staining was performed on paraffin embedded sections, while immunofluorescent staining was carried out on frozen sections.

3.2.1. Paraffin sections

To create paraffin sections, first, skin pieces were fixed in 4 % PFA solution and kept at 4 °C. Next, samples were transferred to embedding cassettes and were run in a tissue processor. The tissue processor dehydrated samples by incubation in ethanol and xylol (ethanol: 2x70 %, 2x80 %, 90 %, 96 %, 2x100 %, xylol: 2x, 1 h of incubation for each), as well as paraffinized the skin samples. Then, samples were embedded in paraffin and 7 µm sections were produced with a rotary microtome. The sections were transferred to glass slides and were dried o. N. in a 37 °C oven and afterwards stored at RT until staining.

3.2.2. Toluidine Blue staining

Mast cell granules have metachromatic properties, which means that staining with a dye such as Toluidine Blue will shift the absorption maxima from blue to purple. With this histological method, mast cell granules can easily be identified in tissues. Therefore, paraffin embedded skin sections were heated in a 65 °C oven for 30 min to eliminate paraffin from the sections. Then sections were incubated in xylol 2x for 5 min each, followed by incubation in ethanol (99 %, 95 %, 90 %, 80 %,70 %) for 5 min each to re-hydrate sections. Slides were then hydrated in water for 5 min, followed by staining in 0.01 % Toluidine Blue solution for 10 min. Afterwards, the sections were washed in water 3x for 5 min and were air-dried. Lastly, sections were mounted with coverslips in one drop of Euparal per section and were dried O/N and kept at RT until microscopic analysis.

3.2.3. Frozen sections

For the generation of frozen sections, back skin pieces were fixed in 4 % PFA at 4 °C for 4 h, followed by incubation in 5 % and 10 % sucrose in PBS for 2 h each and in 20 % sucrose solution O/N at 4 °C. These sucrose incubation steps allow de-hydration of the samples, as water crystals might destroy the structural integrity of the samples once frozen. Then, skin pieces were cut in smaller pieces, embedded in plastic molds using Tissue Tek®, directly frozen on dry ice and stored at -80 °C. Sectioning of the skin was performed with a cryostat, the skin was cut in 10 µm sections and transferred to glass slides which were air-dried for at least 30 min. Afterwards, the slides were stored at -80 °C until further processing.

3.2.4. Immunofluorescence staining

For staining of skin tissue with fluorescent antibodies and dyes, frozen sections were thawed. A hydrophobic border around each section was created with the help of the ImmEdge™ pen to prevent mixing of antibody solutions from different sections on the same slide. The sections were then re-hydrated in PBS for 5 min, followed by permeabilization in 0.1 % Triton-x-100 for 10 min (if mast cell granule staining was included). Sections were then washed thrice for 5 min each in PBS before they were blocked in blocking buffer for 1 h at RT. Then, the buffer was tapped off and the primary antibody solution was pipetted to the sections and incubated O/N at 4 °C. The next day, the antibody solution was removed and slides were washed three times for 5 min each in PBS. The secondary antibody solution was applied to the sections and incubated for 2 h at RT, followed by three rounds of washing for 5 min each. If the staining included directly conjugated antibodies, these were co-incubated together with the secondary antibodies, if possible. Afterwards, slides were washed thrice with PBS for 5 min then counterstained with DAPI (1:1000) for 5 min, followed by two times washing in PBS for 5 min and one washing step in water for 5 min. Finally, glass slides were air-dried, mounted with Mowiol containing mounting solution with DABCO (10 % w/v). All incubation and washing steps were carried out at RT in the dark if not mentioned elsewise. The slides were dried O/N at RT, then kept at 4 °C until microscopic analysis.

3.2.5. Whole ear mounts

In addition to back skin sections, mast cell and DC interactions were analyzed in more depth by staining whole ears. Therefore, mice were sacrificed and hair was removed from ears using depilation cream. Ears were then excised and fixed with 2 % PFA O/N on a rocker at 4 °C. The

next day ears were rinsed five times with PBS and the dorsal and ventral halves of the ear were carefully separated. Then, ears were permeabilized and blocked with blocking buffer O/N on a rocker at 4 °C. On the following day, ears were stained with unconjugated primary antibodies in staining buffer on a rocker at 4 °C. After three days of incubation, ears were rinsed with PBS and washed three times for 5 min each, followed by incubation with the secondary antibody solution on a rocker at 4 °C for two days. The ears were again rinsed and washed in PBS three times for 5 min each, followed by a DAPI counterstain for 10 min. Lastly, the ears were rinsed and washed in PBS three times for 5 min each, followed by one washing step in water. The ears were air-dried and finally mounted between two coverslips in Mowiol containing mounting medium with DABCO (10 % w/v).

3.2.6. Mast cell granule staining

Fluorescently-labeled Avidin can be used to visualize mast cell granules in both microscopy and flow cytometry. Avidin is capable of binding to glycosaminoglycans that are present within mast cell granules, such as heparin, heparin sulfate or chondroitin sulfate. For immunofluorescent staining of skin sections, the following procedure was integrated in the protocols of 3.2.4 and 3.2.5. The slides were treated for 10 min with 0.1 % Triton-x-100, before the sections were blocked. The actual staining was performed when antibody staining was completed. Here, FITC-Avidin solution (5 µg/ml) was incubated for 30 min on the sections, followed by three rounds of washing with PBS for 5 min each. The staining then proceeded with DAPI staining and mounting as described in 3.2.4 and 3.2.5.

3.2.7. Microscopy

The microscopic analysis was performed with the Keyence BZ-9000 fluorescence microscope or the Zeiss LSM 780 confocal microscope. Images were further edited and analyzed with the BZ-II Analyzer or Fiji.

3.3. Cell isolation

3.3.1. Isolation of skin cells

For the isolation of immune cells from the skin, ears were harvested and stored in PBS at 4 °C. The dorsal and ventral side of the ear were separated using forceps and cut into small pieces in a 12-well plate. Then, the minced tissue was digested in a shaking incubator (100 rpm) at

37 °C for 90 min in 500 µl of digestion buffer. After incubation, the tissue was further dissociated by pipetting the suspension with a blunted tip and filtering through 100 µm and subsequently through 70 µm cell strainers. Finally, the suspension was centrifuged at 4000 rpm 10 min 4 °C, the cell pellet was resuspended in 1 ml PBS and then stained for flow cytometry analysis.

3.3.2. Isolation of lymph node cells

Surrounding connective and fat tissue was removed from auricular or brachial lymph nodes (aLN, bLN). Then, lymph nodes were mashed through 70 µm cell strainers with the plunger of a syringe, the strainer was washed with 15 ml PBS and the cell suspension was centrifuged at 400 g 5 min 4 °C. The cell pellet was resuspended in PBS and cells were further stained for flow cytometry analysis.

3.4. Flow cytometry

Phenotypes and functional properties of cells can be characterized by flow cytometry. With the help fluorophore-conjugated antibodies and fluorescent dyes cell-specific markers can be stained. The flow cytometer acquires cells in a suspension and uses different lasers, dichroic mirrors and filters to analyze these fluorescent signals, making it possible to measure multiple parameters per cell.

3.4.1. Cell surface staining

For staining of surface antigens, cells were transferred to FACS tubes or V-bottom plates and washed in PBS at 400 g 5 min 4 °C. The antibody mix containing fluorescent labeled antibodies, Trustain FcX™ blocking reagent (5 µg/ml) and Viability dye (1:1000) was mixed, and 50 µl of this mix were added to the cells and incubated for 20 min at 4 °C in the dark. Then, 2 ml PBS were added and cells were washed at 400 g 5 min 4 °C. After washing, cells were either resuspended in 200 µl PBS and stored at 4 °C until measurement or further processed for staining of intracellular markers. Before cell acquisition, 10 µl counting beads were added for calculation of total cell counts.

3.4.2. Intracellular transcription factor staining

After staining of surface antigens, the FoxP3 Fixation/Permeabilization Kit was used according to the manufacturer's instructions. Briefly, cells were fixed and permeabilized for 30 min at

RT, followed by washing twice at 400 g 5 min RT. Antibodies for the intracellular staining against FoxP3 were incubated o. N. at RT on a rocker, the next day cells were washed twice at 400 g 5 min RT, resuspended in 200 µl PBS and stored at 4 °C until the measurement. Before cell acquisition, 10 µl counting beads were added for calculation of total cell counts.

3.5. Cell culture and in vitro assays

3.5.1. Bone marrow cell isolation

The bone marrow harbors many different immune cell types and hematopoietic cell progenitors. Cultivation of bone marrow with cell type-specific growth factors induces the differentiation of hematopoietic progenitor cells, which then can give rise to various immune cell types, such as macrophages, dendritic cells or mast cells.

For the isolation of bone marrow, femur and tibia were removed, cleaned from muscle tissue and opened at the epiphysis. The bone marrow was then flushed out with PBS using a syringe, collected in a falcon tube and pelleted by centrifugation at 300 g 5 min 4 °C.

3.5.2. Generation of bone marrow-derived dendritic cells (BMDC)

For the generation of BMDC, the bone marrow cell pellet was resuspended in complete medium, counted and adjusted to a concentration of 0.5 x 10^6 cells/ml. On d0, 5 x 10^6 cells were seeded in a 10 cm bacteriological dish in 10 ml of complete medium with 2 % GM-CSF containing supernatant (of GM-CSF transfected X63Ag8-653 cells) and incubated at 37 °C and 5 % CO_2. On d3, 10 ml complete medium with 2 % GM-CSF containing supernatant were added to each dish. On d6, non-adherent and loosely adherent BMDC were collected and pelleted at 300 g 5 min RT. BMDC were counted, the concentration was adjusted according to the subsequent assay and BMDC differentiation was confirmed. Therefore, 0.5 x 10^6 cells were stained with antibodies against the surface receptors CD11c and MHCII and measured by flow cytometry.

3.5.3. Generation of bone marrow-derived mast cells (BMMC)

For the generation of BMMC, the bone marrow cell pellet was resuspended in complete medium, counted, and adjusted to a concentration of 2 x 10^6 cells/ml with 20 ng/ml IL-3. Bone marrow cells were then seeded in 6-well plates with 6 x 10^6 cells/well and incubated at 37 °C and 5 % CO_2. On d4, 2 ml of complete medium with 20 ng/ml IL-3 were added per well. On d7,

suspension cells were harvested, centrifuged at 300 g 5 min RT and resuspended in fresh complete medium with 20 ng/ml IL-3 in a concentration of 1-2x10^6 cells/ml. Like for the first week, a complete medium change was performed once a week with addition of fresh medium containing IL-3 in between. The purity of the BMMC cultures was tested regularly by flow cytometry measurement. The cultures usually reached a purity of >90 % after six to eight weeks, which was measured by expression of the markers c-kit and FcεRIα. Pure BMMC cultures were then used for further experiments.

3.5.4. Co-cultivation of BMDC and BMMC

For the BMDC and BMMC co-cultures, the cells were mixed in a ratio of 2:1 and 0.2 x 10^6 cells in 200 µl complete medium were seeded per well of a flat bottom 96-well plate. Cells were then stimulated in triplicates for 24 h with LPS and CCL21 (100 ng/ml + 50 ng/ml), zymosan (1 µg/ml) or were left untreated. The next day, 96-well plates were centrifuged at 400 g 5 min RT and supernatants were stored at -20 °C for cytokine measurements. The pelleted cells were resuspended in PBS and kept at 4 °C for subsequent flow cytometry staining.

3.5.5. Enrichment of peritoneal cell-derived mast cells (PCMC)

A different source of mast cells for *in vitro* cultures is the peritoneum. Here, primary mature mast cells can be obtained by peritoneal lavage, the proliferative capacity of these cells however is rather limited compared with BMMC. For isolation, mice were sacrificed and the abdominal skin was removed, exposing the intact peritoneum. Mice were i.p. injected with 6 ml PBS and 2 ml air and the peritoneal cavity was gently washed several times, before the peritoneal cell suspension was collected with a syringe. Cells were then centrifuged at 300 g 5 min RT and resuspended in complete medium with IL-3 (10 ng/ml) and SCF (30 ng/ml) and incubated at 37 °C and 5 % CO_2 in 3 ml in a well of a 6-well plate. On d2, suspension and loosely adherent cells were removed, washed at 300 g 5 min RT and resuspended in fresh medium with SCF (30 ng/ml) and IL-3 (10 ng/ml). On d5, the whole medium was changed by centrifugation of the cells at 300 g 5 min RT and replaced with fresh medium containing SCF (30 ng/ml) and IL-3 (10 ng/ml) and seeded in a concentration of 1-2x10^6 cells/ml in 3 ml in 6-well plates. This procedure was continued with a medium change every 5-6 days and addition of fresh medium in between. After three weeks of cultivation, the purity of the cultures was tested via c-Kit and FcεRIα staining and cells were used for degranulation experiments.

3.5.6. Apoptosis assay

To examine the role of MyD88 in BMMC survival, cells were seeded on d0 in a concentration of $1x10^6$ cells/ml with 200 µl/well in 96-well plates and were treated with IL-33 (100 ng/ml), SCF (100 ng/ml) or left untreated. Apoptosis was monitored daily from d1 to d4 using AnnexinV and Propidium Iodide (PI) staining. With the help of these two markers, cell populations can be analyzed for early apoptosis ($AnnexinV^+ PI^-$), late apoptosis ($AnnexinV^+ PI^+$), necrosis ($AnnexinV^- PI^+$) and living cells ($AnnexinV^- PI^-$). For that, cells of every condition were harvested, centrifuged at 400 g 5 min 4 °C and subjected to surface staining against c-Kit and FcεRIα. Following the surface staining, cells were resuspended in 50 µl AnnexinV binding buffer and 2.5 µl AnnexinV APC was added. Cells were incubated for 15 min at RT in the dark, followed by addition of another 150 µl AnnexinV binding buffer and of 2.5 µl PI (of a 50 µg/ml stock) immediately before cells were measured by flow cytometry.

3.5.7. Transwell migration assay

To test mast cell migration towards a certain stimulus, transwell migration assays, also known as the Boyden Chamber assay, were performed. This assay system consists of a bottom well and a smaller insert with a porous membrane that is installed on top of the well. The lower compartment is filled with chemoattractant containing medium, while cells are resuspended in the upper insert in chemoattractant-free medium. Cells then migrate towards the lower compartment and the proportion of migrated cells can then be determined. In detail, BMMC were first incubated for 2 h in starving media at 37 °C, 5 % CO_2. In the meantime, stimuli were prepared and 600 µl of medium with SCF, CCL17, CCL5 (all 100 ng/ml) or without stimulus were pipetted to the wells of a 24-well plate. Each chemoattractant was tested in duplicate. After 2 h, BMMC were centrifuged at 300 g 5 min RT, resuspended and were counted. Then, 100 µl of the BMMC cell suspension (1 x 10^6 cells/ml) were introduced to the inserts with a pore size of 8 µm. The plate was incubated at 37 °C and 5 % CO_2 and cells migrated for 5 h. Afterwards, the insert was carefully removed from the well and the whole medium from the lower compartment together with the trans-migrated cells was transferred to FACS tubes and centrifuged at 500 g for 5 min. Finally, cells were resuspended in 500 µl PBS and were measured by flow cytometry to determine cell counts.

3.5.8. Ca^{2+} mobilization assay

Upon IgE-receptor crosslinking a downstream signaling cascade resulting in the degranulation of mast cells is induced. During this process, intracellular Ca^{2+} liberation from the endoplasmic reticulum and Ca^{2+} influx from the extracellular environment are key events. Therefore, Ca^{2+} mobilization within mast cells can be used to gain knowledge about mast cell degranulation. For this, $1x10^6$ cells/ml PCMC were treated O/N with anti DNP-IgE (1 µg/ml) at 37 °C 5 % CO_2. The next day, cells were washed twice with HBSS (w/o Ca^{2+} and Mg^{2+}) at 300 g 5 min and resuspended in HBSS (w/o Ca^{2+} and Mg^{2+}) at a concentration of 5 x 10^6 cells/ml and stained with indo-1 (4 µM) for 30 min at 37 °C. Indo-1 is a fluorescent dye that binds to Ca^{2+} ions, thereby shifting its emission spectrum and allows to differentiate between the presence and absence of Ca^{2+} within a cell. After incubation, cells were washed twice with HBSS (w/o Ca^{2+} and Mg^{2+}) at 300 g 5 min, resuspended in HBSS (w/o Ca^{2+} and Mg^{2+}) and incubated for further 20 min at RT. Thereafter, cells were washed another time at 300 g 5 min, resuspended in HBSS (with Ca^{2+} and Mg^{2+}) at a concentration of $1x10^6$ cells/ml, distributed to tubes with $0.5x10^6$ cells/tube and incubated in a heating block at 37 °C just until flow cytometry measurement. For this, the cell suspension was transferred to FACS tubes and the baseline indo-1 signal intensity was acquired, followed by addition of DNP-HSA (1 µg/ml) and immediate continuation of measurement for further 3 min.

3.5.9. Degranulation assay

A different assay to monitor mast cell degranulation is by FITC-labeled Avidin staining of mast cell granules (3.2.6 for comparison). In this assay, PCMC were counted and 0.2x 10^6 cells/ml were stimulated per well of a 96-well plate with anti-FcεRIα (2.5 µg/ml) antibodies, IL-33 (100 ng/ml), ionomycin (1 µg/ml) or left untreated for 1 h at 37 °C with 5 % CO_2. After incubation, the mast cell surface markers c-Kit and FcεRIα were stained as described in chapter 3.4.1. Then, cells were fixed for 15 min with 100 µl 2 % PFA, followed by centrifugation at 300 g 5 min. Cells were then permeabilized using 100 µl of 1 % Triton-x-100 for 15 min. Subsequently, cells were washed with PBS at 300 g 5 min and stained with FITC-Avidin (5 µg/ml) in 2 % Triton-x-100 with milk powder (50 mg/ml) for 1 h, followed by washing of the cells at 300 g 5 min. All incubation and centrifugation steps were carried out at RT in the dark if not mentioned elsewise. Stained PCMC were then measured via flow cytometry and the decrease of FITC-Avidin signal intensity, indicating degranulation, was examined.

3.6. Protein quantification

3.6.1. Protein isolation from back skin

Back skin was snap frozen in liquid nitrogen after organ harvest and stored in cryotubes at -80 °C until protein isolation. For isolation, the skin was thawed on ice and the subcutaneous fat was removed using forceps. Then, the skin was cut into small pieces and transferred to a screw cap tube filled with glass pearls and 500 µl of 1x RIPA buffer with 1x protease inhibitor. Next, the skin tissue was disrupted at 6500 rpm 3 x 30 s using the Percellys®24 tissue homogenizer and lysates were transferred to a fresh tube. The screw cap tube was washed with another 500 µl of 1x RIPA buffer with protease inhibitor and lysates were centrifuged at 16000 g 15 min 4 °C to clear proteins from residual tissue. Finally, the protein concentration was determined using the NanoDrop™ spectrophotometer.

3.6.2. Enzyme-linked immunosorbent assay (ELISA)

The ELISA measurement is a method to determine the concentration proteins or other molecules in liquid samples. Here, cytokines and chemokines from cell culture supernatants and back skin lysates were quantified. The here utilized ELISA method is an indirect sandwich ELISA. The measurements were performed according to the manufacturer's instructions with the exception of using only half the amounts indicated in the instructions using half-area 96-well plates. In brief, capture antibodies were incubated O/N at RT, followed by three rounds of washing with ELISA washing buffer the next day. Afterwards, free binding spots on the plate were blocked with 1 % BSA in PBS for 1 h at RT. Then, the blocking buffer was removed and the samples were pipetted to the wells. In order to calculate protein concentrations, a serial dilution of a protein standard was included, which was incubated together with the samples for 2 h at RT, followed by three rounds of washing. Thereafter, biotinylated detection antibodies were pipetted to the wells and incubation took place for 2 h at RT, followed by three rounds of washing. Then, horse radish peroxidase (HRP) -coupled streptavidin solution was added to the wells for 20 min RT that leads to binding of streptavidin to the biotinylated detection antibody, followed by three rounds of washing. Lastly, TMB Plus2 solution was added to the wells which serves as a substrate for HRP and is converted to a blue colored product. The conversion is terminated by addition of 2 N sulfuric acid, leading to color change from blue to yellow. Measurement of the optical density at 450 nm/630 nm then enables calculation of the protein concentration with the help of a standard curve. For protein lysates

from the skin, the cytokine concentration was further normalized to the whole protein concentration.

3.7. Statistical analysis

The statistical analysis was performed using GraphPad Prism. For the comparison of three or more independent groups within one experiment, the one-way ANOVA was used. The two-way ANOVA was used to test mean differences in experiments where groups were split by two independent variables. For some experiments, only significant differences within one experimental group are depicted in the graphs for better clarity, this is however mentioned in the figure legends. All data are represented as mean +Standard Error of the Mean (SEM) if not mentioned elsewise. Significant differences are indicated as the following: * $p < 0.05$, ** $p < 0.01$, *** $p < 0.001$, **** $p < 0.0001$.

4. Results

Mast cells are granulated tissue-resident innate immune cells that fulfil different functions in both, health and disease. Previous findings of our group could show that dermal mast cells are affected MyD88-dependently in the context of chronic UVB irradiation (Opitz, 2016). More precisely, UVB-induced mast cell accumulation was not observed in the absence of MyD88, as well as the epidermal thickening and the amount of damaged DNA that were altered. Mast cell specific re-induction of MyD88 was able to restore these observed effects, which reveals a special importance of MyD88 signaling in mast cells.

Many TLRs and IL-1 receptors utilize the adaptor protein MyD88 for signal transduction, mediating the induction of inflammatory genes. In mast cells, TLR and IL-1 receptor signaling was shown to influence different mast cell functions such as activation and degranulation. To investigate, whether MyD88 signaling specifically has an effect on other mast cell functions, BMMC and PCMC of MyD88 proficient and MyD88 KO mice were generated and tested to explore different functional capacities upon stimulation.

4.1. The role of MyD88 in *in vitro* generated mast cells

4.1.1. MyD88 deficiency does not majorly affect BMMC differentiation from bone marrow cells

For *in vitro* testing of mast cell functions, BMMC were generated from bone marrow cells. To exclude effects of MyD88 deficiency on mast cell progenitors (MCp) within the bone marrow compartment prior to BMMC differentiation, MCp frequencies were quantified based on a flow cytometry gating strategy described by Chen and colleagues (Chen et al., 2005). In this sense, bone marrow cells form WT, MyD88 KO and MyD88^{Mcpt5IND} mice was isolated, stained and analyzed by flow cytometry (Figure 10).

First, living, Lin$^-$ single cells were selected and further subdivided in Ly6C$^-$, Sca1$^-$, FcεRIα$^-$, c-Kit$^+$, CD27$^-$, β7 integrin$^+$ and ST2$^+$ cells, which are MCps (Figure 10 A). In general, around 1 % of all viable Lin$^-$ bone marrow cells were identified as MCps (Figure 10 B). MyD88 proficient mice showed slightly higher MCp frequencies of 1.2 %, while the lack of MyD88 in MyD88 KO and MyD88^{Mcpt5IND} mice led to slightly decreased numbers of 1 % MCps in the bone marrow. This

observation did not reach significance, but however clearly shows a minor MyD88-dependent difference in precursor frequencies.

Similar results in full MyD88 KO mice and MyD88^{Mcpt5IND} mice might be explained by the fact that both strains are deficient for MyD88 (except for mast cells in MyD88^{Mcpt5IND} mice) and that MCp numbers and their development might be regulated by MCp extrinsic effects by other cells. Moreover, Mcpt5 expression was described to be present in MCps, mature mast cells however express higher levels of Mcpt5 (Dahlin et al., 2015). Therefore, Mcpt5-driven recombination in MCps of MyD88^{Mcpt5IND} mice might occur in a much lower degree than in mature mast cells, possibly explaining similar results to cells from MyD88 KO mice.

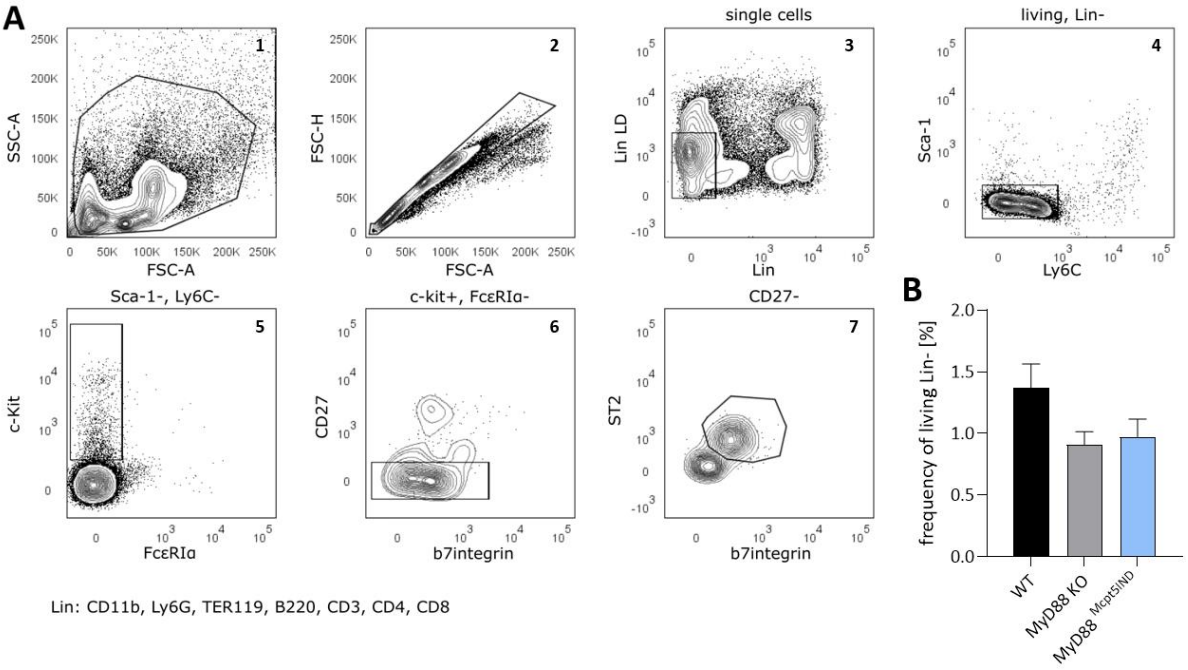

Figure 10 MCps in the bone marrow are slightly reduced in the absence of MyD88.
Bone marrow was isolated from femur and tibia of MyD88 proficient, MyD88 KO and MyD88^{Mcpt5IND} mice. **A** The gating strategy of stained bone marrow cells is shown. Mast cell precursors were identified as a living, single cell, Lin$^-$, Ly6C$^-$, Sca1$^-$, FcεRIα$^-$, c-Kit$^+$, CD27$^-$, β7 integrin$^+$ and ST2$^+$ cell population. **B** The percentage of mast cell precursors from all living, Lin$^-$ cells is depicted for all genotypes (mean ± SEM, n=5-7).

Since MCps were present in bone marrow, the bone marrow cells of MyD88 proficient (see 3.1.1 for comparison) and MyD88 KO mice were cultured in the presence of IL-3 to induce mast cell differentiation. Over the course of differentiation, the BMMC cultures were tested regularly for purity of the cultures and cell proliferation (Figure 11). A representative plot of >90 % pure BMMC cultures of MyD88 proficient and MyD88 KO cultures is shown in Figure 11 A, BMMC were gated as single, c-Kit$^+$ and FcεRIα$^+$ cells. No remarkable difference in mast cell differentiation was observed between MyD88 proficient and MyD88 deficient cultures. In

addition, BMMC proliferation was measured by cell counting (Figure 11 B). The total cell counts decreased rapidly within 2 weeks of culture and remained stable until week 5. After that, BMMC proliferated massively, which also correlates to the time when cultures became pure. Also, the absence of MyD88 did not affect cell proliferation.

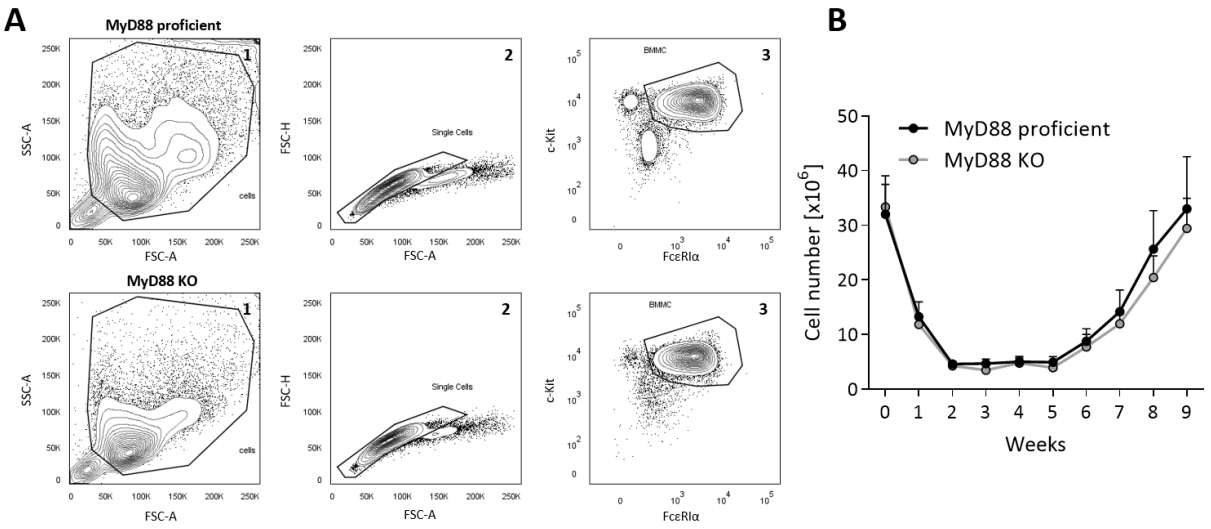

Figure 11 Differentiation of BMMC is not altered in the absence of MyD88.
Bone marrow was isolated from femur and tibia of MyD88 proficient and MyD88 KO mice and cultured for up to 10 weeks in the presence of IL-3. **A** BMMC Differentiation was monitored regularly via flow cytometry, mast cells were gated as single, c-Kit$^+$ and FcεRIα$^+$ double positive cells. **B** The total cell number was determined weekly over the course of differentiation to assess differences in cell proliferation (mean +SEM, n=6).

In summary, slightly less MCps among bone marrow cells were detected in the complete absence of MyD88 and in cells from MyD88^{Mcpt5IND} mice. But this did not affect the differentiation or proliferation to BMMC, indicating that the BMMC generation between MyD88 proficient and MyD88 KO cells was very comparable, which was important for the further analysis of the role of MyD88 for mast cell functionality.

4.1.2. BMMC migration is unaltered in the absence of MyD88

Following chronic UVB irradiation, mast cells accumulated MyD88-dependently in the dermis. This effect could likely be attributed to increased migration of MCps to the dermis caused by inflammatory cues, or by increased emigration from the dermis to lymph nodes. In inflammation, cell migration of several immune cell types, such as neutrophils or Langerhans cells, has been shown to depend on MyD88 signaling (Castoldi et al., 2012; Didovic et al.,

2016). For these reasons, we tested if MyD88 might facilitate the migration of mast cells as well.

Therefore, BMMC were tested in a transwell migration assay. FCS starved cells were seeded to a semi-permeable insert with 8 µm pores on a cell culture plate and were let migrate for 5 h towards chemoattractant containing medium, in these experiments SCF, CCL5 and CCL17, or medium only. Subsequently, transmigrated cells were counted by flow cytometry and the fold increase in migration for each condition over the respective medium control was calculated. BMMC showed the highest migratory capacities towards SCF, which was around 6-fold higher than the medium control while migration towards CCL5 containing medium was around 3-fold increased (Figure 12). Interestingly, for both chemoattractants no difference between MyD88 proficient and MyD88 KO cells could be detected. For CCL17, MyD88 proficient BMMC showed a very minor increase in migration.

Taken together, only SCF and CCL5 were able to induce migration in MyD88 proficient and MyD88 KO BMMC, indicating that BMMC are migratory. In vitro, MyD88 does not appear to play a role in migration towards SCF and CCL5, but it might still have an effect in vivo or if an additional MyD88 dependent stimulus is introduced together with SCF or CCL5.

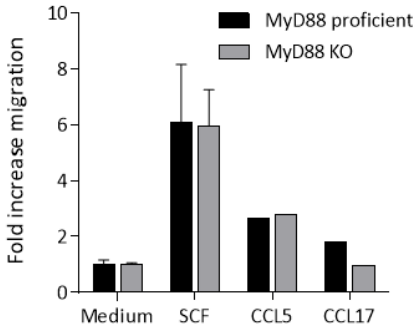

Figure 12 BMMC transmigration does not depend on MyD88.
BMMC were generated and tested in a transwell setup for migration towards SCF, CCL5, CCL17 or medium without chemokines as control. The number of transmigrated cells was determined by flow cytometry in the forward and sideward scatter and depicted as fold change over the respective medium control (mean +SEM, n=3 medium and SCF, n=1 CCL5 and CCL17).

4.1.3. BMMC release great amounts of IL-6 and IL-13 upon IL-33 treatment

BMMC were stimulated for 24 h with the TLR ligands LPS or Pam3Cys, SCF, IL-33 or mast cell degranulation-inducing FcεRIα antibodies to discover the role of MyD88 in cytokine secretion by mast cells. After the incubation period, cells were sedimented, the supernatant was

collected and IL-6 and IL-13 levels were measured by ELISA (Figure 13). LPS and Pam3Cys stimulation both induced IL-6 release in MyD88 proficient BMMC only, while SCF did not lead to remarkable cytokine secretion (Figure 13 A). Stimulation with antibodies directed against the high affinity IgE receptor FcεRIα has been shown to activate mast cells, for this reason we tested whether this activation happens MyD88-dependently (Hübner et al., 2011). Here, FcεRIα stimulation led to IL-6 secretion independent of MyD88. Stimulation with IL-33 however, significantly increased IL-6 secretion in a MyD88-dependent manner. Similar trends could be seen for IL-13 release. While Pam3Cys and IL-33 affected the IL-13 release MyD88-dependently, FcεRIα stimulation induced IL-13 secretion independent of MyD88 (Figure 13 B).

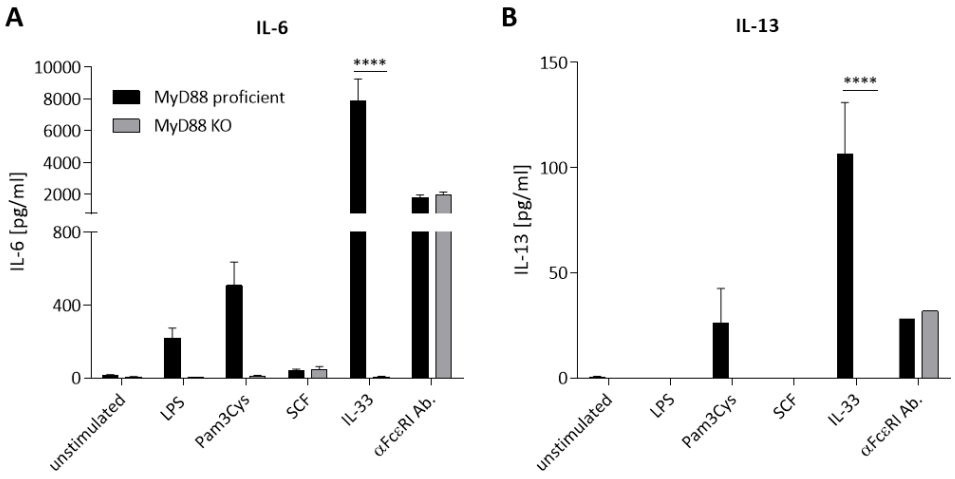

Figure 13 BMMC secrete considerable amounts of IL-6 and IL-13 upon IL-33 stimulation.
BMMC were generated and stimulated for 24 h with LPS, Pam3Cys, SCF, IL-33, αFcεRI antibodies (Ab.) or left unstimulated. After 24 h of treatment, supernatants were collected and **A** IL-6 and **B** IL-13 cytokine levels were determined by ELISA (mean +SEM, n=2-5 for IL-6, n=1-4 for IL-13, **** p<0.0001).

4.1.4. IL-33 ameliorates mast cell survival MyD88-dependently

Another hypothesis how MyD88-dependent accumulation of dermal mast cells in the model of chronic UVB irradiation might have occurred is that MyD88 deficient mast cells might have lower survival rates. To study mast cell apoptosis, BMMC were cultured in medium containing IL-33, SCF or medium only for 4 days and tested daily for apoptosis rates by AnnexinV/PI staining (Figure 14 A). Leaving BMMC unstimulated mainly led to an increase in early apoptosis (AnnexinV$^+$, PI$^-$), while late apoptosis (AnnexinV$^+$, PI$^+$) was minorly affected. Therefore, the whole fraction of all AnnexinV$^+$ BMMCs was utilized for quantification. Without any stimulation, a daily increase in all AnnexinV$^+$ cells could be measured which was MyD88-independent (Figure 14 B). After 4 days of cultivation, the cultures constituted of around 60 %

apoptotic cells. Strikingly, cultivation in IL-33 containing-medium was able to significantly reduce apoptosis in MyD88 proficient cells; after 4 days of treatment only 10 % of the cells were apoptotic (Figure 14 C). MyD88 KO cells on the other hand were unable to respond to IL-33 within the cultures and showed apoptosis rates comparable to the unstimulated condition. Interestingly, SCF treatment decreased apoptosis compared to the unstimulated condition in both BMMC cultures independent of the genotype (Figure 14 D). Still, SCF was not as potent as IL-33 in the induction of survival, after 4 days of culture SCF treated cells constituted of around 30 % apoptotic cells. In summary, only IL-33 could efficiently induce survival in MyD88 proficient BMMC, while SCF acted MyD88-independently.

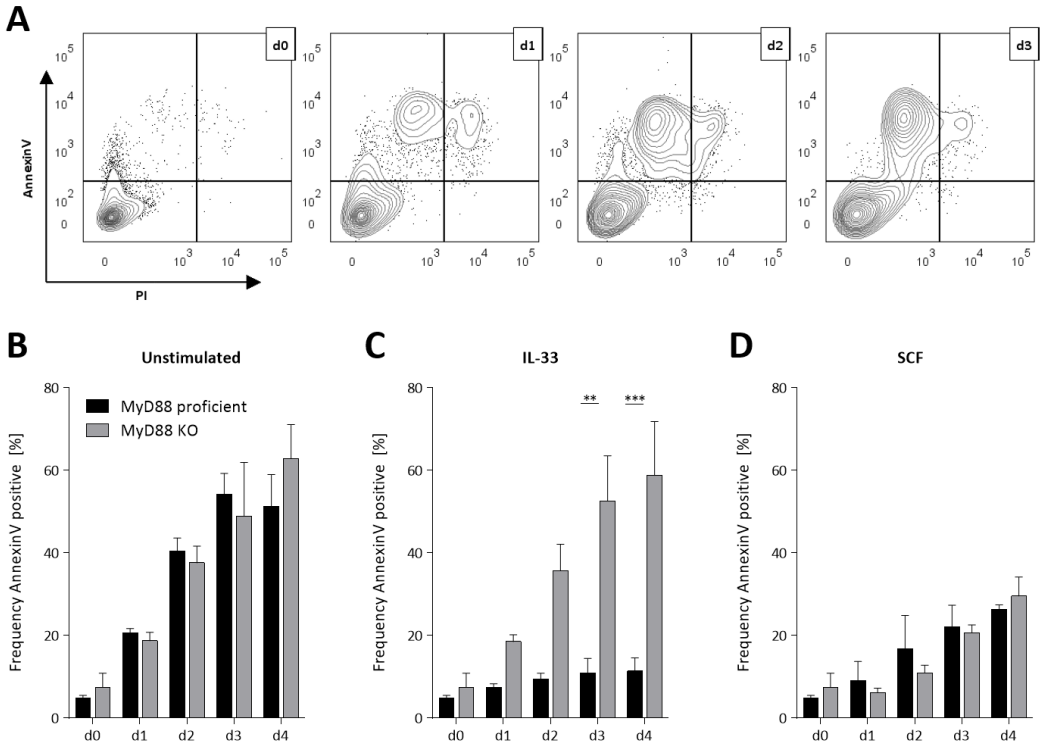

Figure 14 BMMC survival takes place MyD88-dependently in IL-33 treated mast cell cultures.
BMMC were differentiated by cultivation of bone marrow cells in the presence of IL-3. When cultures consisted of > 90 % BMMC, $0.2x10^6$ cells were seeded per well in 96-well plates and stimulated with 100 ng/ml IL-33, 100 ng/ml SCF or left unstimulated. **A** Over the time of 5 days, cells were analyzed daily and therefore stained with AnnexinV and PI to monitor apoptosis by flow cytometry. The frequency of $AnnexinV^+$ cells of the BMMC population was quantified for **B** unstimulated cells, **C** IL-33 stimulated cells and **D** SCF stimulated cells (mean +SEM, n=3, **p<0.01, ***p<0.001).

4.1.5. Mast cell degranulation

A hallmark of mast cells is their ability to degranulate upon stimulation. In this process, pre-formed granules containing cell-mediators are rapidly exocytosed and released into the cellular environment. Here, we studied the degranulation capacity of PCMC with two different

approaches and analyzed whether MyD88 signaling interferes in this process. In contrast to the other assays, PCMC were used instead of BMMC, since BMMC failed to degranulate although containing granules (data not shown). PCMC were isolated from the peritoneal cavity by lavage with PBS and further expanded by cultivation with IL-3 and SCF (see 3.5.5 for comparison). After 3 weeks of cultivation, PCMC were utilized for experiments.

In the first approach, PCMC were treated with degranulation inducing stimulant FcεRIα or ionomycin as a positive control for 1 h. Mast cells were then stained with FITC-Avidin and analyzed by flow cytometry. FITC conjugated Avidin specifically stains negatively charged glycosaminoglycans of mast cell granules such as heparin, thereby enabling to study mast cell granule content (Kett et al., 2003; Tharp et al., 1985). The decrease of the FITC-Avidin signal intensity within the mast cell population was an indicator for granule release (Figure 15 A). The gMFI values were determined, normalized to the respective unstimulated control and depicted as the decrease in FITC-Avidin signal intensity (Figure 15 B). FcεRIα engagement alone led to a signal reduction in MyD88 proficient and MyD88 KO cells, but was more prominent in the presence of MyD88. Co-treatment with IL-33 did not affect FcεRIα-mediated degranulation. Ionomycin stimulation was used as a positive control and induced a much stronger decrease in signal intensity, which seemed to be MyD88-dependent as well. A general reduction of granule content in MyD88 KO mast cells compared to MyD88 proficient cells however might explain this observation.

In a second approach to study degranulation, PCMC were pre-incubated with anti-DNP IgE antibodies and were stained with the Ca^{2+} indicator dye indo-1 and subjected to Ca^{2+} flux measurements by flow cytometry (Figure 15 C). Indo-1 is a ratiometric dye that shifts its emission maximum when bound to Ca^{2+} ions. The Ca^{2+} unbound form emits fluorescence at 475 nm, while Ca^{2+} bound indo-1 shifts emission to 400 nm. The 400/475 ratio of the indo-1 median fluorescence intensity is presented here. After 1 min of baseline measurement, DNP-HSA was added to the cells and the acquisition was continued for further 3 min. Immediately after the addition, the indo-1 signal peaked, but then declined within the following 20 s and formed a stable signal intensity. Interestingly, during the peak WT PCMC showed a slightly higher signal than MyD88 KO cells, indicating that there might be slightly more Ca^{2+} release and degranulation, supporting the finding of the other degranulation assay in Figure 15 A and

B. However, this Ca^{2+} measurement approach in PCMC was rather unstable and was only observed in few experiments.

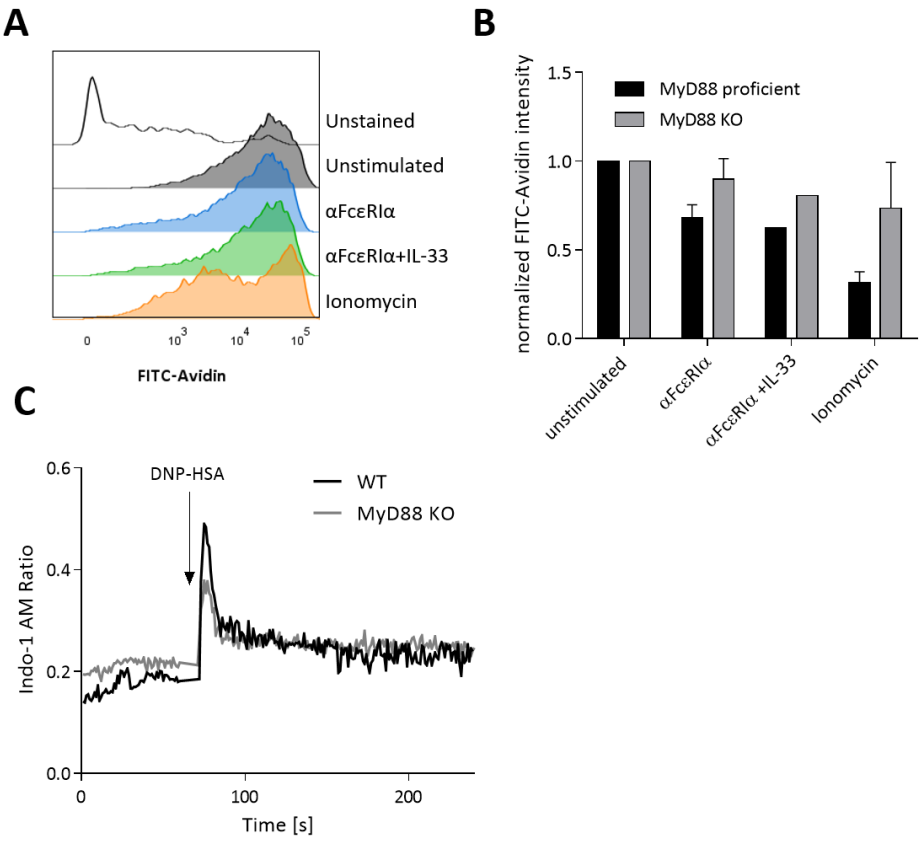

Figure 15 MyD88 contributes to PCMC degranulation.
PCMC were differentiated by cultivation in the presence of IL-3 and SCF. Cells were seeded in 96-well plates with $0.2x10^6$ cells/well and were left unstimulated or were treated with anti-FcεRIα alone or with anti-FcεRIα together with IL-33, or with ionomycin for 1 h. Then, cells were harvested and mast cell granules were stained with FITC-Avidin. **A** Representative histograms of the FITC-Avidin signal in PCMC throughout the different conditions are depicted. **B** The FITC-Avidin gMFI values for the different conditions were normalized to the unstimulated control to show the relative decrease of the FITC-Avidin signal (mean +SEM, n=3, αFcεRIα+IL-33 n=1). **C** Ca^{2+} flux measurements were performed using PCMC and the Ca^{2+} indicator indo-1 (n=1).

4.2. MyD88 contributes to cutaneous anaphylactic reactions

Mast cells are key effector cells in allergic reactions. Especially in type I hypersensitivity reactions, mast cell degranulation upon IgE receptor crosslinking is one of the hallmark events, leading to the release of mast cell granules. Since MyD88 was involved in survival and cytokine secretion of BMMC (Figure 13, Figure 14), as well as in degranulation of PCMC *in vitro* (Figure 15) it was tested whether MyD88 might as well be engaged in the process of degranulation *in vivo*. To examine whether MyD88 signaling influences mast cell degranulation, MyD88 proficient, MyD88 KO and MyD88^{Mcpt5IND} mice were analyzed in the model of passive cutaneous anaphylaxis, which is a mouse model of a type I hypersensitivity reaction. Therefore, PBS or anti-DNP IgE antibodies were i.d. injected into the ear skin, followed by i.v injection of DNP-HSA with Evans Blue 24 h afterwards. Subsequently, ears were excised to measure the Evans Blue leakage into the ear tissue. PBS injected ears did not appear blue, while anti-DNP IgE treated ears exhibited blue spots indicative of vascular leakage (Figure 16 A, B). As a second control, a group of MyD88 proficient mice did not receive any i.d injection and showed similar results as PBS injected mice, revealing that the injection per se did not lead to major trauma. Intriguingly, anti-DNP IgE injected MyD88 proficient mice showed a greater Evans Blue signal than MyD88 KO mice. Mice expressing MyD88 in mast cells specifically however had again a higher Evans Blue leakage than MyD88 deficient animals. This suggests that MyD88 signaling in mast cells is involved in mast cell degranulation.

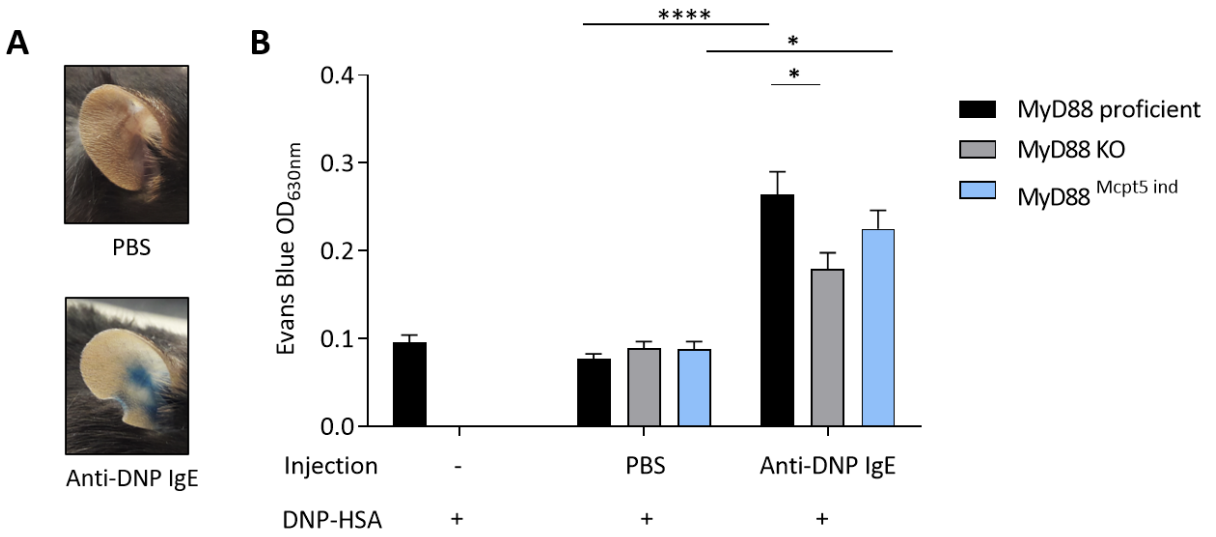

Figure 16 MyD88-signaling contributes to the anaphylactic reaction.
Mice were i.d. treated with anti-DNP IgE antibodies (20ng) or PBS and 24 h later i.v. injected with DNP-HSA (1 µg/ml) and 1 % Evans Blue in PBS. 1 h after the injection, mice were sacrificed and leakage of the blue dye into the ear tissue was determined. **A** Exemplary photos of a control PBS injected ear and an anti-DNP-IgE injected ear. **B** The leaked dye was extracted from ear tissue and measured in a spectrophotometer in duplicates at 630 nm (mean +SEM, each dot represents one ear, *p<0.05, ****p<0.0001).

These results highlight that mast cell-specific MyD88 signaling affects mast cell functionality *in vivo*. *In vitro* however, MyD88 only slightly affected PCMC degranulation. Strikingly, mast cell activation and survival were massively regulated by IL-33, which is known to act MyD88-dependently. Therefore IL-33 is an interesting candidate to study, if it is able to modify mast cell functions *in vivo*.

4.3. Impacts of IL-33 signaling in chronic UVB irradiation

IL-33 has been shown to be expressed after UVB irradiation by a human keratinocyte cell line, as well as in murine skin, where IL-33 secreting cells are closely associated with skin neutrophils and mast cells (Byrne et al., 2011; Suhng et al., 2018).

In vitro data revealed that BMMC are strongly affected by IL-33 in a MyD88-dependent manner (Figure 13, Figure 14). To explore if the UVB-induced mast cell accumulation occurs due to IL-33 release, to which MyD88 KO mice cannot respond, WT mice were irradiated using a chronic UVB irradiation protocol and IL-33 signaling was blocked for the last three weeks of irradiation by i.p. injection of anti-ST2 antibodies (100 µg, Chen et al., 2018), that are directed against the IL-33 receptor ST2, twice a week. As a control, UVB irradiated WT mice were i.p. injected with the same amount of IgG1 antibodies. By the end of the experiment, the back skin was histologically examined and immune cell populations in the ear skin were analyzed. Furthermore, protein lysates of skin specimens were prepared for IL-33 measurements by ELISA (Figure 17). In line with the literature, enhanced IL-33 levels were detected in mice that were exposed to UVB irradiation. Blocking of IL-33 signaling could further increase IL-33 levels.

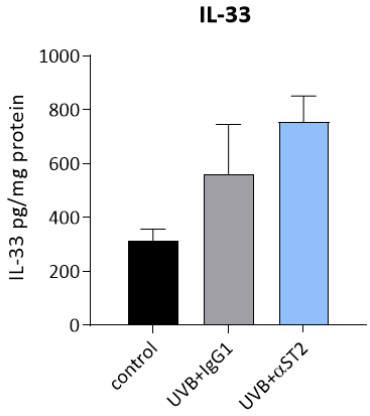

Figure 17 IL-33 expression in the skin rises after chronic UVB irradiation.
WT mice were irradiated with UVB for six weeks, during the last three weeks of irradiation IL-33 signaling was blocked by i.p. injection of anti-ST2 or IgG1 antibodies as a control. Protein lysates from the back skin were prepared and tested by ELISA for IL-33 expression. The detected protein concentration was normalized to the total amount of proteins per sample (mean +SEM, n=4).

The back skin tissue was fixed, embedded in paraffin, sectioned and subjected to Toluidine Blue staining. Toluidine Blue stains metachromatic mast cell granules in a violet color while the background is stained in lighter violet/blue (Figure 18 A). Mast cell numbers in the dermis were counted and the number of mast cells in a certain dermal area was calculated (Figure 18

B). Unirradiated control mice had the lowest number of mast cells per mm^2, both irradiated groups showed significantly increased mast cell counts in the dermis which were not altered by blocking of IL-33 signaling. UVB exposure is known to induce keratinocyte proliferation, which leads to epidermal thickening (acanthosis). To discover if IL-33 signaling influences the UVB-induced acanthosis, the epidermal thickness was measured using Fiji (Figure 18 C). Similar to the mast cell counts, UVB irradiation led to an increase in thickness of the epidermal skin layer.

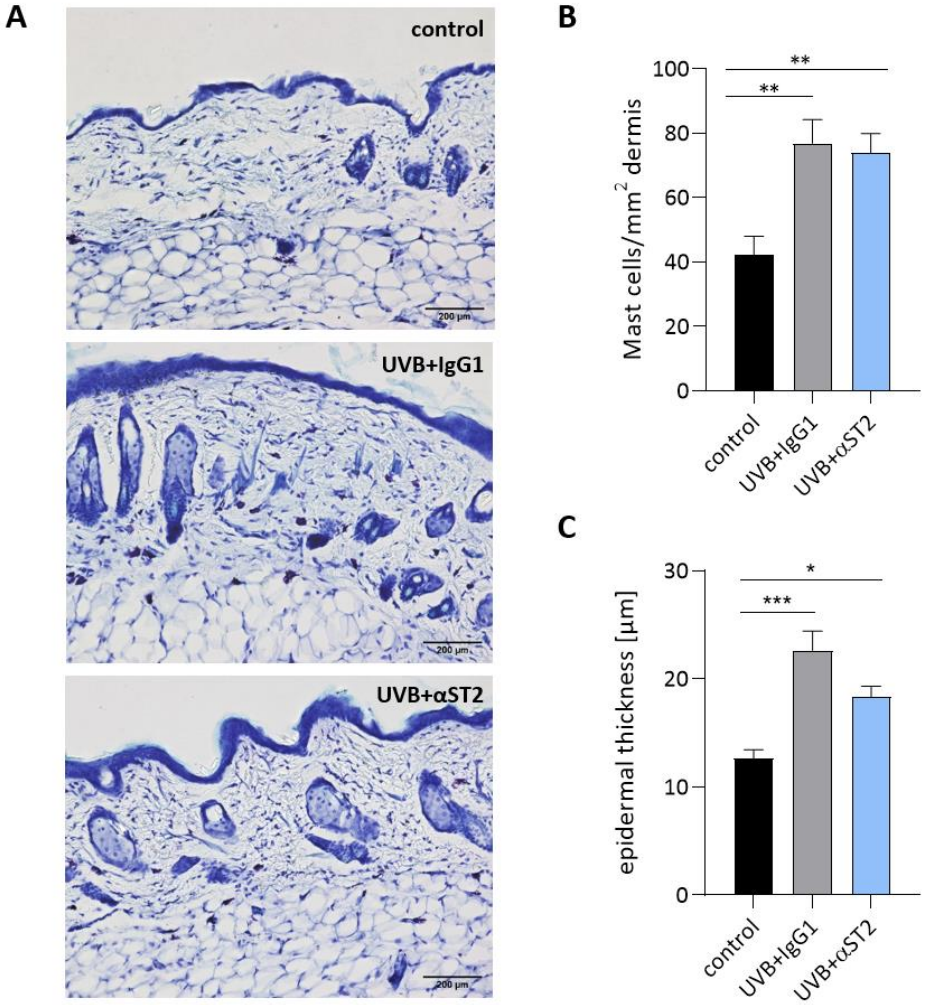

Figure 18 IL-33 signaling is involved in the formation of UVB-induced acanthosis of the epidermis, but not in accumulation of dermal mast cells.
WT mice were irradiated with UVB for six weeks, during the last three weeks of irradiation IL-33 signaling was blocked by i.p. injection of αST2 or IgG1 antibodies as a control. **A** The back skin was sectioned and stained with toluidine blue to visualize mast cells. **B** Mast cells were counted and numbers were normalized to the dermal area. **C** The epidermal thickness was measured (mean +SEM, n=7, *p<0.05, **p<0.01, ***p<0.001).

Interestingly, in contrast to the mast cell numbers ST2 blocking attenuated acanthosis (Figure 18 C). IL-33 is described to be released by keratinocytes, but also influences keratinocyte

function in an autocrine manner and thereby contributes to keratinocyte function in skin inflammation (Byrne et al., 2011; Zeng et al., 2021). For this reason, it was further tested if ST2 blocking in the context of UVB exposition directly affects keratinocyte proliferation in order to prove that absent IL-33 signaling reduces proliferation and therefore causes attenuated epidermal thickening (Figure 18 C). This was performed by staining of the nuclear marker Ki-67, which is only detectable during interphase in cell division and is therefore used as an indicator of cell proliferation. Frozen sections of back skin samples were stained for Ki-67 expression and cell nuclei were counterstained with DAPI (Figure 19 A). The number of Ki-67 expressing cells in the epidermis was determined and is presented as the number per epidermal length (mm, Figure 19 B). Keratinocytes of both UVB irradiated conditions showed more cells expressing Ki-67 than unirradiated controls. Blocking of IL-33 signaling diminished Ki-67 expressing keratinocyte numbers in comparison to IgG1 injected controls, demonstrating that IL-33 signaling partially contributes to keratinocyte proliferation after UVB exposure and is the cause for reduced epidermal thickening (Figure 18 C).

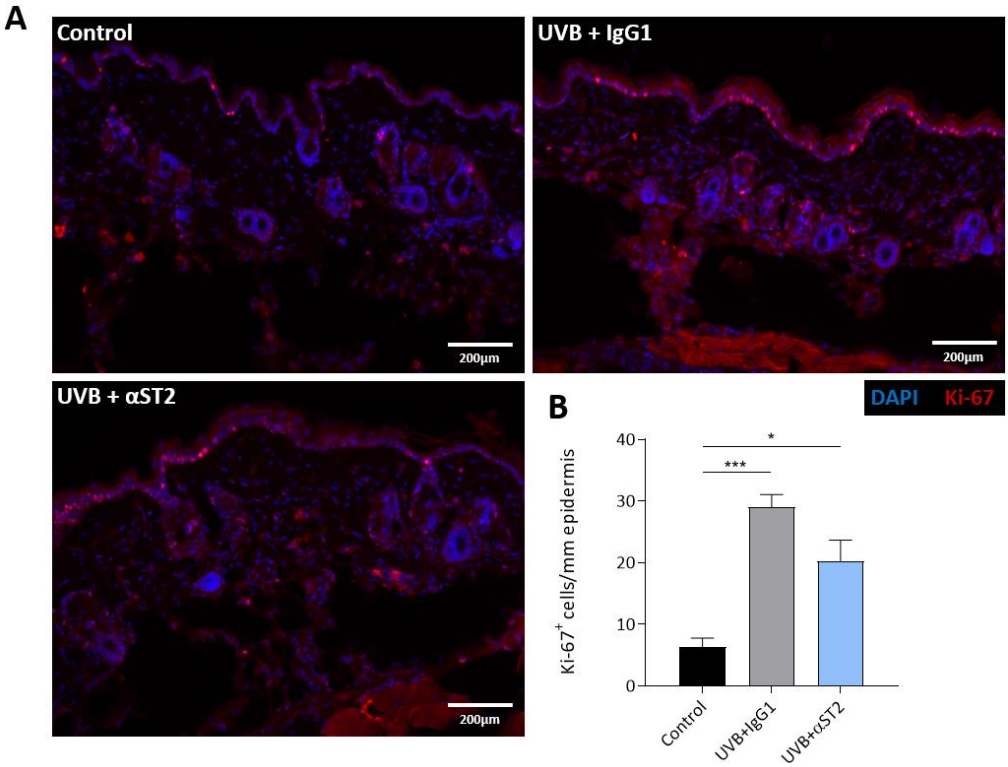

Figure 19 IL-33 receptor blocking suppresses UVB-induced proliferation of epidermal cells.
WT mice were irradiated with UVB for six weeks, during the last three weeks of irradiation IL-33 signaling was blocked by i.p. injection of αST2 or IgG1 antibodies as a control. **A** The back skin was sectioned and stained against Ki-67 (red) to visualize proliferating cells and with DAPI to label cell nuclei. **B** Ki-67$^+$ cells in the epidermis were quantified and presented as the cell number per mm epidermis (mean +SEM, n=4, *p<0.05, ***p<0.001).

To find out how IL-33 signaling influences immune cells in UVB irradiated skin, immune cell populations in the ear skin were isolated and stained for flow cytometry (Figure 20 A). The gating strategy applied is based on a strategy presented by Bouladoux and colleagues (Bouladoux et al., 2017). For this, first three single cell gatings (FSC-W vs- FSC-A, FSC-A vs. FSC-H, SSC-A vs. SSC-H) were performed to remove all doublets and undesired cell aggregates from analysis. Single cells were then further gated on $CD45^+$ and viable cells. Then, TCRγδ expressing cells were identified and assigned to the DETC gate (TCRγδ high) and the dermal γδ T-cell gate (TCRγδ intermediate). All residual $TCR\gamma\delta^-$ cells were plotted against CD11b and Ly6G to identify neutrophils, all non-neutrophil cells were next separated in $CD11b^+$ and $CD11b^-$ populations. From the $CD11b^-$ population, mast cells were identified as c-Kit^+ and $Fc\varepsilon RI\alpha^+$ cells, while $CD11b^+$ cells were further selected by Ly6C and CD64 expression. From there, macrophages were gated as F4/80 and CD64 expressing cells, the residual cells were gated based on Ly6C and MHCII expression as $Ly6C^+$ $MHCII^-$ monocytes, $Ly6C^+$ $MHCII^+$ moDCs and $Ly6C^-$ $MHCII^+$ moDCs. The total amount of $CD45^+$ immune cells in the skin remained unaltered throughout the different experimental groups (data not shown), which is why population frequencies are depicted here (Figure 20 B-I). The proportion of DETC and dermal γδ T-cell in the skin significantly decreased after UVB irradiation, likewise ST2 blocking further lowered the percentage of DETC while having no effect on dermal γδ T-cells (Figure 20 B, C). Mast cell frequencies remained largely unaltered in all experimental groups (Figure 20 D). Neutrophils however accumulated in UVB irradiated skin in an IL-33-mediated manner, since the accumulation was almost absent when ST2 was blocked (Figure 20 E). A similar trend as for the neutrophils was also observed for macrophages and $Ly6C^+$ $MHCII^-$ monocytes (Figure 20 F, G). UVB irradiation induced the expansion of these populations, while additional ST2 blocking decreased their abundance. The $Ly6C^+$ $MHCII^+$ moDC population was significantly enlarged upon UVB irradiation independent of ST2 blocking, in contrast, the $Ly6C^-$ $MHCII^+$ population remained unchanged (Figure 20 H, I).

In summary, γδ T-cell populations, neutrophils, macrophages, monocytes and $Ly6C^+$ $MHCII^+$ moDCs experienced altered frequencies in the ear skin, while mast cells and $Ly6C^-$ $MHCII^+$ remained stable. UVB exposure led to a decrease of γδ T-cell populations, whereas neutrophils, macrophages, monocytes and $Ly6C^+$ $MHCII^+$ moDC mainly expanded. Additional blocking of IL-33 signaling did not affect γδ T-cell populations after UVB exposure, but innate cells like neutrophils, macrophages and monocytes were reduced. In contrast to the *in vitro*

BMMC results, which showed great impact of IL-33 on mast cell activation and survival, here IL-33 blocking did not affect mast cell numbers in the back skin and ear skin as detected by histology and flow cytometry.

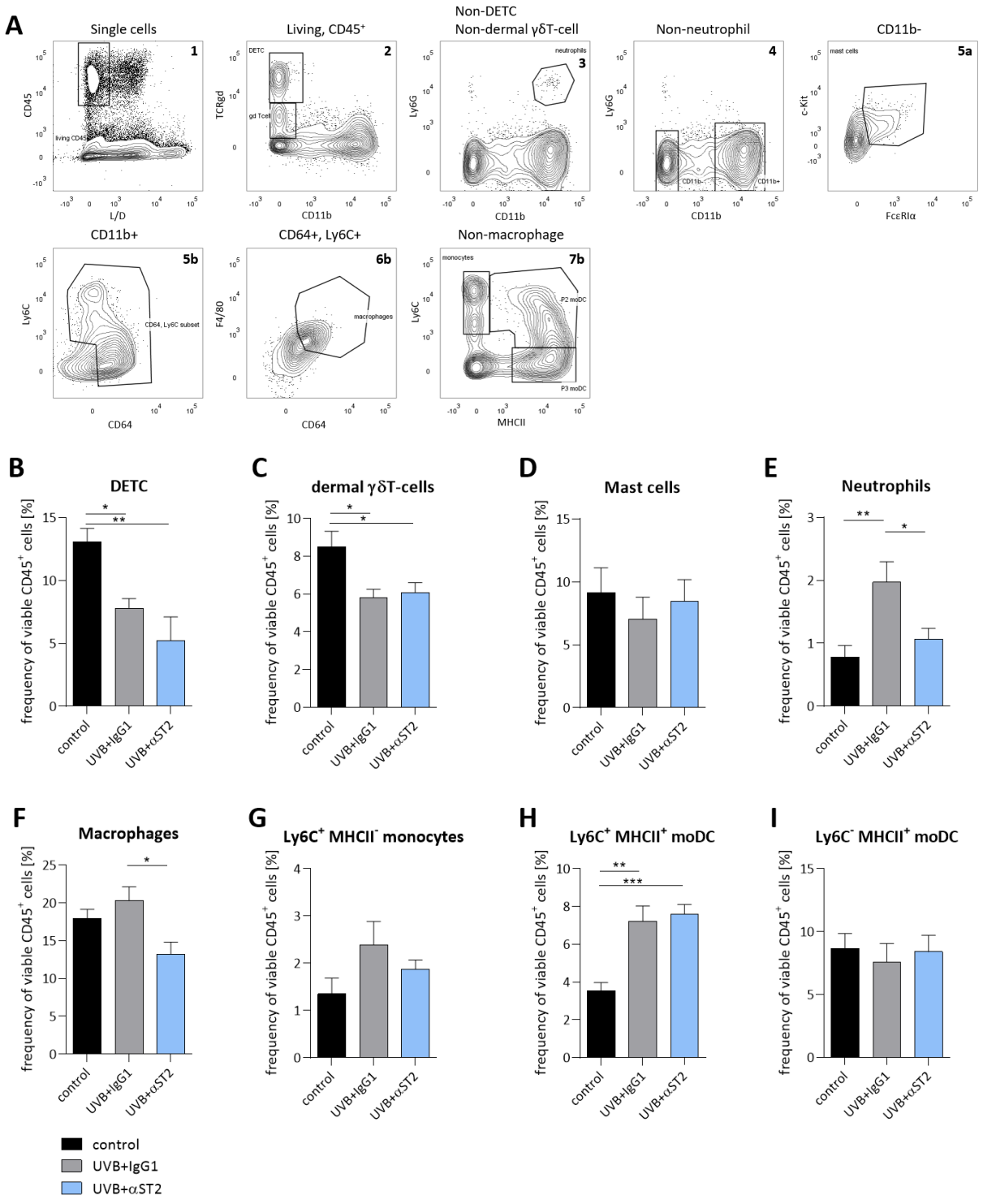

Figure 20 IL-33 signaling mainly influences DETC, neutrophils and macrophages in the skin.
WT mice were irradiated with UVB for six weeks, during the last three weeks of irradiation IL-33 signaling was blocked by i.p. injection of αST2 or IgG1 antibodies as a control. **A** Gating strategy of immune cells in the skin and **B-I** their quantification is presented. Single cells were gated for viable, CD45$^+$ immune cells. Among these, **B** DETC and **C** dermal T-cells were selected. Further on, among the residual cells **E** neutrophils were identified and **D** mast cells within the CD11b$^-$ portion of the non-neutrophil cells. CD11b$^+$ cells were further selected for **F** macrophages, **G** monocytes, **H** Ly6C$^+$ MHCII$^+$ moDC and **I** Ly6C$^-$ MHCII$^+$ moDC (mean +SEM, n=7, *p<0.05, **p<0.01, ***p<0.001).

In addition to the analysis of immune cells in the skin, Tregs in secondary lymphoid organs were studied. It is well known that UVB irradiation mediates immunosuppression by the expansion of Tregs. To study, whether IL-33 signaling supports UV-induced Treg generation, immune cells from the spleen and bLN were isolated, stained an analyzed by flow cytometry (Figure 21 A). First, single cells were gated and selected further for viable, CD45 expressing immune cells. Then, TCRβ$^+$ conventional T-cells were identified and further gated for CD4$^+$ and CD8$^+$ T-cells. Within the CD4$^+$ population, FoxP3$^+$ Tregs were gated. The quantification showed, that around 12-13 % of all CD4$^+$ T-cells were Tregs in both, the bLN and the spleen (Figure 21 B, C). UVB irradiation led to a significant expansion of Tregs independent of ST2 blocking. This observation was more prominent in the bLN, but could also be observed in the spleen.

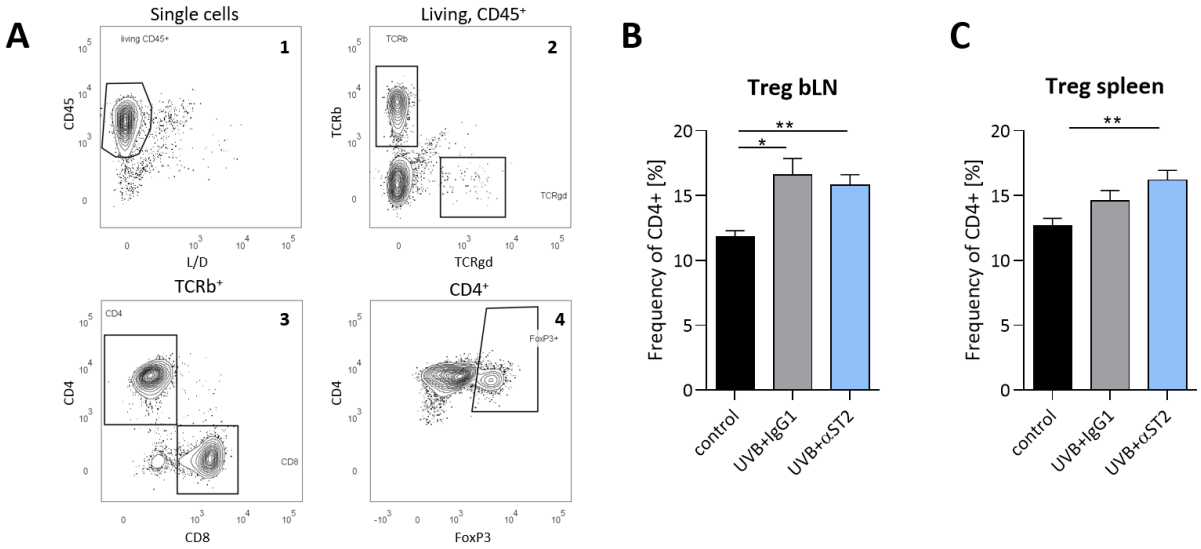

Figure 21 UVB irradiation leads to an increase of Treg in secondary lymphoid organs independent of IL-33 signaling.
WT mice were irradiated with UVB for six weeks, during the last three weeks of irradiation IL-33 signaling was blocked by i.p. injection of αST2 or IgG1 antibodies as a control. **A** Gating strategy of T-cells in the bLN, after filtering single cells, viable CD45$^+$ immune cells were gated. TCRβ$^+$ were selected and further gated for CD4$^+$ and CD8$^+$ cells. Among the CD4$^+$ cells, FoxP3 expressing Tregs were identified. Quantification for Tregs is shown in **B** for the bLN and in **C** for the spleen (mean +SEM, n=7, *p<0.05, **p<0.01).

Taken together, IL-33 blockade in WT mice exposed to chronic UVB doses affected keratinocyte proliferation and thus epidermal thickening. Moreover, it dampened the recruitment of inflammatory cells, therefore IL-33 signaling in UVB exposed skin contributes to skin inflammation. Mast cell accumulation in the back skin appeared to happen IL-33-independently, in the ear skin however no mast cell expansion was detectable. In contrast to

the effect on mast cell survival and activation in the *in vitro* experiments, IL-33 does not play a role in mast cell accumulation *in vivo*. Surprisingly, through chronic UVB exposition Treg differentiation was induced in secondary lymphoid organs which confirms that our model of chronic UVB irradiation might create an immunosuppressive environment.

4.4. DC-mast cell crosstalk in the skin

4.4.1. DCs and mast cells are located close together in the skin

Although mast cell-specific MyD88 signaling was able to induce mast cell accumulation in chronic UVB irradiation, it cannot be excluded that also another cell type might be involved in this process. Indeed. previous findings from our group showed that not only mast cell intrinsic MyD88 signaling but also DC specific MyD88 signaling contributes to dermal mast cell accumulation upon chronic UVB irradiation (Opitz, 2016). This suggests, that both, mast cell intrinsic and extrinsic MyD88 signaling from DCs, can influence mast cell numbers in the skin. It is described that mast cells and DCs closely interact and can shape each other's functions (Sumpter et al., 2019). To visualize these mast cell-DC niches, back skin and ear skin samples of naïve R26eYFP^{Mcpt5IND} mast cell reporter mice were studied (Figure 22 A, B). Skin sections (for back skin) and whole mount samples (ear skin) were stained with anti-GFP antibodies to enhance the endogenous reporter signal and MHCII expressing cells were stained to label DCs. Furthermore, nuclei were marked with DAPI and blood vessels in the ear were labeled by staining of CD31 expressing endothelial cells. In back skin, eYFP expressing mast cells and DCs were found within the dermis, some of the DCs appeared to be in close proximity and to be interacting with to mast cells. In ear skin, mast cells were located in perivascular dermal regions and similar to the back skin, DCs were located near mast cells. This confirms that mast cell-DC niches are present in the murine skin and that their crosstalk might regulate each other's functions.

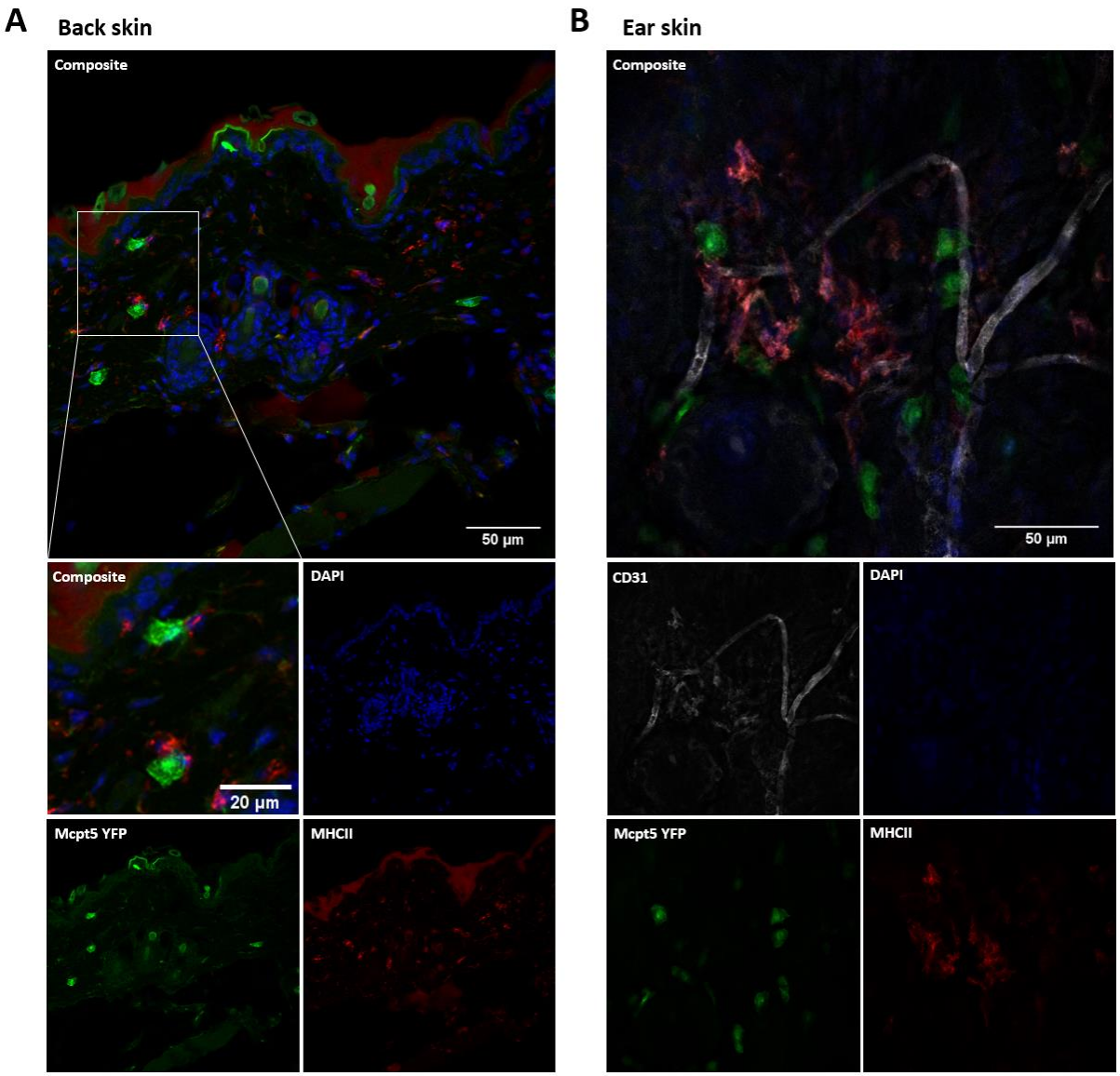

Figure 22 DCs and mast cells communicate in back and ear skin.
A Back skin and **B** ear skin specimens of R26eYFP^{Mcpt5IND} mice were withdrawn, fixed, sectioned and stained with fluorescently labeled antibodies and dyes. The endogenous eYFP signal in Mcpt5 expressing cells is depicted in green while MHCII positive cells are displayed in red. Cell nuclei were counterstained and are represented in blue, CD31^{+} endothelial cells are presented in grey (representative images are presented, n=2).

Since mast cells and DCs could be found in close contact to each other, I wondered whether the absence of MyD88 might affect the mast cell-DC interaction. For this, whole mount samples of ears were prepared and stained like the samples shown in Figure 22, except that mast cells did not contain the endogenous fluorescent reporter, instead they were stained using FITC-Avidin. Z-stacks of the tissue were acquired and depicted as maximal Z-projections with orthogonal views in x- and y-direction (Figure 23 A-C). In all samples, mast cells can mainly be found in perivascular regions of the dermis. Some direct interactions between mast cells and DCs could be observed (marked with yellow arrows) in all genotypes, implying that the

absence of MyD88 did not influence the ability of DCs and mast cells to co-localize under homeostatic conditions.

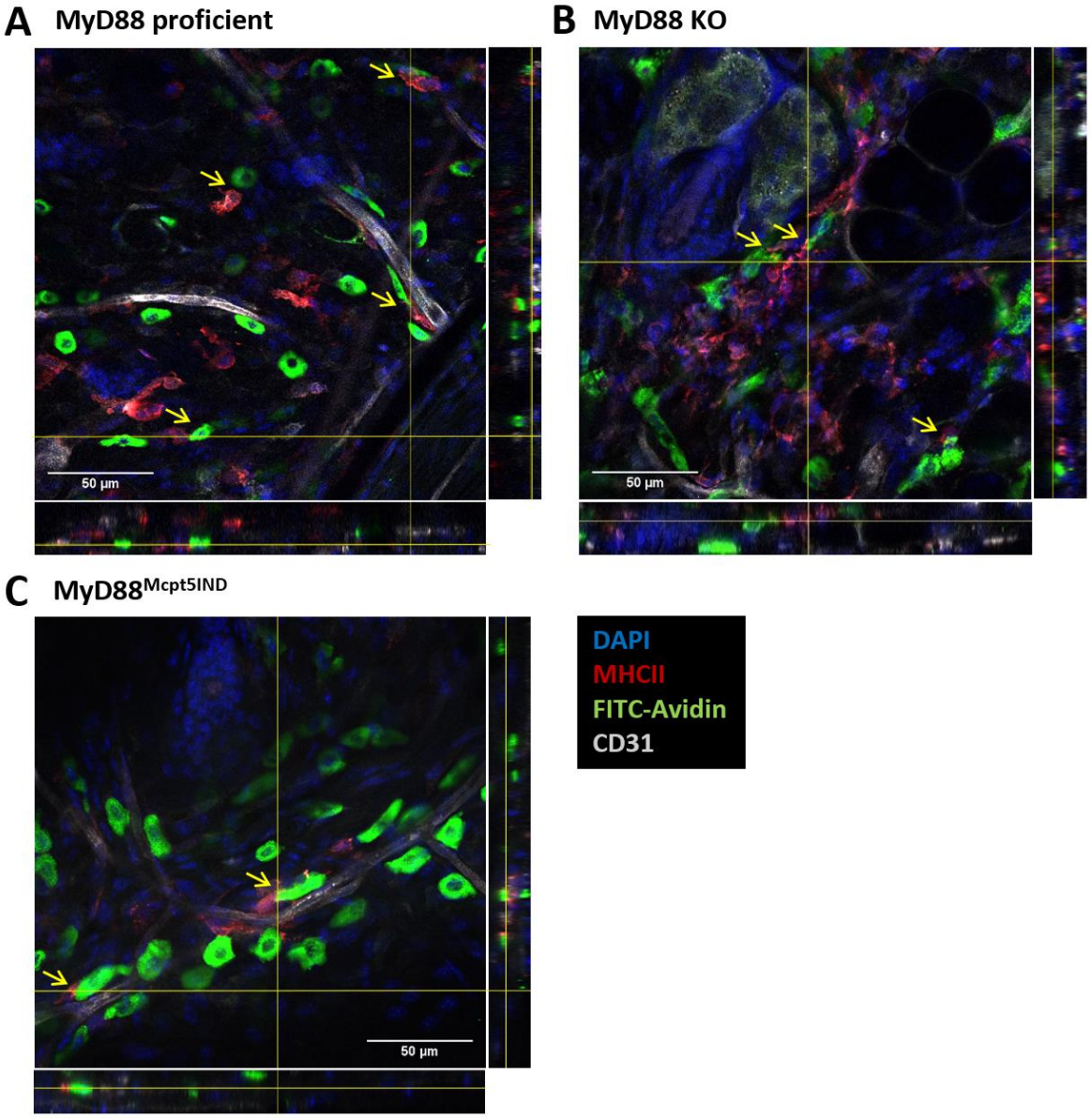

Figure 23 DCs and mast cells in the ear skin interact MyD88-independently.
Ear skin of **A** MyD88 proficient, **B** MyD88 KO and **C** MyD88^{Mcpt5IND} mice was fixed and stained as a whole ear with fluorescently labeled antibodies and dyes. Mast cells are depicted in green (FITC-Avidin), while MHCII expressing cells are represented in red. Grey signals indicate the presence of endothelial cells (CD31), cell nuclei can be detected in blue (DAPI). Z-projections were recorded with the LSM 780, with the yellow lines indicating the x- and y-position of the orthogonal views. The yellow arrows highlight the contact between FITC-Avidin and MHCII-positive cells (representative images are presented, n=2).

4.4.2. DC activation is mildly affected by mast cell internal MyD88 signaling

Next, we studied the DC and mast cell interaction in more depth and tried to elucidate whether MyD88 signaling in one cell type might affect activation of the other cell type. To test

this, BMDC and BMMC were generated and co-cultured for 24 h with LPS + CCL21, zymosan or left untreated. The stimuli LPS + CCL21 were chosen based on a protocol presented in by Otsuka and colleagues to achieve a robust BMDC activation (Otsuka et al., 2011). Zymosan was included as a second stimulus since it acts only partially via TLR2/6 and can also signal via Dectin-1, which signals independent of MyD88. Then, the cells were subjected to antibody staining and measured by flow cytometry.

For the detection of activation markers, viable singlets were gated and mast cells were selected based on c-Kit and FcεRIα expression (Figure 24 A). Within the mast cell population, the expression level of FcεRIα did not alter after stimulation and co-culturing, but a small proportion of BMMCs carrying MHCII molecules was detected. Similar to Dudeck and colleagues, mast cells were described to build immune synapses with DCs where molecules, such as MHCII, can be exchanged (Dudeck et al., 2017). Quantification of these MHCII expressing BMMC showed that MHCII was present on about 0.5-1 % of all BMMC whenever these were cultured in the presence of BMDC, this was however independent of the stimulation presence of MyD88-dependent signaling (Figure 24 B).

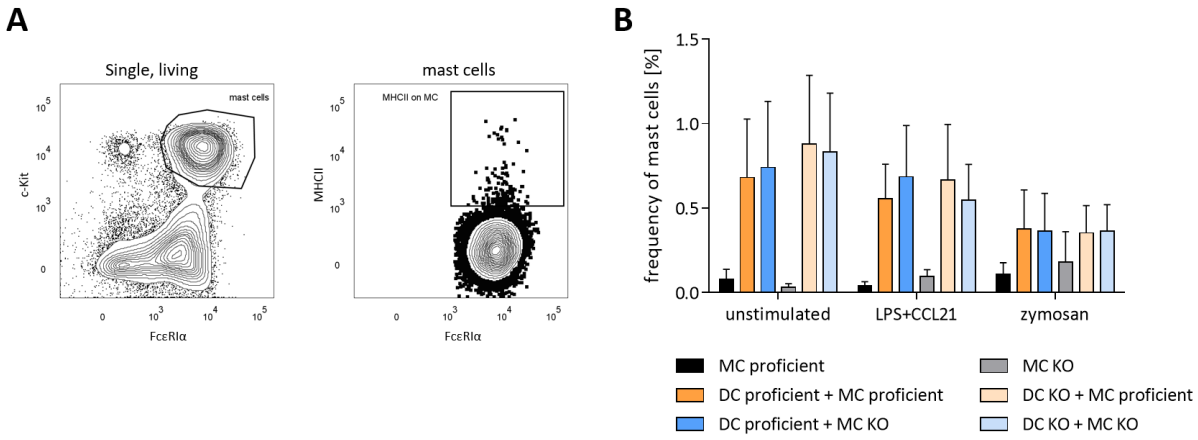

Figure 24 Co-cultivation of BMDC with BMMC leads to the exchange of MHCII to the BMMC surface.
BMDC and BMMC were co-cultured with LPS+CCL21, zymosan or left untreated for 24 h. Then, cells were subjected to antibody staining and analyzed by flow cytometry. **A** Within the mast cell population (viable, single cell, c-Kit$^+$, FcεRIα$^+$ cells) MHCII expression was analyzed. **B** The quantification of MHCII$^+$ cells in the mast cell population is presented (mean +SEM, n=3-4).

Next, BMDC activation markers were characterized. Therefore, again based on viable single cells, all non-mast cells were selected and further gated on CD11c and MHCII intermediate to high expression to identify BMDCs (Figure 25 A). Within this population, the activation markers CD86 and CD40 were analyzed, as well as MHCII and MAR-1$^+$ cells (Figure 25 B). Increased expression of CD86, MHCII and CD40 are typical for activated DCs. It is proposed that FcεRIα

antibodies (clone MAR-1) cross-react with Fcγ receptors on inflammatory cDC2, therefore we evaluated whether activated BMDCs might as well be MAR-1$^+$ upon activation (Bosteels et al., 2020; Tang et al., 2019). Expectedly, both LPS+CCL21 and zymosan, led to an increase of CD86, MHCII, CD40 and even MAR-1 expression on BMDCs, rather independent of the presence of mast cells within the cultures compared to unstimulated cultures (Figure 25 C-F). While MyD88 KO BMDC exhibited decreased surface expression of CD40 and MAR-1 upon LPS+CCL21 stimulation (Figure 25 E, F), they interestingly showed elevated CD86 and MHCII expression upon zymosan treatment (Figure 25 C, D). MAR-1$^+$ cells were strongly elevated upon both types of stimulation in MyD88 proficient BMDCs, but not in MyD88 KO cells (Figure 25 F). The requirement of MyD88 signaling in BMDCs for activation was also observed for CD40 expression, but only after LPS+CCL21 stimulation. CD86 and MHCII expression however were comparable between MyD88 proficient and MyD88 KO cells, or were even further enhanced in MyD88 KO cells upon zymosan stimulation. For all these activation markers, the presence of mast cells within the stimulated cultures did not induce any differences in BMDCs upon stimulation. Intriguingly, in the unstimulated conditions the addition of mast cells to BMDC cultures could slightly elevate the expression of the activation markers, especially in cultures with MyD88 proficient mast cells, which was discovered for CD86 and CD40 expression quite clearly. This suggests that MyD88 signaling in mast cells clearly augmented BMDC activation in unstimulated cultures, while the more robust effects of LPS+CCL21 and zymosan stimulation on BMDCs might conceal the small mast cell induced differences from the unstimulated conditions.

In summary, these experiments show that mast cells and DCs are able to interact, thus influencing each other's function. The presence MyD88 proficient mast cells enhanced DC activation in unstimulated cultures, while MyD88 deficient mast cells were less potent in inducing DC activation. These findings furthermore strengthen the hypothesis that the absence of MyD88 signaling in the mast cell-DC crosstalk shows effects on skin immunity *in vivo,* such as in UV irradiation where both, DC and mast cell specific MyD88 signaling affected mast cell accumulation.

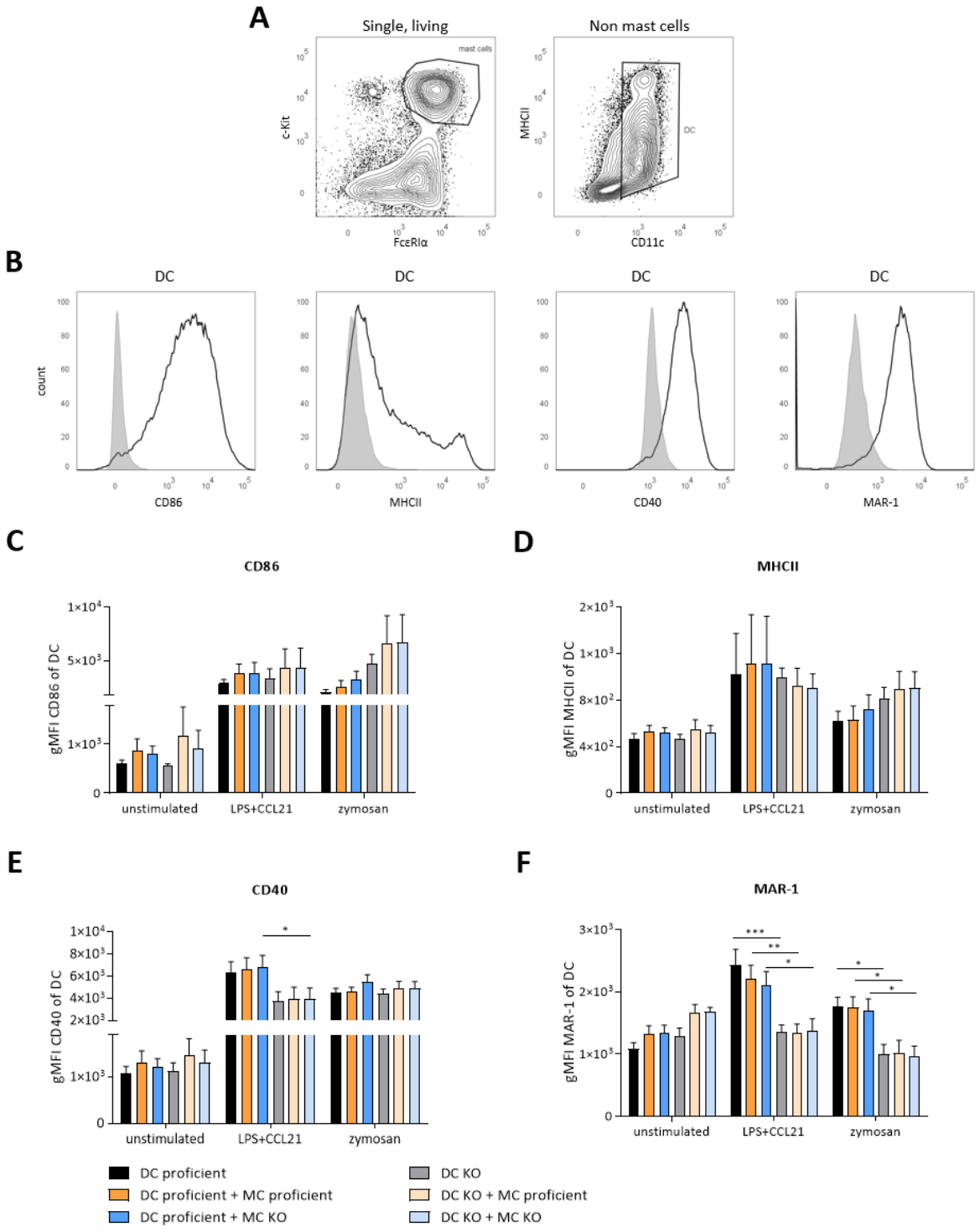

Figure 25 Co-culturing of BMDC and BMMC slightly increases activation marker expression on BMDC in unstimulated cultures.

BMDC and BMMC were co-cultured and stimulated with LPS+CCL21, zymosan or left untreated for 24 h. Then, cells were subjected to antibody staining and analyzed by flow cytometry. **A** DCs were identified (viable, single, CD11c$^+$ MHCII int-high cells) and **B** activation marker expression within the DC population was studied. **C** The expression of the co-stimulatory receptor CD86 was assessed, **D** as well as MHCII. **E** Moreover, CD40 expression was studied and **F** the presence of MAR-1$^+$ cells were examined (mean +SEM, n=3-4, *p<0.05, **p<0.01, ***p<0.001, other significant differences between the different treatment conditions of the same groups are not depicted here for better clarity of the graphs).

4.5. Role of MyD88 in UVB-induced immunosuppression

UVB-irradiation has been known for many years to induce immune suppression through different mechanisms (chapter 1.4.2). Especially, mast cells have been described to participate in these processes by the release of suppressive mast cell-derived factors, the cross-talk to DCs and by initiating adaptive responses in lymph nodes. We could observe that Treg frequencies rose in bLN and the spleen of chronic UVB irradiated mice, independent of IL-33 signaling (Figure 21). Therefore, we wanted to gain deeper knowledge about whether MyD88 signaling could contribute to immunosuppressive effects of UVB and if so, whether mast cell specific MyD88 signaling would be sufficient.

4.5.1. UVB-induced immune suppression is established independent of MyD88

To examine the role of MyD88 signaling pathways in dermal mast cells for the generation of UVB-induced immune suppression, MyD88 proficient, MyD88 KO and MyD88^{Mcpt5IND} mice were shaved on the back and subjected to UVB irradiation on 4 consecutive days, controls were left unirradiated. Following irradiation, mice were sensitized with the hapten DNFB on the back skin and challenged with the same hapten on the ear skin 5 days after sensitization. As a readout of the immune response in the ear skin, the ear swelling was measured over the course of 3 days after the challenge. The experiment was terminated 3 days after challenge and the immune cell populations in the ear skin and the ear draining auricular lymph nodes (aLN) were analyzed.

To measure the ear thickness, mice were anesthetized daily after the challenge and the ear swelling was determined as the percentage increase in swelling over the ear thickness prior challenge (Figure 26). While one ear was treated with DNFB, the other ear was treated with vehicle only, which served as an internal control. For all genotypes, the vehicle treated ears did not show any ear swelling, while DNFB treated ears exhibited a significant increase in ear swelling (Figure 26 A-C). The response was the highest on d1 and gradually decreased until d3 in all genotypes. In mice, which were exposed to UVB irradiation prior to sensitization the ear thickness was 10-20 % lower than that of control mice, which was largely independent of MyD88. Of note, the ear swelling curve of MyD88 KO mice was clearly higher than that of MyD88 proficient and MyD88^{Mcpt5IND} mice, but did not reach statistical significance. In previous experiments from our group, MyD88 proficient and MyD88 KO mice were characterized in a regular CHS reaction without prior UVB irradiation (Thomanek, 2020,

unpublished data). There, MyD88 KO mice displayed an increased ear thickening compared to MyD88 proficient mice, similarly to the findings here. In summary, MyD88 KO mice showed increased ear swelling after DNFB compared to the other genotypes, but all mice were able to achieve immune suppression since UVB irradiation was able to reduce the ear swelling response in the presence and in the absence of MyD88.

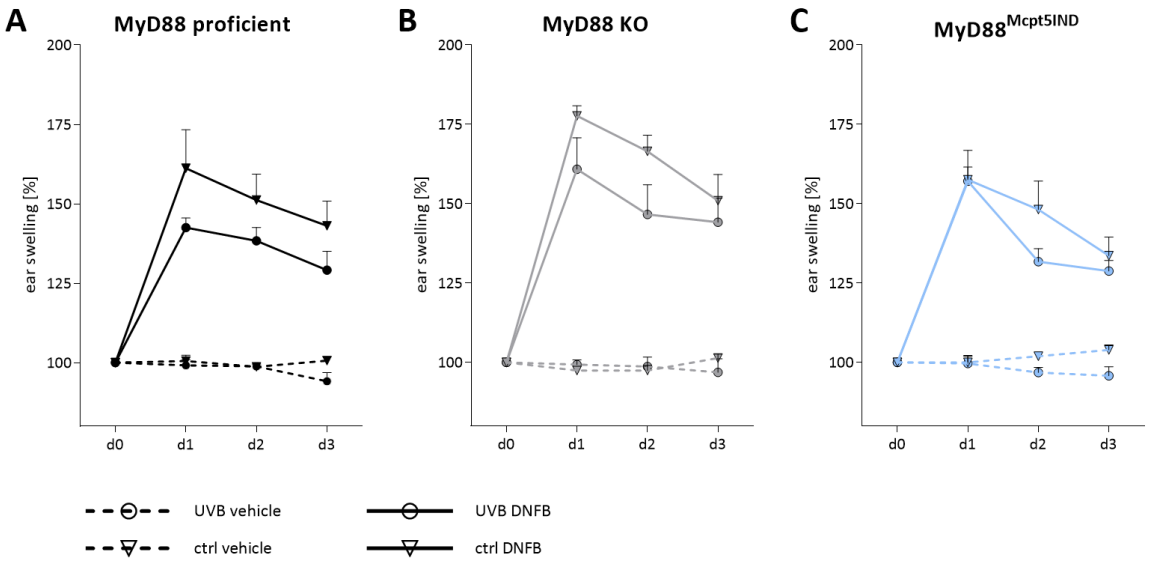

Figure 26 UVB-treatment prior to the CHS reaction reduces the ear swelling response.
A MyD88 proficient, **B** MyD88 KO and **C** MyD88^{Mcpt5IND} mice were irradiated with UVB for 4 days or left untreated, followed by sensitization with DNFB on the back skin. 5 days later (on d0), mice were challenged with DNFB on one ear, while the other ear was treated with vehicle solution. The ear swelling response was monitored daily for 3 days (d0-d3) on the DNFB treated ears (solid lines) and vehicle treated ears (dashed lines) of UVB irradiated (circle symbol) and control (triangle symbol) mice, before they were sacrificed and immune cell infiltrates were analyzed (mean +SEM, n=4-6).

Since all genotypes reacted to the UVB-induced immunosuppressive effects and MyD88 KO mice showed increased ear swelling, we sought to gain further insight on the immune response during this reaction by analyzing the immune cell infiltrated in the ear skin. For this, the ear skin was digested and immune cells were isolated and stained for flow cytometry analysis (Figure 27). Cells were first selected based on three single cell gates (as in the IL-33 blocking experiments) and then further divided as CD45$^+$ viable and Lin$^-$ cells. Among these immune cells, within the CD11b$^-$ fraction mast cells were identified. Neutrophils were gated as CD11b$^+$ Ly6G$^+$ cells, while the CD11b$^+$ Ly6G$^-$ population was further selected for CD64$^+$ Ly6C$^+$ cells. Within these, the cell population was further analyzed for CCR2$^+$ monocytes/moDCs, which were subsequently analyzed by the expression of Ly6C and MHCII. Returning to dot blot 2, based from all non-neutrophil cells DCs were selected as CD11c$^+$ and MHCII$^+$ cells and

further gated as CD24$^+$ CD11b$^+$ LCs, CD24$^-$ CD11b$^+$ cDC2, CD24$^+$ CD11b$^-$ cDC1 and the so-called CD11b$^-$ CD24$^-$ double negative (DN) dermal DC population. Moreover, cDC1 were classified in CD103$^+$ and CD103$^-$ cDC1 and cDC2 were more stringently gated as Ly6C$^-$ CD64$^-$ cells.

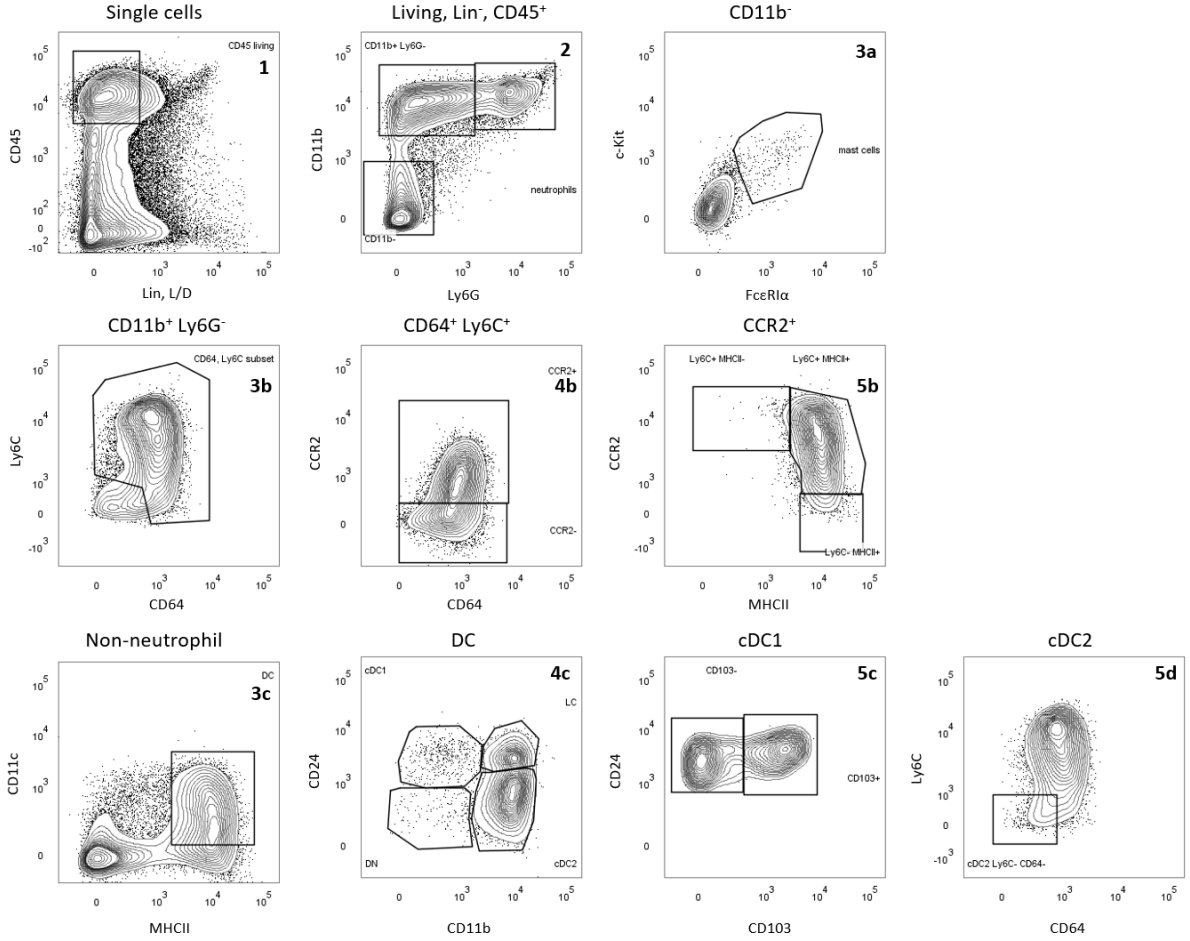

Figure 27 Gating strategy of myeloid cell populations in the skin.
MyD88 proficient, MyD88 KO and MyD88^{Mcpt5IND} mice were irradiated with UVB for 4 days or left untreated, followed by sensitization with DNFB on the back skin. 5 days later, mice were challenged with DNFB on one ear, while the other ear was treated with vehicle solution. After three days, mice were sacrificed and the ear skin was digested, cells were stained with antibodies for myeloid cell populations and analyzed by flow cytometry. Cells were first gated on their FSC/SSC profile, before three single cell gate strategies were applied. Viable, Lin$^-$ (CD3 and B220), CD45$^+$ immune cells (1) were gated and further separated in Ly6G$^+$ and CD11b$^+$ neutrophils (2), and CD11b$^-$ cells which were further gated as c-Kit$^+$ and FcεRIα$^+$ mast cells (3a). For the identification of monocytes, CD11b$^+$, Ly6G$^-$ cells were selected and gated as Ly6C$^+$ and CD64$^+$ (3b), CCR2$^+$ (4b) and then based on Ly6G and MHCII (5b) as monocytes and moDCs. Within all non-neutrophil cells DCs (3c) were separated and gated as cDC1, cDC2, LC and DN DC (4c). cDC1 were further analyzed for CD103 expression (5c) while cDC2 were more precisely gated as CD64$^-$ and Ly6C$^-$ cells. An exemplary gating strategy for a UVB-treated, DNFB applied ear of a MyD88 proficient mouse is depicted here.

DNFB treatment led to a massive expansion of immune cells in the ears, MyD88 deficient mice showed even higher immune cell numbers that MyD88 proficient and MyD88^{Mcpt5IND} mice, corresponding to the increased ear swelling response (Figure 28 A). When analyzing the

myeloid cell populations in more detail, it became evident that mast cell numbers in the skin rather decreased by DNFB treatment compared to the vehicle treated skin, while all other myeloid populations largely expanded (Figure 28 B). The mast cell decrease was most prominent in MyD88 KO mice and MyD88 proficient mice, while MyD88^{Mcpt5IND} mice displayed similar numbers, all mainly independent of UVB irradiation. Neutrophil populations however increased the most in DNFB treated MyD88 KO mice UVB-dependently, followed by MyD88 proficient mice (Figure 28 C). This UVB-dependent increase in neutrophils however could not be observed in MyD88^{Mcpt5IND} mice. Apart from neutrophils, another inflammatory cell population that infiltrates the skin are monocytes, which differentiate to moDCs at the site of inflammation (Tamoutounour et al., 2013). In all of these populations, UVB treatment alone at the vehicle treated ear elevated the number of Ly6C$^+$ MHCII$^-$ monocytes, Ly6C$^+$ MHCII$^+$ moDCs and Ly6C$^-$ MHCII$^+$ moDCs, which were indicating minor inflammation compared to the numbers in DNFB treated skin (Figure 28 D-F). The infiltration of monocytes appeared to occur MyD88-independetly. The DNFB treated ears displayed higher monocyte and moDC counts than the vehicle treated controls. Interestingly, UVB irradiation reduced the infiltration of monocytes to the DNFB treated ears in all genotypes, MyD88 KO mice which were not irradiated with UVB had the highest monocyte counts. For Ly6C$^+$ MHCII$^+$ moDCs, UVB irradiation did not show large effects on the abundance, but for Ly6C$^-$ MHCII$^+$ moDCs UVB-dependent trends were observed. Here, UVB irradiated MyD88 proficient and MyD88 KO mice displayed higher moDC numbers than unirradiated mice, mast cell specific MyD88 reconstitution however abolished the UVB dependent effects. Next, LC populations were studied and while the vehicle treated ears did not display large differences between experimental groups, DNFB treated ears revealed that irradiated MyD88^{Mcpt5IND} mice had significantly lower numbers of LC than irradiated MyD88 proficient or MyD88 KO mice (Figure 28 G). Finally, CD103$^+$ cDC1 were analyzed (Figure 28 H). UVB-exposition expanded this population in the vehicle treated ears, as well as in DNFB treated ears. This UVB-induced augmentation was not found in DNFB treated ears of MyD88^{Mcpt5IND} mice. Similar observations as for cDC1 were made for cDC2 (data not shown).

In summary, DNFB treatment induced a massive infiltration of inflammatory myeloid cells, which was further regulated by UVB irradiation. Only mast cell numbers remained comparable or rather decreased by DNFB treatment. MyD88 KO mice showed the highest cell numbers for most myeloid subsets, which also correlates with the increased ear swelling response, while

MyD88^{Mcpt5IND} mice showed rather reduced counts. In contrast, for the mast cell population numbers were lowest in MyD88 KO mice.

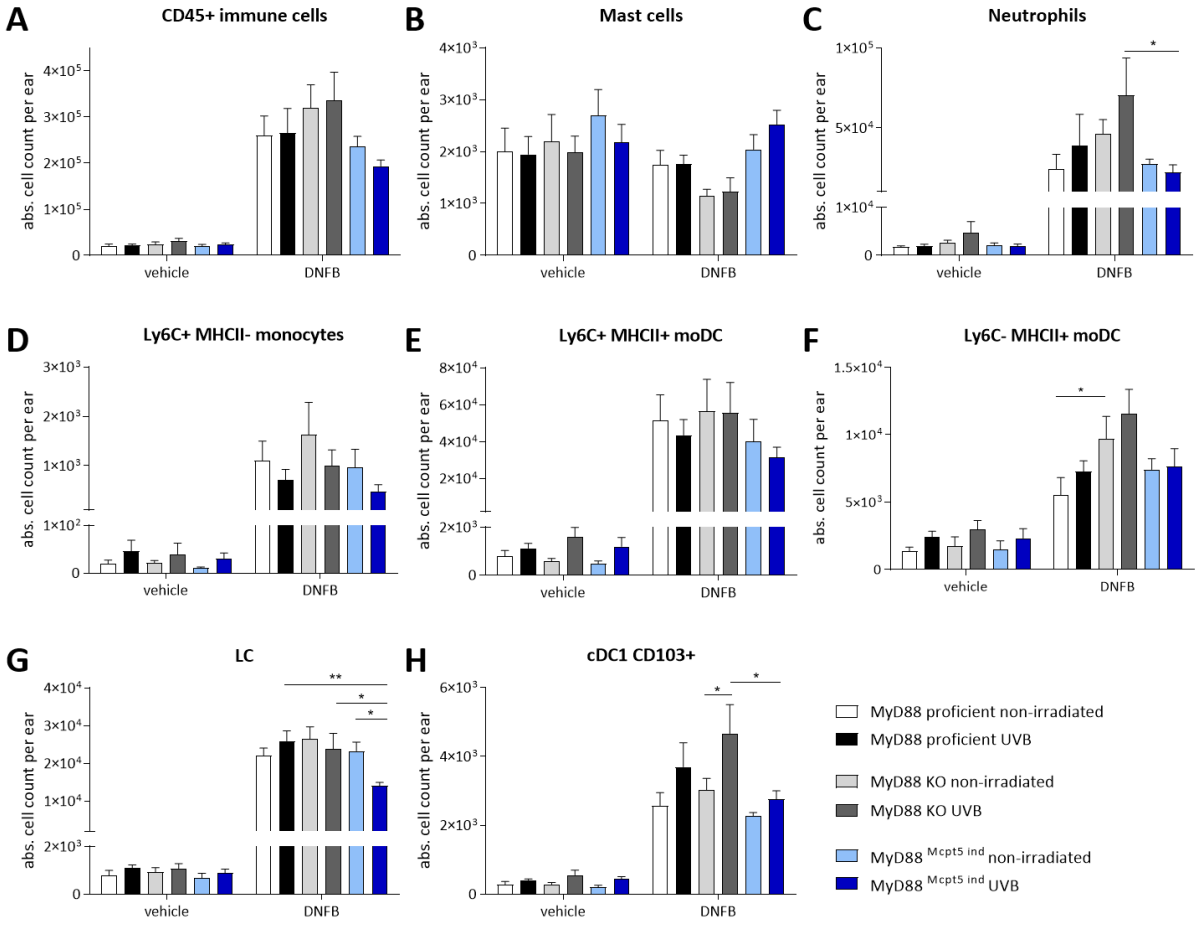

Figure 28 A larger number of infiltrated immune cells can be detected in DNFB treated ears of MyD88 KO mice. MyD88 proficient, MyD88 KO and MyD88^{Mcpt5IND} mice were irradiated with UVB for 4 days or left untreated, followed by sensitization with DNFB on the back skin. 5 days later, mice were challenged with DNFB on one ear, while the other ear was treated with vehicle solution. After three days, mice were sacrificed and the ear skin was digested, cells were stained with antibodies for myeloid cell populations and analyzed by flow cytometry. The gating strategy is depicted in Figure 27. **A** CD45$^+$ immune cells, as well as **B** mast cell, **C** neutrophil, **D** monocyte and the two moDC populations (**E** Ly6C$^+$ MHCII$^+$, **F** Ly6C$^-$ MHCII$^+$) are presented. For the DCs, **G** LC and **H** CD103$^+$ cDC1 are shown here (mean +SEM, n=4-6, *p<0.05, **p<0.01, other significant differences between vehicle and DNFB treatment of the same groups are not depicted here for better clarity of the graphs).

APCs in the skin initiate a T-cell response in the ear draining lymph nodes upon application of DNFB. T-cells then migrate towards the site of inflammation and mediate adaptive immunity. To study the adaptive immune response in the skin, immune cells were isolated from the ears and stained with antibodies to analyze them by flow cytometry (Figure 29). First, cells were selected by size and granularity, followed by single cell gating based on three single cell gates, which were then further selected for viable CD45 expressing cells. Next, CD19$^+$ B-cells were identified and all non-B-cells were analyzed for TCRγδ and TCRβ expression. DETCs have a high

TCRγδ expression, while dermal γδ T-cells are rather intermediately expressing TCRγδ. All conventional T-cells could be identified as TCRβ$^+$ cells, among these, CD4$^+$ and CD8$^+$ conventional T-cells were selected. Subsequently, CD4$^+$ T-cells were analyzed for FoxP3 and CD25 expression to determine Treg populations and for CD69 to analyze activated CD4$^+$ T-cells.

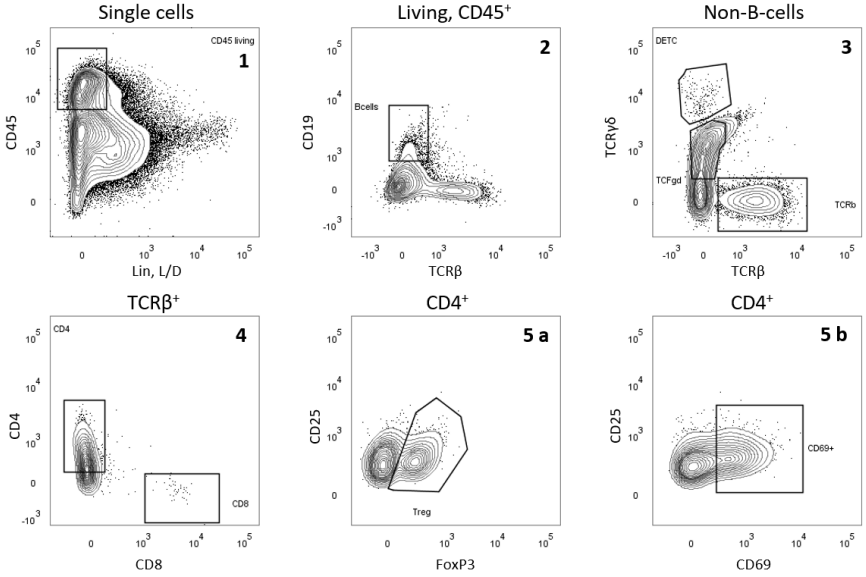

Figure 29 Gating strategy for skin T-cells.
MyD88 proficient, MyD88 KO and MyD88^{Mcpt5IND} mice were irradiated with UVB for 4 days or left untreated, followed by sensitization with DNFB on the back skin. 5 days later, mice were challenged with DNFB on one ear, while the other ear was treated with vehicle solution. After three days, mice were sacrificed and the ear skin was digested, cells were stained with antibodies for T-cell populations and analyzed by flow cytometry. Cells were first gated on their FSC/SSC profile, before three single cell gate strategies were applied. Within the viable CD45$^+$ population (1), B-cells were gated as CD19$^+$ cells, all CD19$^-$ cells were gated for TCRβ expression and TCRγδ expression (3). TCRβ$^+$ cells were then subdivided in CD4$^+$ and CD8$^+$ fractions (4), for the CD4$^+$ fraction, the amount of FoxP3$^+$ Tregs (5a) and CD69$^+$ activated T-cells (5b) was analyzed. An exemplary gating strategy for a UVB-treated, DNFB applied ear of a MyD88 proficient mouse is depicted here.

DETCs are γδ T-cells of the epidermis are known to be activated upon allergen exposure by stress-induced signals (Jameson et al., 2004). In this experimental model, DETC numbers remained stable in vehicle and DNFB treated ears. Although UVB induced effects were observed which led to reduced DETC numbers in irradiated mice in both DNFB treatment and controls, MyD88-dependent effects could not be observed (Figure 30 A). Surprisingly, MyD88 proficient mice already displayed a DETC reduction in unirradiated vehicle treated ears. In contrast to the DETC fraction, all other T- and B-cell populations expanded upon DNFB treatment.

DNFB treated MyD88 KO mice displayed highest numbers of dermal γδ T-cells, followed by MyD88 proficient and MyD88^{Mcpt5IND} animals (Figure 30 B). For B-cells, UVB irradiation could slightly elevate cell numbers in vehicle treated ears while DNFB treatment induced expansion of the B-cell population (Figure 30 C). Especially, UVB treated MyD88 proficient and MyD88 KO cells showed many B-cells in the skin. The exact phenotype of these B-cells was not characterized, but it might very likely be that these B-cells were Bregs since it was shown that UV exposure induces the generation of Bregs, thus improving CHS symptoms (Liu et al., 2018). Due to the heterogeneity of Bregs, the analysis largely relies on functional assays, in which the ability to secrete IL-10 is studied (Peng et al., 2018), which should be addressed in future experiments. The conventional T-cell population largely increased upon DNFB application and similar to γδ T-cells, MyD88 KO mice had a higher influx of conventional CD4$^+$ and CD8$^+$ T-cells than MyD88 proficient and MyD88^{Mcpt5IND} mice (Figure 30 D). UVB irradiation was able to slightly reduce the infiltration of T-cells. Importantly, in vehicle treated ears, UVB irradiation induced Treg expansion MyD88 independently (Figure 30 E). In DNFB treated ears, the Treg expansion was eminent and also there UVB could positively affect Treg numbers. MyD88 KO mice however showed high Treg numbers independent of UVB irradiation. Very similar trends were observed for the presence of activated CD69$^+$ CD4+ T-cells, this cell population increased after DNFB treatment which appeared to be affected by UVB irradiation in MyD88 KO mice, but not in MyD88 proficient and MyD88^{Mcpt5IND} mice (Figure 30 F).

In summary, UVB irradiation influenced the abundance of adaptive immune cells in the ear skin, especially DETCs, B-cells and Tregs were affected. MyD88 KO mice showed the highest number of conventional T-cells and dermal γδ T-cells, which correlated with the increased numbers of immune cells in general (Figure 28 A). It is of importance to mention that MyD88^{Mcpt5IND} mice had generally lower numbers of immune cells in the skin, which might explain the decreased amount of adaptive immune cells compared to the other genotypes as well as reduced ear swelling in comparison to full MyD88 KO mice.

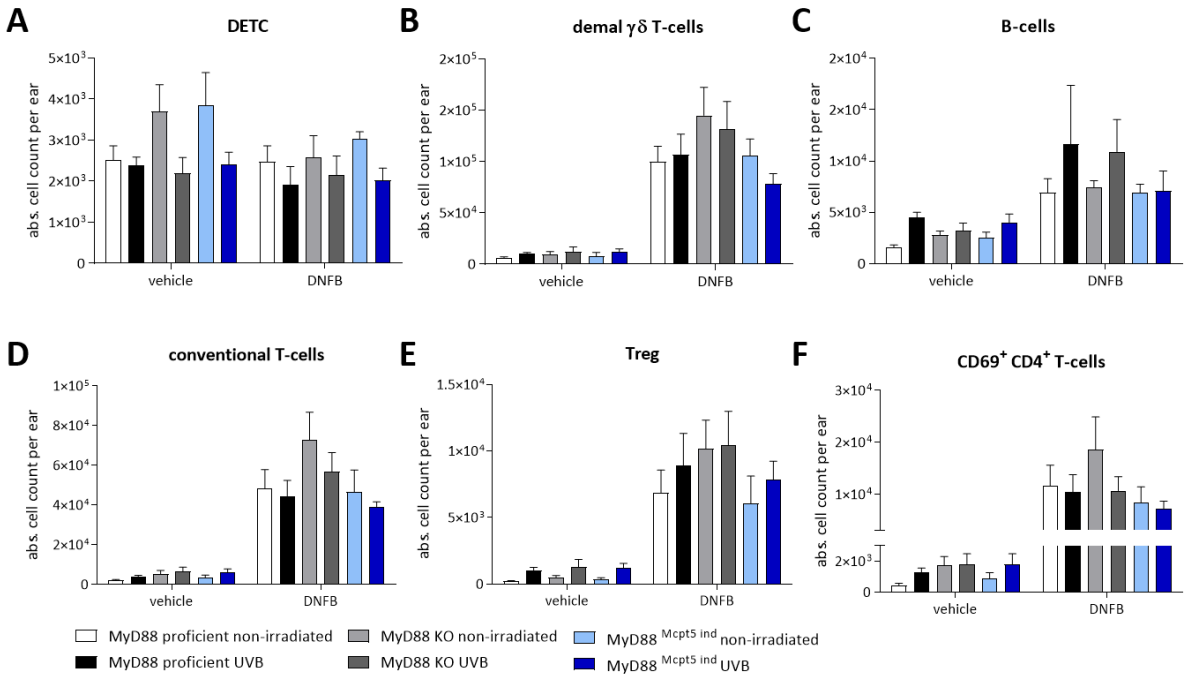

Figure 30 T-cell and B-cell populations in the skin reveal changes after DNFB treatment.
MyD88 proficient, MyD88 KO and MyD88^{Mcpt5IND} mice were irradiated with UVB for 4 days or left untreated, followed by sensitization with DNFB on the back skin. 5 days later, mice were challenged with DNFB on one ear, while the other ear was treated with vehicle solution. After three days, mice were sacrificed and the ear skin was digested, cells were stained with antibodies for T-cell populations and analyzed by flow cytometry. The gating strategy is depicted in Figure 29, **A** DETC and **B** dermal γδ T-cells were analyzed, as well as **C** B-cell populations. Moreover, **D** conventional T-cell populations are presented, with this population **E** Tregs and **F** CD69$^+$ CD4$^+$ T-cells are depicted (mean +SEM, n=4-6, significant differences between vehicle and DNFB treatment of the same groups are not depicted here for better clarity of the graphs).

4.5.2. UVB exposition prior to CHS changes the immune cell composition in skin-draining lymph nodes

In addition to the skin tissue specific immune response, the ear-draining aLN were studied to gain further insight on the adaptive immune response. Therefore, lymph node cells were isolated and stained for flow cytometry analysis (Figure 31). Similar to the gating strategy for the skin, cells were first selected by size and granularity, followed by single cell gating and further selection for viable CD45 expressing cells. Next, CD19$^+$ B-cells were identified and all non-B-cells were analyzed for TCRγδ and TCRβ expression. All conventional T-cells could be identified as TCRβ$^+$ cells, and among these, CD4$^+$ and CD8$^+$ conventional T-cells were selected. CD4$^+$ cells were gated on CD25 and FoxP3 to identify Tregs, these Tregs were furthermore studied for CD44 and CD62L expression, selecting CD44$^+$ effector memory (EM) Tregs, CD62L$^+$ naïve Tregs and CD44$^+$ CD62L$^+$ central memory (CM) Tregs. Moreover, all CD4$^+$ and CD8$^+$ T-

cells were separately studied for these naïve and memory cell subsets, and were also analyzed for activation by selecting for CD69 expression on CD4 or CD8 T-cells.

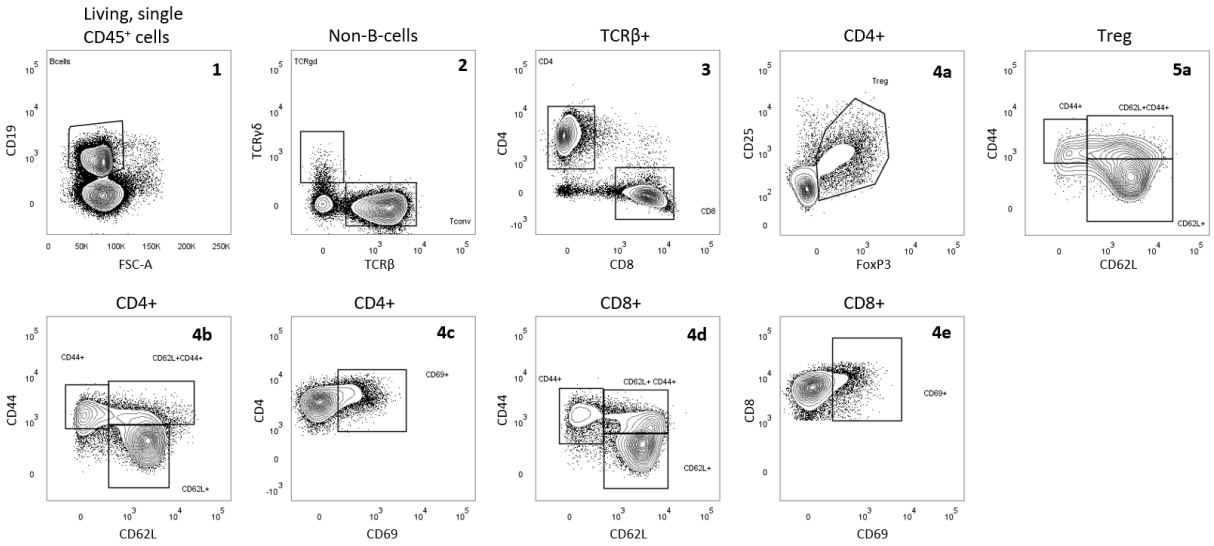

Figure 31 Gating strategy of T-cells in the aLN.
MyD88 proficient, MyD88 KO and MyD88^{Mcpt5IND} mice were irradiated with UVB for 4 days or left untreated, followed by sensitization with DNFB on the back skin. 5 days later, mice were challenged with DNFB on one ear, while the other ear was treated with vehicle solution. After three days, mice were sacrificed and the ear draining lymph nodes were digested, cells were stained with antibodies for T-cell populations and analyzed by flow cytometry. Cells were first gated on their FSC/SSC profile, before a single cell gating strategy was applied. Living, CD45$^+$ immune cells were identified and B-cells were selected based on CD19 expression (1). All non-B-cells were next classified in TCRγδ expressing T-cells and TCRβ expressing conventional T-cells (2). CD4 and CD8 expression was then assessed within the conventional T-cell population (3). CD4$^+$ T-cells were further studied in different gates, CD25$^+$ and FoxP3$^+$ Tregs were analyzed, as well as the distribution of these in CD44$^+$ effector memory Tregs, CD62L$^+$ naïve Tregs and double positive CD44$^+$ CD62L$^+$ central memory Tregs. The same gating for the analysis of memory and naïve T-cell populations was furthermore applied to all CD4$^+$ T-cells and all CD8$^+$ T-cells. Activated CD69 expressing CD4$^+$ T-cells and CD8$^+$ T-cells were evaluated in addition. An exemplary gating strategy for a UVB-treated MyD88 proficient mouse with a lymph node on the side of the DNFB applied ear depicted here.

As expected, draining lymph nodes of DNFB treated ears contained more CD45$^+$ immune cells than the ones from vehicle treated ears (Figure 32 A). So not only in the skin, but also in the aLN MyD88 deficiency induced higher cellularity. However, UVB irradiated MyD88 proficient mice did not show that much of an increase regarding immune cell counts, likely because of the lower number of biological replicates (n=2 for MyD88 proficient UVB irradiated DNFB treated mice). To level out this effect, the frequencies of all viable CD45$^+$ immune cells of the respective subset are presented. In general, immune cell populations in the aLN did not show large differences. DNFB treatment induced higher frequencies of B-cells, which was affected by UVB irradiation, resulting in decreased frequencies when mice were irradiated (Figure 32 B). Conventional T-cells on the other side, expanded number-wise (data not shown), but remained stable between genotypes when evaluating percentages (Figure 32 C). Among

these, UVB irradiation could decrease frequencies of activated $CD4^+$ T-cells in MyD88 proficient mice independent of DNFB treatment, while MyD88 KO and $MyD88^{Mcpt5IND}$ mice displayed rather similar frequencies (Figure 32 D). Consistent with these results, UVB irradiation was able to elevate frequencies of naïve $CD4^+$ T-cells in draining lymph nodes of DNFB treated ears (Figure 32 E). EM and CM T-cell frequencies in draining lymph nodes of DNFB treated ears appeared to occur MyD88-independently. Interestingly, DNFB increased the frequencies of CM T-cells, while EM T-cell frequencies were similar between vehicle and DNFB treated sides (Figure 32 F, G). DNFB experienced unirradiated lymph nodes of MyD88 proficient mice even showed elevated frequencies of CM T-cells. Frequencies of Tregs in the lymph node expanded in all UVB animals compared to unexposed mice, furthermore highlighting the ability of UVB light to induce immune suppression (Figure 32 H). Moreover, the frequencies of the memory, activated and naïve T-cell populations for $CD8^+$ T-cells and Tregs (data not shown) behaved similarly to these of $CD4^+$ T-cells (Figure 32 D-G).

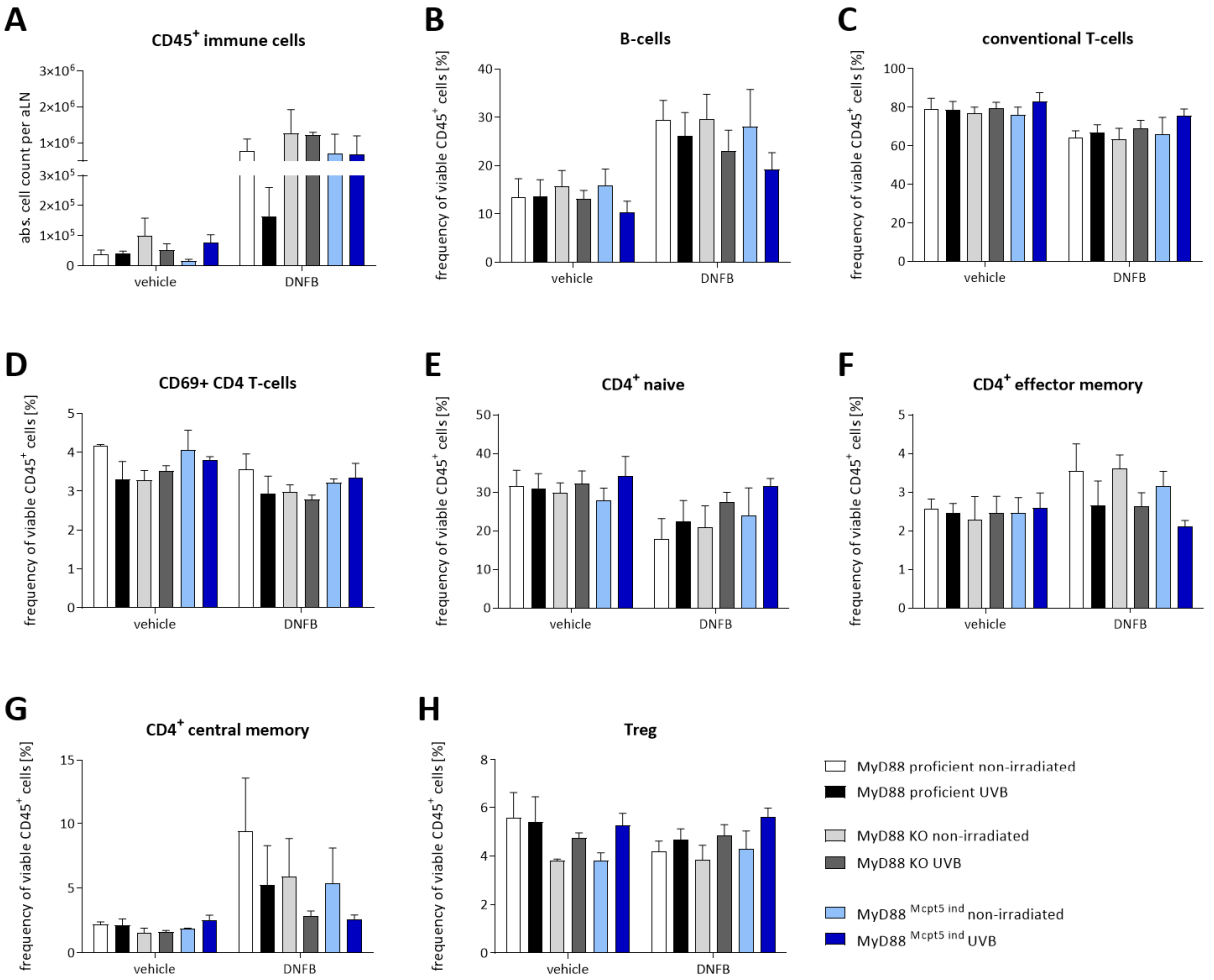

Figure 32 UVB-induced immune suppression regulates B-and T-cell frequencies in the aLN.
MyD88 proficient, MyD88 KO and MyD88^{Mcpt5IND} mice were irradiated with UVB for 4 days or left untreated, followed by sensitization with DNFB on the back skin. 5 days later, mice were challenged with DNFB on one ear, while the other ear was treated with vehicle solution. After three days, mice were sacrificed and the ear draining lymph nodes were digested, cells were stained with antibodies for T-cell populations and analyzed by flow cytometry with the gating strategy depicted in Figure 31. All immune cells, B-cells and conventional T-cells were evaluated, as well as certain populations of CD4$^+$ T-cells. Among these, activated CD69$^+$ T-cells, naïve T-cells, EM T-cells, CM T-cells and Tregs were studied (mean +SEM, n=2-6, significant differences between vehicle and DNFB treatment of the same groups are not depicted here for better clarity of the graphs).

In summary, UVB treatment prior to CHS could lead to the reduction of the ear swelling response. This effect was observed in all of the mice, independent of MyD88. But, MyD88 deficient mice interestingly showed a generally increased immune response, which was also reflected by the enhanced infiltration of immune cells in the skin, while MyD88^{Mcpt5IND} mice mainly resembled to MyD88 proficient animals. This shows, that mast cell specific MyD88 signaling might dampen the immune response in CHS, although the effects of MyD88 signaling to UV-induced immune suppression were quite small. The experimental model of UV-induced immune suppression was functional and was able to diminish inflammation in the ear skin

likely due to increased Treg and B-cell expansion. Although there was evidence for slightly higher numbers of neutrophils, cDC1 and Ly6C$^-$ MHCII$^+$ mo-DCs, UV exposure was also able to reduce numbers of and monocytes and Ly6C$^-$ MHCII$^+$ mo-DCs and induce Treg and B-cell expansion. These results show that UV irradiation can modulate skin immune cell populations thereby mediating immune suppression in the context of CHS.

4.6. Role of MyD88 in Photocarcinogenesis

One of the main risk factors that accompanies UV irradiation is the development of skin tumors. The reasons for this are increased formation of DNA damage, inflammation and suppression of the immune system which together facilitate the development of non-melanoma skin cancers upon UV irradiation (Prasad & Katiyar, 2017). Since MyD88 was previously shown to regulate expression of DNA repair enzymes and therefore influence DNA damage (Opitz, 2016), we wanted to further analyze how mast cell-specific MyD88 signaling might influence the formation of skin tumors. Moreover, the observation that MyD88 deficient mice showed enhanced inflammation in the experimental model of UV-induced immune suppression, might also influence the tumor outcome.

4.6.1. MyD88 KO mice develop more tumors after long-term UVB exposition

MyD88 proficient, MyD88 KO and MyD88^{Mcpt5IND} mice were exposed to UVB three times a week for a total duration of 33 weeks. After each irradiation, tumor numbers and sizes were recorded. Generally C57BL/6 mice do not develop as many UV-induced tumors (Kitajima et al., 1995). But beginning after 16 weeks of irradiation, the first tumors were detected on the skin of MyD88 KO mice, while MyD88 proficient and MyD88^{Mcpt5IND} mice began to develop tumors after 20 and 21 weeks (Figure 33 A). Over the experimental course MyD88 KO mice developed the highest number of tumors, while MyD88 proficient mice showed very low numbers. Until week 25 MyD88^{Mcpt5IND} mice behaved very similar to MyD88 proficient animals, but from week 26 onwards the tumor numbers increased a lot more than in the MyD88 proficient animals, so that by the end of the experiment the frequency of tumors was rather intermediate. The analysis of the tumor size revealed that at the end point of the experiment, the mean tumor sizes did not differ between genotypes, the interindividual variations however were considerable (Figure 33 B). A general observation about this experiment was that UVB exposed MyD88 KO mice had increased experimental scores due to skin inflammation. For this reason, 40 % of MyD88 KO mice (2 out of 5) had to be taken out of the experiment before the end of the experiment, while only 28.5 % of MyD88 proficient mice (2 out of 7) had to be taken out before week 33 (data not shown). The higher scores of MyD88 KO mice reflects the observations from the UV-induced immune suppression experiments; MyD88 KO mice showed increased skin inflammation there as well (Figure 26). But interestingly, none of the MyD88^{Mcpt5IND} mice needed to be removed from the photocarcinogenesis experiment before week 33.

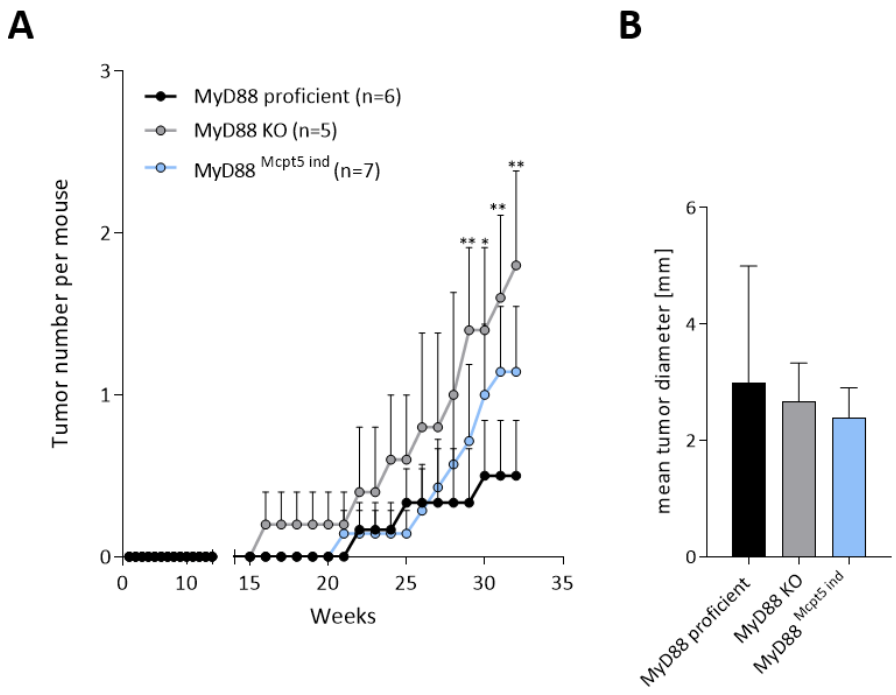

Figure 33 Global MyD88 deficiency leads to a higher number of skin tumors, but does not affect tumor size. MyD88 proficient, MyD88 KO and MyD88^{Mcpt5IND} mice were irradiated thrice a week with UVB over the course of 33 weeks. **A** The tumor numbers and were documented after each irradiation and are represented over the whole duration of the experiment, significant differences refer to the MyD88 proficient group. **B** Tumor sizes were registered and are shown for the end of the experiment in week 33 (mean+ SEM, n=5-7, *p<0.05, **p<0.01).

Next, long-term irradiated tumor unaffected skin regions and control skin were histologically analyzed by Toluidine Blue staining (Figure 34 A). UVB irradiation led to an increase of the epidermal thickness (Figure 34 B). The epidermis of MyD88 KO mice however only showed minor thickening, which was again higher in in MyD88^{Mcpt5IND} mice. This MyD88-dependent thickening upon long-term irradiation coincides with the results of mice, which were exposed to chronic UVB doses for 6 weeks (Opitz, 2016). The dermal thickness as well as the numbers of dermal mast cells were not altered after UVB irradiation and the absence of MyD88 did not change mast cell numbers compared to proficient animals (Figure 34 B, C). But in this experiment, mast cell numbers were remarkably higher than in the skin of younger mice (Figure 18 B).

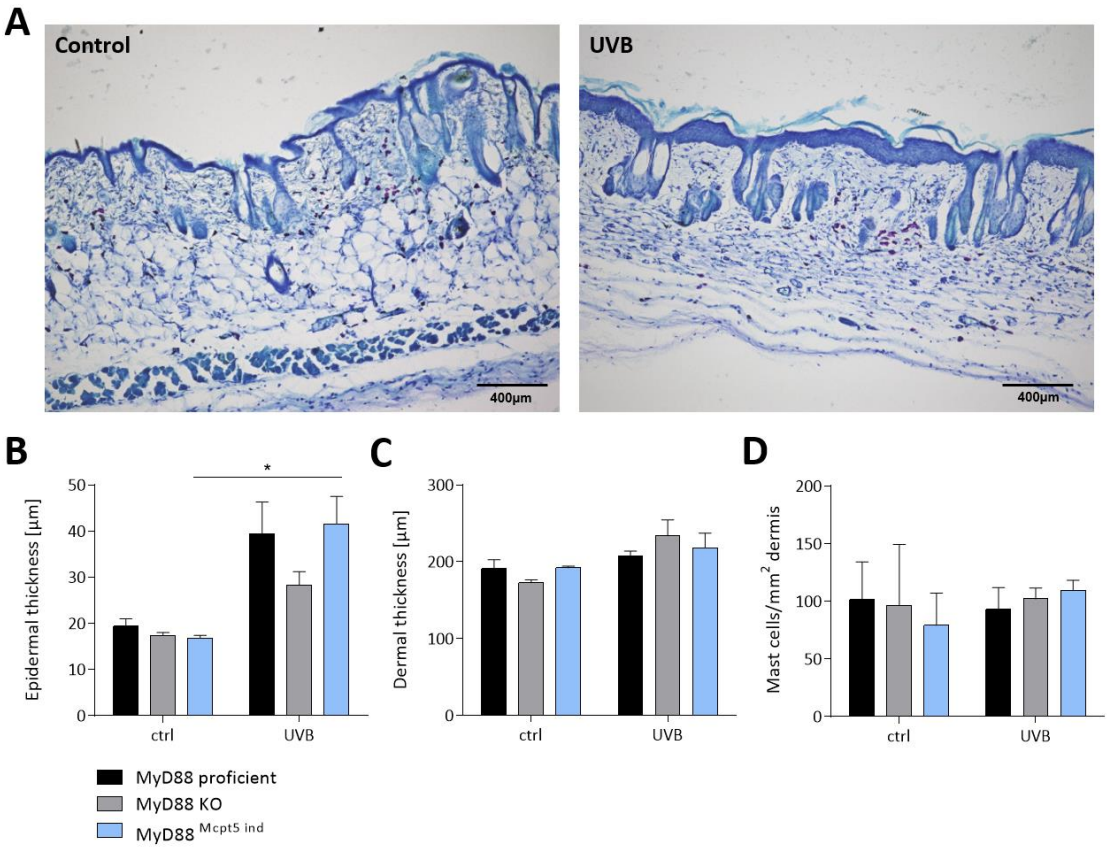

Figure 34 Long-term UVB treatment induces acanthosis, but does not affect mast cell numbers.
MyD88 proficient, MyD88 KO and MyD88^{Mcpt5IND} mice were irradiated thrice a week with UVB over the course of 33 weeks. Skin sections of control and UVB irradiated mice were prepared and stained with Toluidine Blue to visualize mast cells. **A** Depicts exemplary images of control and UVB treated skin sections. **B** The epidermal and **C** the dermal thickness were quantified, as well as **D** the number of mast cells/mm^2 dermal area (mean +SEM, n=3-7, *p<0.05).

To shed light on the cytokine expression after long-term UVB exposure, skin protein lysates were generated and measured by ELISA. TSLP was reported to be highly associated to allergic skin diseases like atopic dermatitis, but was also shown to be upregulated in UVB irradiated keratinocytes (Jang et al., 2013; Ziegler, 2012). Here, TSLP was slightly enhanced in MyD88 proficient skin after UVB irradiation, while MyD88 deficient and mast cell-specific MyD88 reconstituted skin displayed a strong induction in TSLP expression. Similarly, TNF-α expression was increased in UVB exposed skin of MyD88 KO mice the most, but was not further induced in mice of other genotypes. Lastly, IL-10 was analyzed since this cytokine was reported to contribute to the UV-induced immunosuppressive environment in the skin (Loser et al., 2007). In our model however, UVB induced only a minimal increase in IL-10 secretion, but also here control MyD88 KO mice and UVB irradiated MyD88 KO mice showed the largest IL-10 expression.

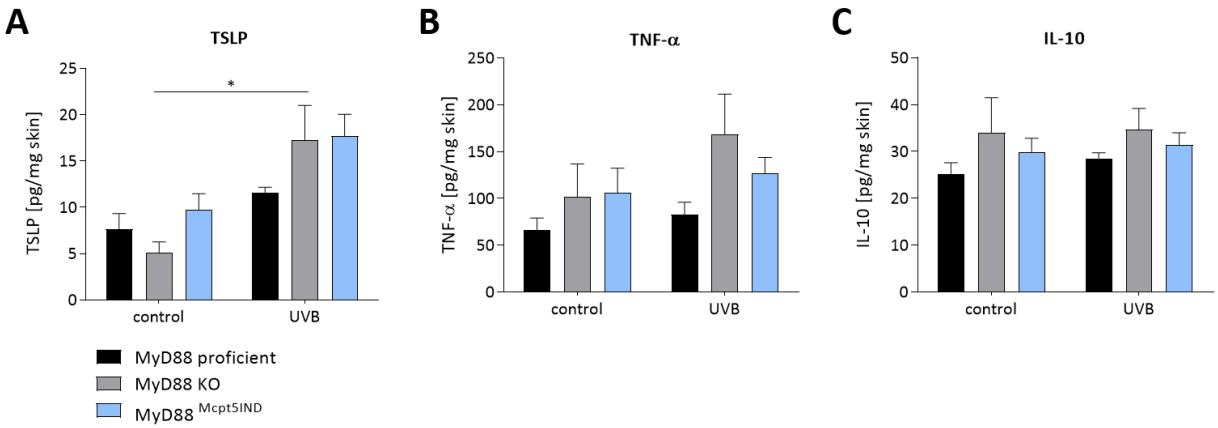

Figure 35 MyD88 signaling influences TSLP and TNF-α protein levels in the skin.
MyD88 proficient, MyD88 KO and MyD88^{Mcpt5IND} mice were irradiated thrice a week with UVB over the course of 33 weeks. Skin lysates of control and UVB irradiated mice were prepared and analyzed by ELISA measurements for **A** TSLP, **B** TNF-α, and **C** IL-10 protein levels (mean +SEM, n=3-7 * $p<0.05$).

4.6.2. Long-term UVB irradiation influences adaptive immune cells in skin and lymph nodes

To analyze the exact effects of long-term UVB irradiation on adaptive immune cells in the skin, ears of MyD88 proficient, MyD88 KO and MyD88^{Mcpt5IND} mice were digested, immune cells were isolated and stained for flow cytometry analysis. The gating strategy for the different immune cell subsets is the same as in Figure 29. It should be stated that the bars of the UVB irradiated MyD88 KO group constitute of two individual mice only, therefore the results for this genotype need to be interpreted cautiously. CD45$^+$ immune cells in the skin only expanded in MyD88^{Mcpt5IND} mice, while in the other genotypes the numbers remained stable or were rather decreased (Figure 36 A). Expectedly, DETCs were massively depleted from the skin after long-term irradiation (Figure 36 B). Dermal γδ T-cells however marginally increased MyD88-dependently after UVB exposition, similar to conventional T-cells (Figure 36 C, D). Within the conventional T-cell population, Tregs expanded upon UVB irradiation in all mice (Figure 36 E). Having a closer look at the Treg frequencies, irradiated MyD88 KO mice had a higher percentage of Tregs in the skin than MyD88 proficient and MyD88^{Mcpt5IND} (Figure 36 F).

Taken together, long-term irradiation drastically reduced DETC counts, while Tregs were increased. The slightly increased Treg frequencies in MyD88 KO mice could also suggest greater immunosuppressive capacities, which correlates to the increased IL-10 levels in the

skin and more tumor formation, though this suggestion would require additional evidence by testing more mice.

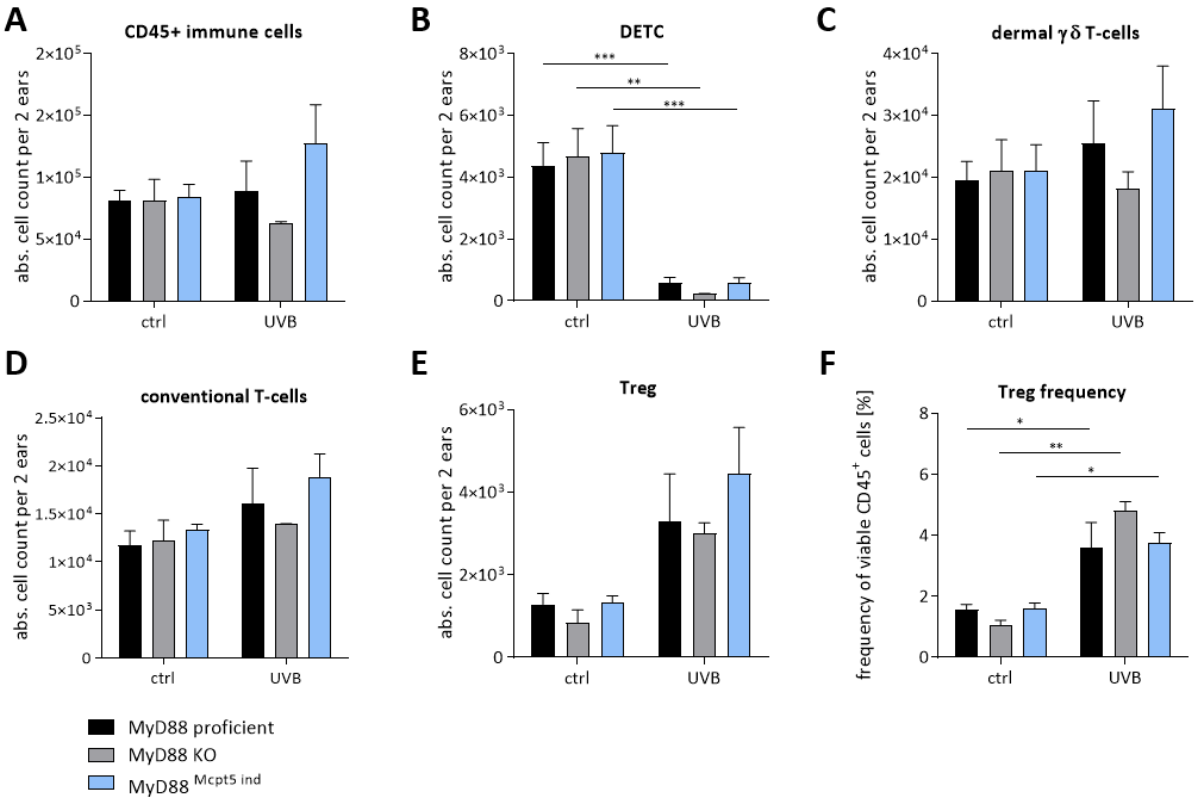

Figure 36 T-cell populations in skin reveal MyD88-dependent differences.
MyD88 proficient, MyD88 KO and MyD88^{Mcpt5IND} mice were irradiated thrice a week with UVB over the course of 33 weeks. Immune cells in the skin were analyzed, the same gating strategy as in Figure 29 was applied here. **A** CD45^{+} immune cell populations, as well as **B** DETC and **C** dermal γδ T-cell populations were evaluated. In addition, **D** conventional T-cell and **E, F** Treg numbers were studied. All of the mentioned graphs depict absolute cell counts of the respective population, while **F** displays Treg frequencies of all CD45^{+} immune cells (mean +SEM, n=2-7, *p<0.05, **p<0.01, ***p<0.001).

In addition to the skin-specific immune response, likewise the adaptive immune response in the back skin draining bLN was explored. Therefore, bLN were isolated, single cell suspensions were prepared from the tissue, counted and stained for flow cytometry analysis (Figure 37). The gating strategy for the immune cell subsets in the lymph node is the same as in Figure 31. CD45^{+} immune cells were strongly elevated after chronic UVB irradiation, which indicates that long-term UVB exposure induces a robust adaptive immune response (Figure 37 A). Here, MyD88^{Mcpt5IND} mice showed the highest cell numbers compared to WT and MyD88 KO mice. The increase of immune cells in the bLN can be explained by a general rise in B-cell and conventional T-cell numbers in all genotypes upon UVB exposition (Figure 37 B, C). Notably, Tregs were slightly elevated in the complete absence of MyD88 and in MyD88^{Mcpt5IND} mice,

corresponding to the Treg counts in the skin (Figure 37 D). Moreover, the percentage of activated, naïve and EM T-cells from all $CD4^+$ T-cells was determined. While the percentage of $CD69^+$ activated T-cells increased MyD88-independently, frequencies of naïve T-cells ($CD62L^+$, $CD44^-$) were rather decreased after UVB exposition (Figure 37 E, F). Interestingly, aged MyD88 KO and $MyD88^{Mcpt5IND}$ control mice exhibited higher frequencies of naïve T-cells which suggests contribution of MyD88 signaling in the activation of T-cells apart from UVB exposition. In line, EM T-cells generally increased after UVB exposition, MyD88 proficient mice showed the largest proportion of this population (Figure 37 G).

In summary, B-cells, Tregs and activated $CD4^+$ T-cells expanded by UVB irradiation. These results indicate, that long-term UVB irradiation indeed induces Treg expansion in the lymph nodes, which might contribute to UV-induced immune suppression, favoring tumor progression. These results however need to be interpreted cautiously since the number of individual mice in the UVB irradiated MyD88 KO group was quite low. But, the importance of MyD88 signaling in lymph node cells and in the skin was still apparent; MyD88 deficient mice showed less acanthosis, had more Tregs and higher IL-10 levels in the skin, which together might promote the increased development of UV-induced skin tumors.

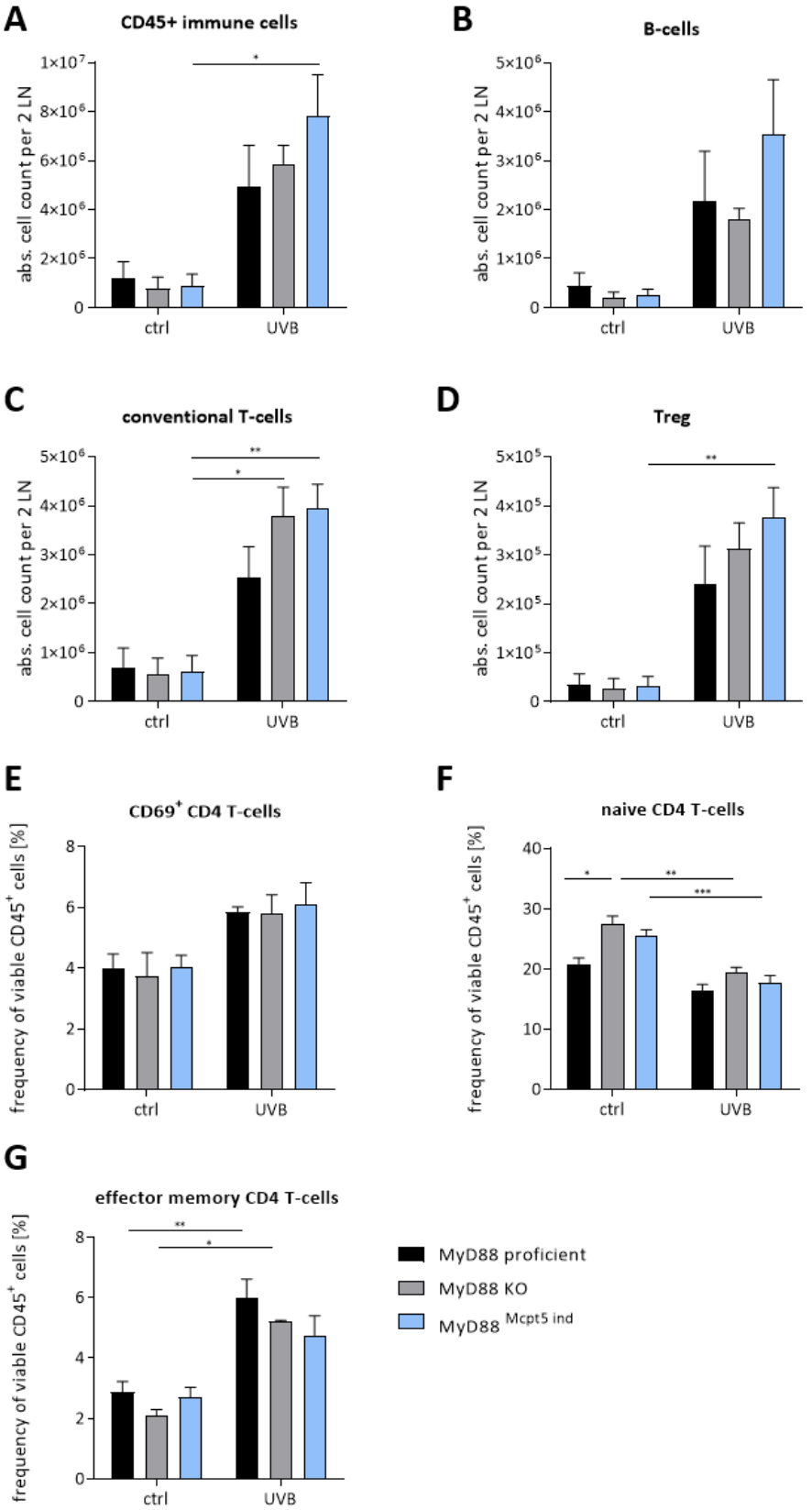

Figure 37 Long-term UVB irradiation changes B- and T-cell proportions in the bLN.
MyD88 proficient, MyD88 KO and MyD88^{Mcpt5IND} mice were irradiated thrice a week with UVB over the course of 33 weeks. Immune cells in the bLN were analyzed, the same gating strategy as in Figure 31 was applied here. **A** CD45$^+$immune cells, **B** B-cells, **C** conventional T-cells and **D** Treg cell counts in the bLN were quantified. Moreover, frequencies of CD4$^+$ **E** activated CD69$^+$ T-cells, **F** naïve T-cells and **G** EM T-cells was determined (mean +SEM, n=3-7, *p<0.05, **p<0.01, ***p<0.001).

5. Discussion

Mast cells are granulated innate immune cells that reside in connective (e.g., skin) and mucosal tissues (e.g., gut mucosa) of the body. Their granules contain different types of cell mediators such as histamine, prostaglandins, leukotrienes and cytokines, which can be released after mast cell activation (Valent et al., 2020). A central molecule in innate immune signaling is MyD88, which transduces signaling upon TLR and IL-1R engagement by PAMPs and DAMPs. In the skin, MyD88 has been shown to regulate DNA damage as well as acanthosis after chronic UVB irradiation (Opitz, 2016). Besides, mast cell accumulation was observed in a MyD88-dependent manner, mast cell specific and DC specific MyD88 expression was able to restore the defects in mast cell accumulation, but also DNA damage and acanthosis were back at WT levels (Opitz, 2016). Thus, mast cell specific MyD88 signaling was shown to take an important function in UVB irradiation.

In this thesis, the functional role of MyD88 in mast cells was analyzed and in addition, their interaction with DCs was examined. In these functional studies, IL-33 was found to be an important regulator of different mast cell functions, therefore IL-33 signaling was studied in an *in vivo* model of chronic UVB irradiation. Furthermore, mast cells are relevant for the induction of UV-induced immune suppression and since mast cell specific MyD88 signaling was found to impact mast cell numbers, it was addressed how MyD88 might affect the generation of immune suppression. Thus, UV-induced immune suppression in a model of CHS was studied and moreover, it was tested how long-term UVB irradiation affects tumor formation.

5.1. MyD88 signaling influences mast cell survival, activation and degranulation

Since previous data revealed a role for mast cell-specific MyD88 signaling (Opitz, 2016), first, the function of MyD88 in *in vitro* generated mast cells was studied. For this, bone marrow cells were differentiated to mast cells and different properties were analyzed. However, to identify if MyD88 deficient mast cells already show any defects in their precursor numbers that might affect their differentiation, MCps were analyzed. MCp numbers in the bone marrow were slightly lower in MyD88 KO and MyD88^{McptI5ND} mice (Figure 10). An explanation for similar MCp numbers in MyD88 KO and MyD88^{Mcpt5IND} mice might be that Mcpt5 drives re-expression of MyD88 rather in mature mast cells (Scholten et al., 2008). Yet, the difference between MyD88

proficient and MyD88 KO MCps did not further influence mast cell differentiation *in vitro* as cells of both genotypes developed equally well (Figure 11). Even if *in vitro*, this did not influence mast cell differentiation, the slightly decreased MCp counts can potentially affect the mast cells *in vivo*. Unlike in UVB-exposed skin, unirradiated MyD88 proficient, MyD88 KO and MyD88^{Mcpt5IND} mice had comparable numbers of mast cells in the back skin, indicating that MyD88 does not play an essential role in the primary seeding and maintenance of mast cell populations under physiologic conditions (Opitz, 2016). Chronic UVB irradiated skin however displayed a MyD88-dependent reduction of mast cells, that is again restored in MyD88^{Mcpt5IND} mice (Opitz, 2016). Indeed during health, mast cells have been shown to maintain their population in the skin independent from MCp contribution (Gentek et al., 2018; Li et al., 2018). In skin inflammation however, a recent study identified that mast cells accumulate in the skin after DNFB application in two different ways (Weitzmann et al., 2020). On the one hand, skin resident mast cell precursors proliferate locally, and on the other hand, additional precursors are recruited from the bone marrow to the site of inflammation, where these cells complete maturation. So, in their experiments, it was clearly shown that the pool of skin mast cells is of heterogenous origin and that in inflammation, bone marrow derived precursors contribute to the skin population (Weitzmann et al., 2020). In line with the study by Weitzmann et al., decreased MCp numbers or defects in MCp recruitment could explain lower mast cell numbers in UVB exposed skin of MyD88 KO mice. Additional investigations are required to test whether this dual origin of skin mast cells can also be observed upon UVB exposure. *In vitro* assays on mast cell migration however appeared to happen independent of MyD88 (Figure 12), but it is not clear yet whether MyD88 plays a role in the migration of MCps to the skin in inflammation.

Besides the recruitment of mast cells in inflammation, an increased survival and proliferation of local mast cells might explain elevated numbers. In *in vitro* generated mast cells, survival and activation after stimulation were diminished in MyD88 KO cells (Figure 13 ,Figure 14). TLR engagement induced IL-6 and IL-13 release in a MyD88-dependent manner, while FcεRIα engagement induced cytokine release independent of MyD88. Especially, IL-33 stimulated cells showed a significantly higher cytokine release, and IL-33 was also able to induce mast cell survival MyD88-dependently, which can in the context of UVB irradiation explain the importance of MyD88 for mast cell survival in the skin. These findings resemble results from a study, which shows that IL-33 stimulation or FcεRIα engagement alone lead to the production of IL-6 and IL-13 in mast cells, and IL-33 at a higher dose is able to enhance mast

cell survival independent of additional FcεRIα engagement (Ho et al., 2007). Moreover, in other studies IL-33 was also shown to be expressed by keratinocytes and dermal fibroblasts upon UVB exposure (Byrne et al., 2011; Suhng et al., 2018) and improve survival of mast cells (Iikura et al., 2007; Wang et al., 2014). The here detected pro-survival activity of IL-33/ST2 can thus possibly contribute to mast cell accumulation in inflamed tissues. Furthermore, IL-33 signaling can modulate mast cell degranulation (Joulia et al., 2017; Jung et al., 2013; Nian et al., 2020). Although containing granules, bone marrow derived mast cells failed to degranulate (data not shown), therefore, degranulation was studied using peritoneal cell derived mast cells. Here, MyD88 deficient cells showed slightly decreased degranulation capacities after FcεRIα engagement, indicating that MyD88 might regulate degranulation (Figure 15). But, additional IL-33 stimulation with FcεRIα engagement together did not further modulate degranulation in these experiments. In contrast to the above-mentioned studies concerning the role of IL-33 in degranulation, the results from Ho et al. again resemble the results here, indicating that IL-33 is not able to further modulate mast cell degranulation *in vitro* (Ho et al., 2007). Moreover, ionomycin treatment should induce degranulation MyD88-independently, but this was not the case here. This suggests that MyD88 could be involved in granule formation itself and thus MyD88 mice could have generally lower degranulation capacities because of lower amounts of granules or less mature granules. Kaieda et al. reported that IL-33 treatment of mast cells contributes to their maturation (Kaieda et al., 2010), leading to the hypothesis that here, MyD88 deficient cells could contain more immature mast cell granules. The observed effect of decreased degranulation in MyD88 deficient PCMCs however was quite unstable, which is why these results have to be interpreted cautiously. However, in line with the *in vitro* findings on mast cell degranulation, the passive cutaneous anaphylaxis assay showed a MyD88-dependent reduction of the anaphylactic reaction (Figure 16), which can be explained by less efficient degranulation of mast cells and basophils. Anaphylaxis was again partially restored in mice with mast cell specific MyD88 induction. This suggests that MyD88 expression in mast cells, is important for the development of local anaphylaxis, validating the observed trends in PCMCs, but also that MyD88 signaling in other cell types like basophils is necessary since the anaphylactic reaction was not fully restored in MyD88^{Mcpt5IND} mice. Engagement of TLR2 or TLR4 together with FcεRI on BMMCs was reported to enhance cytokine production of BMMCs, without a potentiating effect on mast cell degranulation, whereas others showed that TLR2 ligation can induce mast cell degranulation (Qiao et al., 2006; Sandig

& Bulfone-Paus, 2012; Selander et al., 2009). Furthermore, IL-33 was found to play an essential role during passive cutaneous anaphylaxis as it is released by mast cells after degranulation and acts in an autocrine manner (Hsu et al., 2010). Especially in a later phase of anaphylaxis (>20 h) IL-33 dependent effects were evident since mice blocked with anti-ST2 and anti-IL-33 antibodies failed to develop skin inflammation (Hsu et al., 2010). All these studies show how several different MyD88-dependent pathways can aid the development of anaphylactic reactions, specifically IL-33 could be partially responsible in degranulation *in vivo*. Further examinations of the anaphylactic ear tissue would be useful to determine cytokines and visualize mast cells by microscopy to analyze in more detail how MyD88 deficiency affects the anaphylactic reaction.

Overall, BMMC developed normally in the absence of MyD88, although MCp numbers in the bone marrow were slightly reduced, indicating that mast cell development *in vivo* might be reduced in MyD88 KO mice. But, in functional assays MyD88 KO mast cells showed decreased activation, degranulation and survival, but only cytokine secretion and survival were IL-33-dependent, while degranulation occurred independent of IL-33 *in vitro*. One hallmark of mast cells is their ability to release preformed granules, which was impaired in MyD88 deficiency in the experimental model of passive cutaneous anaphylaxis. Re-expression of MyD88 expression in mast cells partially rescued this effect, which suggests that IL-33 or other alarmins could still influence degranulation *in vivo*.

5.2. IL-33 signaling affects keratinocyte proliferation and immune cell recruitment to UVB exposed skin

In the present work, IL-33 was shown to have a large impact on mast cell survival and activation in a MyD88-dependent manner, therefore non-responsiveness of MyD88 KO mice to IL-33 might be a cause for decreased mast cell accumulation in the skin after UVB exposure. IL-33 levels were elevated upon UVB exposure (Figure 17), similar to findings by Byrne et al. (Byrne et al., 2011), showing that elevated IL-33 levels could explain altered mast cell frequencies. To test if mast cells accumulate IL-33-dependently, IL-33 signaling was inhibited in UVB irradiated WT mice. Unexpectedly, these mice showed very comparable mast cell numbers in the back skin to irradiated IgG1 injected UVB exposed mice (Figure 18 B). Studies highlight, that IL-33 directly acts on mast cells resulting in increased proliferation *in vitro* and *in vivo* whereas other studies demonstrate that IL-33 rather sustains mast cell survival without

changing their proliferation rates (Saluja et al., 2014; Wang et al., 2014). Here as well, IL-33 driven mast cell survival was detected *in vitro*, an IL-33-dependent effect on mast cell accumulation however was not observed *in vivo*. Although, the mast cell numbers were very similar with and without IL-33 blockade, it is still possible that mast cells of irradiated and ST2 blocked mice are impaired in their maturation or functionality, similar to studies by Hsu et al. and Kaieda et al. (Hsu et al., 2010; Kaieda et al., 2010). Another likely explanation for the unchanged mast cell counts in UVB irradiated skin with and without ST2 blocking is that the accumulation could have already occurred at an earlier timepoint (between week 1 to week 3 of irradiation) before the injection of ST2 blocking antibodies was performed. Mast cells were indeed shown to accumulate in the dermis as early as 6 h after UV exposure (Byrne et al., 2008, 2015). Since mast cells are long-lived cells with a low turnover rate in steady-state (Gentek et al., 2018; Hatanaka et al., 1979; Kitamura et al., 1977, 1979), an early beginning of mast cell accumulation after UV irradiation could sustain in a long-term accumulation of mast cells in the skin. The exact dynamics of the dermal mast cell population after UVB exposure have not been assessed yet and should be the objective of future studies, to find out when accumulation occurs and how long it remains.

The blocking of IL-33 signaling did not affect UVB-induced mast cell accumulation, but regulated other cell types in the skin. Interestingly, ST2 blockade dampened keratinocyte proliferation and thus, the formation of acanthosis (Figure 18 C, Figure 19). An autocrine mechanism for IL-33 signaling in keratinocytes is already described in the model of imiquimod-induced psoriasis, in which IL-33 deficient mice display a reduced epidermal thickness compared to WT mice (Zeng et al., 2021), which correlates quite well with the results in the present work. Conversely, mice with inducible keratinocyte specific IL-33 overexpression have an increased epidermal and dermal thickness and also show enhanced mast cell accumulation in naïve skin compared to WT mice (Kurow et al., 2017). This furthermore supports the hypothesis that the time point at which mast cells react to IL-33 is important for their accumulation, since already two weeks after the induction of IL-33 overexpression the mast cell accumulation can be observed (Kurow et al., 2017).

Analysis of other immune cell types in the skin showed that blocking of IL-33 signaling during chronic UVB irradiation rather acts on inflammatory innate immune cells in the skin, but to a lesser extent on adaptive immune responses in the spleen and lymph nodes (Figure 20,Figure

21). Especially for neutrophils, macrophages and monocytes, IL-33 blocking reduced the UVB-induced increase of these populations and interestingly, neutrophils have also been shown to be in direct contact with IL-33 expressing fibroblasts of UVB irradiated skin (Byrne et al., 2011), hence blocking of IL-33 signaling could very well explain decreased neutrophil recruitment. Actually, IL-33 was shown to directly act on neutrophils to regulate CXCR2 expression on these cells, which will result in decreased migratory capacities (Artru et al., 2020). In addition to this direct effect of IL-33 on neutrophils, in the corneal epithelium, neutrophil recruitment was shown to be indirectly affected by mast cell-derived CXCL2, which is induced by IL-33 stimulation (Elbasiony et al., 2020). These two different modes of action of IL-33 on neutrophils could therefore explain the decreased recruitment in UVB irradiated skin during ST2 blockade. The IL-33/ST2 axis is known to polarize immune responses towards type 2 immunity. Apart from ILC2, eosinophils and Th2 cells, IL-33 has been shown to facilitate polarization of alternatively activated macrophages, which also are essential in type 2 immunity (Dagher et al., 2020; He et al., 2017; Kurowska-Stolarska et al., 2009). Here, macrophage frequencies were decreased in the skin of ST2 blocked mice, revealing that blockade of IL-33 signaling might affect macrophage survival or infiltration. In UV exposed skin, infiltrating macrophages have been identified as the main producers of IL-10, thus essentially promoting the generation of UV-induced tolerance (Kang et al., 1994; Toichi et al., 2008). Indeed, a recent report suggested that IL-33 indirectly supports the polarization of alternatively activated macrophages and thereby promotes immunosuppression (Finlay et al., 2020). This indirect effect is induced by mast cell-derived IL-6 and IL-13, which induces macrophage polarization (Finlay et al., 2020). In *in vitro* stimulated mast cells here, we also detected a strong induction of IL-6 and IL-13 upon IL-33 stimulation, indicating that in the IL-33 blocking experiments not only macrophage numbers are decreased, but also macrophage polarization might be disturbed and their regulatory role in inflammation might be reduced. Expectedly, γδ-T-cells in the skin were diminished after UVB-irradiation (Aberer et al., 1986), but only DETCs were further affected by the absence of IL-33 signaling, which reveals IL-33 as a cytokine that might maintain DETCs in the skin. IL-33 has been shown by others to stimulate and amplify numbers of γδ T-cells from human peripheral blood (Duault et al., 2016), this might as well be a possible mechanism in these experiments here for DETCs in the epidermis. Since keratinocytes in the skin are directly damaged by UVB exposure and DETCs are important for the recognition of damaged and stressed keratinocytes (Jameson et al., 2004),

it would be very interesting to investigate how IL-33 exactly affects keratinocyte activation. Despite the influence on their proliferation, absence of IL-33 in UVB irradiation might affect keratinocyte damage, which could have an impact on the interaction between keratinocytes and DETCs, similar to Jameson et al. (Jameson et al., 2004).

Studies showed that in different disease models IL-33 can suppress immune responses through the expansion of Tregs, either directly or indirectly, and thereby shape the course of disease (Schiering et al., 2014; Vasanthakumar et al., 2015). In this thesis however, blockade of IL-33 signaling in chronic UVB irradiation did not decrease Treg frequencies in secondary lymphoid organs. This implies that the UVB-induced mechanism of Treg expansion does not require IL-33 signaling in this experimental model, perhaps again earlier injection of anti-ST2 antibodies before week 4 might affect Treg expansion. Tregs execute immune suppression through different ways, one of them is the release of anti-inflammatory cytokines such as IL-10 (Sakaguchi et al., 2009). Apart from the Treg frequencies that were detected here, blockade of IL-33 might still affect Treg functionality and alter their immunosuppressive capacity. In the present thesis, Tregs were only measured based on FoxP3 expression. Inclusion of additional markers for the Treg population and staining for intracellular IL-10 would give more information about their immunosuppressive functions. Nevertheless, in line with the existing literature (Schwarz, 2005), the results shown here clearly demonstrate that chronic UVB irradiation induces Treg expansion, probably resulting in immune suppression.

In summary, although the *in vitro* results showed a remarkable impact of IL-33 on mast cells, ST2 blocking in chronic UVB irradiation did not alter dermal mast cell numbers, but affected the local immune response in the skin. IL-33 blocking diminished keratinocyte proliferation, which resulted in reduced epidermal hyperplasia and blocked innate immune cell infiltration to the skin, such as for neutrophils, monocytes and macrophages.

5.3. MyD88 signaling in mast cell-DC interactions

In this thesis, it was elucidated that IL-33 might not be the direct reason for mast cell accumulation in UVB exposed skin. UV exposure shapes many different cells and processes in the skin. In addition to the direct effects on mast cells, UV irradiation might also influence other cell types in the skin, which in turn might indirectly alter mast cell accumulation and function. Previous results showed that MyD88^{CCL17IND} mice, which express MyD88 in activated and mature DCs (Alferink et al., 2003), behaved like MyD88^{Mcpt5IND} mice and showed again a

higher mast cell accumulation upon UVB exposure compared to MyD88 KO mice (Opitz, 2016). Therefore, we reasoned that a possible crosstalk of DCs and mast cells might be crucial for the expansion of dermal mast cells, and that this crosstalk might as well occur MyD88-dependently. As a matter of fact, mast cell-DC interactions have been observed in skin in allergy and infection experiments, and as a consequence these crosstalks can modulate adaptive immune responses (Carroll-Portillo et al., 2015; Dudeck et al., 2019; Katsoulis-Dimitriou et al., 2020; Shelburne et al., 2009; Sumpter et al., 2019). Therefore, it was hypothesized that this kind of immune synapse formation might also emerge in UV exposed skin, but has not been described so far.

The analysis of mast cell-DC localization in the back skin and ear skin showed, that these cells interact with each other in MyD88 proficient, MyD88 KO and MyD88^{Mcpt5IND} mice (Figure 23). DCs were identified as MHCII expressing cells, although MHCII is not an exclusive DC marker. The use of a different DC marker or reporter mouse line would be more specific and should be utilized in future experiments if possible. But still, MHCII expression gives an impression about probable DC location in the skin. Mast cells have been shown to position in perivascular regions (Tong et al., 2015), which was confirmed in the present experiments here. Due to their perivascular localization, mast cells are able to extend their processes into the vessel lumen, probe vascular content and take up IgE antibodies, which is a central step for binding of IgE antibodies to mast cells (Cheng et al., 2013). Furthermore, dermal cDC2 have been shown to locate to perivascular regions as well and contribute to anaphylactic reactions by transferring captured allergens from the blood in microvesicles to mast cells in the surrounding tissue (Choi et al., 2018). However, the communication between these two cell types can also happen the other way from the mast cells to DCs. Mast cell-derived TNF-α was shown to boost DC maturation and migration, thus enhancing T-cell responses (Dudeck et al., 2015; Suto et al., 2006). Furthermore, similar effects on DCs were observed upon the uptake of secreted mast cell granules by DCs (Dudeck et al., 2019). Especially CD103^{+} DCs in the skin were found to be efficient in the engulfment of mast cell granules.

To study the crosstalk in more detail, co-cultures of mast cells and DCs were used to evaluate if the cell communication is altered in a MyD88-dependent fashion. Although mast cells usually do not express MHCII on the cell surface, the presence of DCs in these cultures induced a low proportion mast cells to be positive for MHCII, however independent of the stimulation and genotype (Figure 24). This finding suggests that DCs might transfer MHCII molecules to

mast cells, which would correspond to findings by Dudeck et al., who were able to show that DCs transfer antigen loaded MHCII molecules to mast cells *in vivo* (Dudeck et al., 2017). In our culture system lower MHCII levels were observed compared to published data (Dudeck et al., 2017). An explanation for this might be the 2D cell culture setting, a 3D setting would perhaps be more suitable for future studies to create an environment closer to the *in vivo* situation, where transfer of molecules between cells can be better studied (Sapudom et al., 2020).

Already in unstimulated co-cultures of mast cells and DCs the presence of mast cells affected DC activation (Figure 25). Cultures, in which MyD88 was expressed in mast cells even showed slightly enhanced activation marker expression on DCs. Additional stimulation of these co-cultures with LPS+CCL21 (Otsuka et al., 2011) or zymosan could furthermore increase DC activation, but the presence of mast cells did then not further affect DC activation. Expectedly, stimulation with LPS+CCL21 or zymosan upregulated the expression of activation markers. CD40 and MAR1 expression were higher in MyD88 proficient DCs, but surprisingly CD86 and MHCII showed rather no differences or were even upregulated in MyD88 deficient DCs. Since LPS signals via TLR4, which can use both, MyD88 and TRIF as adaptor proteins (Kawai et al., 2001; Yamamoto et al., 2002), it is very likely that in the absence of MyD88, TRIF dependent signaling takes over and partially compensates for MyD88 deficiency. Also, a different time kinetic for CD86 expression in MyD88 deficient DCs is described (Shen et al., 2008), which could explain this observation. Shen et al. demonstrate that CD86 expression peaks 6 h after LPS stimulation in WT BMDC, while MyD88 KO BMDC still show sustained CD86 expression until 24 h after stimulation (Shen et al., 2008), which would be an explanation for increased CD86 expression in these co-cultures that were stimulated for 24 h as well. After zymosan stimulation, the increased expression of CD86 and MHCII in MyD88 KO BMDCs became even more evident. Zymosan is a TLR2 and Dectin-1 ligand, therefore zymosan-induced signaling can only be partially awarded to MyD88-dependent signaling pathways (Gantner et al., 2003). MyD88 deficient adipose tissue macrophages for example have been shown to upregulate Dectin-1 levels on their cell surface (Castoldi et al., 2017). If this Dectin-1 upregulation in MyD88 deficient mice would also exist in DCs, possibly more Dectin-1-dependent signaling might occur and explain why MyD88 KO cells express higher CD86 and MHCII levels after zymosan stimulation. Further investigations are required to determine if a direct contact between mast cells and DCs is necessary to influence each other's activation, or if soluble mast cell-derived mediators are sufficient to cause DC activation.

Taken together, these experiments highlighted that DCs and mast cells can interact *in vitro* and thus modify cell activation, which might have also functional consequences *in vivo*. The impact of MyD88 here however was minor in mast cell-DC co-cultures without stimulation, but positively correlated with DC activation when MyD88 was expressed in mast cells.

5.4. MyD88 signaling in immune suppression and photocarcinogenesis

UV exposure is a major risk factor for the development of skin cancer. The DNA damaging and immunosuppressive effects of UV light both promote a skin environment in which tumor development is facilitated (Hart & Norval, 2018). Therefore, it is of high interest to understand how innate immune signaling and mast cells contribute to immune suppression and later on also to tumor formation in the skin.

5.4.1. UVB exposure induces immune suppression MyD88-independently

Immunosuppression describes a state in which the immune reaction towards dangerous substances or pathogens is dampened. In autoimmune diseases or organ transplantation, this is a very desirable reaction, in other diseases however a suppressed immune system is detrimental, impedes the immune system and thus promotes disease or cancer. In the present work, UV-induced immunosuppression was studied in CHS, which is a model for an allergic skin reaction and commonly used to study immunosuppression (Kim et al., 1998; Schwarz et al., 2005). In this model, UVB exposure induced the expansion of Tregs, which mediate immunosuppression in the subsequent CHS reaction. UVB irradiation prior to the CHS reaction was able to suppress the ear swelling response in all genotypes independent of MyD88 signaling (Figure 26). On cellular level however, the differences in the immune cell numbers between non-irradiated and UVB irradiated mice were rather small, which makes it difficult to trace the reduction of the ear swelling response back to one single cell type. In general, it was observed that UVB exposure slightly increased the neutrophil cell population, while at the same time inducing expansion of Tregs, B-cells, as well as reducing T-cell activation, DETCs, and monocytes in DNFB treated ears (Figure 28,Figure 30). Intriguingly, MyD88 deficient mice showed enhanced skin inflammation compared to MyD88 proficient and MyD88^{Mcpt5IND} mice. This observation coincides very well with previous results from our group, revealing that MyD88 KO mice show a slightly increased ear swelling response compared to WT mice in CHS reactions without prior UVB exposure (Thomanek, 2020, unpublished data). Different studies that examined the role of MyD88, TLRs and IL-1 receptors during CHS showed that these

proteins are important for the development of the CHS response, since mice deficient in these molecules showed reduced ear swelling (Klekotka et al., 2010; Martin et al., 2008). On the contrary, MyD88 deficient non-obese diabetic (NOD) mice have been shown to develop an exaggerated CHS response compared to WT NOD mice, because of enhanced DC migration and activation behaviour in the absence of MyD88 (Szczepanik et al., 2018). Moreover, comparing mice in SPF and germ-free animal housing conditions revealed that the ear swelling response during CHS is very similar (Patra et al., 2018). But, with prior UV exposure the loss of microbiome-derived signals in germ-free mice, which can engage TLR signaling, induces more immunosuppression (Patra et al., 2018). Another study however described that MyD88 deficient mice are resistant against UV-induced immune suppression, but unirradiated MyD88 KO mice have a very similar ear swelling response compared to WT mice (Harberts et al., 2015). All these studies show quite contradictory results for the role of MyD88 signaling in CHS, which can possibly be explained by different mouse strains that were utilized, changes in microbiome and slight differences in the experimental protocol. Similar to Harberts et al. and Patra et al., here we could show that the inflammatory response is not impaired, even slightly enhanced, in non-irradiated MyD88 mice. But in contrast to these studies, UV exposure was able to generate immunosuppression independent of MyD88 signaling.

Mast cells have been shown to mediate immunosuppression, e.g. through CXCR4/CXCL12 dependent mast cell migration to the lymph nodes upon UVB irradiation (Byrne et al., 2008; Chacón-Salinas et al., 2011; Guhl et al., 2005; Hart et al., 2000). In these experiments here, immune suppression appeared to be independent of MyD88 signaling in mast cells, and although mast cell numbers were remarkably reduced in MyD88 deficient mice, they still displayed immunosuppression. These findings indicate that an impaired mast cell expansion upon UVB irradiation is not the main mechanism for the induction of immunosuppression, but it still can be associated to an increased CHS response in MyD88 KO mice, similar to findings from Reber and colleagues (Reber et al., 2017). In CHS however, the role of mast cells has not only been described as protective, but also as pro-inflammatory (Dudeck et al., 2011; Gimenez-Rivera et al., 2016; Norman et al., 2008; Reber et al., 2017). The increased skin inflammation in MyD88 KO mice can also be explained by an expansion of neutrophils and Ly6C^{-} MHCII^{+} moDCs, albeit the mast cell population was reduced. Furthermore, a study conducted by Schweintzger and colleagues highlighted the importance of mast cells in UV-induced itch, in that study mast cell deficient mice exhibited increased scratching behaviour,

furthermore underlining the protective role of mast cells in the skin (Schweintzger et al., 2015). Possibly, the decreased mast cell numbers in MyD88 KO mice might be accounted for increased inflammation due to enhanced scratching behaviour in these mice, which is consistent with the increased experimental scores of MyD88 KO mice during long-term UVB irradiation (see 4.6.1). As a consequence, more neutrophils and monocytes/moDCs might infiltrate the skin and exaggerate CHS symptoms. Enhanced neutrophil infiltration to the skin was moreover associated with better moDC recruitment and more efficient initiation of adaptive immunity (Megiovanni et al., 2006), possibly explaining the increased inflammation in MyD88 KO mice. In future experiments, the hypothesis of increased scratching behaviour of MyD88 KO mice should be examined more closely.

In CHS, DETCs become activated by keratinocytes and both, DETCs and dermal γδ T-cells contribute to skin inflammation (Jiang et al., 2017; Nielsen et al., 2014). Interestingly, UVB treatment induced DETC depletion from the ears, and DNFB treatment furthermore induced their reduction in the ear skin, similar to Nielsen et al. (Nielsen et al., 2014). IL-1β has been shown to activate DETCs in CHS (Nielsen et al., 2014) and is known to signal via MyD88, therefore it would be of high interest to study if also DETC activation is impaired in MyD88 KO mice. MyD88 proficient mice lacked a UVB-induced decrease of DETCs in vehicle treated ears, naïve mice however showed very comparable DETC numbers compared to the other genotypes (data not shown), indicating that this result might derive from experimental variations. In contrast, dermal γδ T-cells expanded drastically upon DNFB, the largest population was observed in MyD88 KO mice. Consistent with the increased neutrophil numbers, dermal γδ T-cells were shown to contribute to the CHS response by secretion of IL-17, which leads to increased neutrophil infiltration to the skin (Jiang et al., 2017), which was also observed here. A similar effect was detected for the conventional T-cell population, in which as expected, $CD4^+$ and $CD8^+$ T-cells both expanded upon DNFB treatment. Although CHS is known as a mainly $CD8^+$ driven T-cell disease, $CD4^+$ T-cells also contribute to the pathology (Wang et al., 2000) and were even present in higher in number in the present experiments (data not shown). Interestingly, UVB exposure elevated numbers of Tregs and B-cells, potentially Bregs, in the skin. Circulatory Tregs have been reported to traffic between the skin and skin-draining lymph nodes in steady-state and during CHS to supress inflammation in the ear skin (Tomura et al., 2010), UV-induced Tregs however were shown not to home to ear skin in the elicitation phase of CHS reactions as they lack skin-homing receptors, but they rather

mediate immunosuppression by modifying APCs in the sensitization phase (Schwarz et al., 2004, 2007). Hence, increased Treg numbers in the ear skin here might be explained by the fact that these ears were not covered and have been exposed to the UVB irradiation. In a different approach to study these UV-induced Tregs in the ear and to analyze whether trafficking between the skin-draining lymph nodes and the ear skin actually occurs would therefore be to only expose the skin area to the UVB-light, which is going to be sensitized, rather than both the sensitization and the to be challenged skin. Furthermore, the sensitization phase of the CHS reaction should be studied in more detail in order to measure if there are alterations in sensitization efficiency in MyD88 deficient mice. Although, MyD88 KO mice displayed the highest Treg numbers, UVB irradiation was not able to further increase this population, indicating that absence of MyD88-dependent pathways promotes generation of Tregs even without any contribution of UVB irradiation. According to a study, MyD88 signalling was actually shown to promote Treg generation and tolerance (Hoff et al., 2018), in contrast to the findings in the present thesis. Aside from Tregs, Bregs are induced by UVB exposure and contribute to immunosuppression through secretion of IL-10. Moreover, TLR4 was linked to Breg induction, suggesting that MyD88 could be involved in this process (Wang et al., 2017), but here the absence of MyD88 signaling did not affect B-cell numbers in the skin. But it might still have functional consequences in Breg activity. Therefore, future studies on this cell population should include additional markers to clearly identify these regulatory cells.

UVB irradiated and DNFB treated MyD88 proficient mice showed strongly decreased immune cells in the aLN compared to other DNFB treated mice (Figure 32), which might be attributed to a less effective sensitization of these mice and therefore less proliferation, or to a smaller group size since these mice actually did not show less skin inflammation than MyD88^{Mcpt5IND} mice for instance. But other than that, UVB irradiation did not suppress lymphocyte numbers in DNFB treated skin of MyD88 KO an MyD88^{Mcpt5IND} mice. In the skin-draining aLN, UVB exposure interestingly reduced T-cell activation, as detected by the decreased frequency of antigen-experienced CD4$^+$ EM, CM T-cells and CD69$^+$ T-cells and increased frequency of naïve T-cells, indicating furthermore that immunosuppression did not depend on MyD88 signaling. Similar observations were made for CD8$^+$ memory T-cell populations and in general, CD4$^+$ and CD8$^+$ T-cells were massively decreased in number in UVB-treated mice (data not shown). This is very consistent with findings from Rana and colleagues, who revealed that UVB exposure

reduces effector $CD4^+$ and $CD8^+$ T-cells in the skin draining lymph nodes after sensitization and reduces $CD8^+$ memory cells in the skin (Rana et al., 2008).

In general, immune cell populations of $MyD88^{Mcpt5IND}$ mice behaved slightly different than in MyD88 proficient and MyD88 KO mice. Less immune cells were detected in the skin of DNFB treated mice in almost all populations, except for mast cells and DETCs, compared to the other genotypes. The immune response in the lymph nodes however was very comparable to MyD88 KO mice. This suggests that mast cell-specific MyD88 signalling partially dampens the enhanced skin inflammation of full MyD88 deficiency but has rather no effect on the adaptive immune response in the aLN.

Overall, in these experiments UVB irradiation was able to induce immunosuppression independent of MyD88 signalling. I suppose that the balance between regulatory and inflammatory cells is of importance to determine immunosuppression in a way that the suppressive regulatory cells inhibit adaptive immune responses in the skin and lymph node and inhibit the UVB-induced low-grade inflammation. Future studies should also focus on the different phases in CHS to identify whether the observed changes derive from defects in sensitization or from the elicitation response upon secondary exposure to DNFB.

5.4.2. MyD88 signalling protects from photocarcinogenesis

UV-induced inflammation, DNA damage, and the suppression of immune responses together promote photocarcinogenesis. In this thesis, the development of skin tumors after long-term UVB exposure of 33 weeks was tracked, which was increased by number and began to develop earlier in MyD88 deficient and $MyD88^{Mcpt5IND}$ mice compared to MyD88 proficient animals (Figure 33). In addition, a decreased epidermal thickness was observed in MyD88 KO mice, which was restored to MyD88 proficient levels in $MyD88^{Mcpt5IND}$ animals (Figure 34 B), again supporting that the UV-induced cytokines like IL-33, might affect keratinocyte proliferation (Zeng et al., 2021), similar to the observations here in the IL-33 blocking experiments. Previous experiments from our group showed that after chronic UVB irradiation MyD88 KO mice had decreased expression levels of DNA repair enzymes and elevated levels of DNA damage (Opitz, 2016). So together with the here observed decreased acanthosis, increased DNA damage might be accounted for the higher incidence of tumors in MyD88 KO mice. Interestingly, mast cell specific MyD88 expression was able to reduce the tumor burden, indicating that mast cell

derived cytokines and mediators might regulate immune responses in the skin to protect from carcinogenesis as already described by Siebenhaar et al. (Siebenhaar et al., 2014). Some studies show that MyD88/IL-1R/TLR signaling rather induces skin carcinogenesis, while prevention of inflammation in the absence of these proteins protects from tumors (Cataisson et al., 2012; Mittal et al., 2010). In these two studies, skin carcinogenesis was chemically induced by 7,12-dimethylbenz[a]anthracene (DMBA) and 12-O-tetradecanoylphorbol-13-acetate (TPA), other than in the present experiments. In these models, DMBA induces mutations in genes such as in tumor suppressor genes, while repeated TPA application leads to tissue inflammation, thereby promoting carcinogenesis (Abel et al., 2009). Thus, it might be the case that this model relies to a larger extent on tissue inflammation, which could be mediated by MyD88, than the model of photocarcinogenesis that was used here. In human squamous cell carcinoma samples, however a tumor suppressing role of TLR4 was confirmed (Mikami et al., 2019), which would correspond to the results in photocarcinogenesis. In ongoing investigations, the tumor tissue is analyzed in more detail, to check whether MyD88 deficiency alters the prevalence of a certain type of tumor, especially of squamous cell carcinoma.

In contrast to chronic irradiation, mast cell numbers were generally increased, but no changes were observed between the genotypes and between control and UVB-irradiated skin in the photocarcinogenesis experiment (Figure 34 D). At the time of analysis, mice were around 40-43 weeks old and are therefore considered as aged in comparison to the mice that were analyzed in chronic 6-week UVB irradiation experiments. Indeed, it is known that aged photoprotected skin as well as chronic sun exposed skin similarly show an increase of mast cells and that this accumulation can contribute to altered immune reactions and tissue homeostasis (Grimbaldeston et al., 2003; Pilkington et al., 2019). But, surprisingly, in this thesis I could not observe a cumulative effect of UVB exposure and age on the mast cell numbers and moreover, the previously observed MyD88-dependent effect in mast cell accumulation was lost. This was also the case in the IL-33 blocking experiment, where additional IL-33 blocking was not able to further modulate mast cell accumulation. A potential explanation for this might be a strong effect of skin aging on the mast cells, which cannot be further enhanced by innate immune signaling events. TSLP is upregulated by keratinocytes upon UVB exposure and is associated with protective functions in skin carcinogenesis (Di Piazza et al., 2012), which is contrasting the results in the present work as MyD88 KO mice

show the highest TSLP levels, but are also more susceptible to tumor development. Similarly, Didovic et al. were able to measure elevated TSLP levels in MyD88 deficient mice, and revealing keratinocytes as the main source of TSLP in the skin (Didovic et al., 2016). Studies show that keratinocyte-derived TNF-α acts on keratinocytes in an autocrine way and increases DNA damage after UVB exposure and thereby potentially promotes carcinogenesis (Faurschou, 2010; Moore et al., 1999). Furthermore, the anti-inflammatory cytokine IL-10 is associated with immunosuppression and tumor development in the skin (Loser et al., 2007), but interestingly was not further upregulated in UVB exposed skin. Both, TNF-α and IL-10, were expressed highest in MyD88 KO skin, which could contribute to increased tumor numbers in MyD88 deficient mice (Figure 35).

MyD88 KO mice also showed a distinct immune cell composition in UVB exposed skin (Figure 36). While DETCs were almost entirely depleted in UVB exposed skin in all genotypes, dermal γδ T-cells and conventional T-cells rather expanded in MyD88 proficient and MyD88^{Mcpt5IND} mice, but not in MyD88KO mice. Interestingly, DETCs limit DNA damage in UVB exposed skin and thus have protective functions in carcinogenesis (Cavanagh et al., 1997; MacLeod et al., 2014). A UVB-induced reduction of DETCs that was detected here might therefore contribute to higher tumor development. Moreover, DETCs are known to be activated by UV irradiation and in consequence release cytokines (MacLeod et al., 2014). Since DETC activation might already occur before their depletion, MyD88-dependent effects in DETC activation cannot be entirely ruled out and require further analysis at earlier time points.

UVB induced the expansion of Tregs in the skin and MyD88 KO animals had the highest frequency, potentially implying that MyD88 deficiency might enhance immune suppressive Treg development and thus further support tumor progression. In addition, this observation also correlates with increased Treg numbers of MyD88 KO mice in the immunosuppression experiments. Although the reduction of the ear swelling response was similar in all genotypes, it could be possible that long-term UVB exposure of 33 weeks induces more immunosuppression in MyD88 KO mice, than 4 days of exposure such as in the immunosuppression experiments. In line, frequencies of naïve CD4$^+$ T-cells in the bLN were slightly higher while EM CD4$^+$T-cells were minimally lower in MyD88 KO mice, furthermore suggesting a role for MyD88 in T-cell activation and immune suppression. However, differences between the genotypes regarding immune cells in the bLN were rather low.

As another aspect, the experiments in this thesis point out the importance of MyD88 signaling in the emergence of skin tumors, likely due to increased inflammation. A study by Harberts et al. shed light on the question how MyD88 deficiency can lead to increased inflammation (Harberts et al., 2014). They described decreased apoptotic cell death of MyD88 deficient macrophages after UV irradiation *in vitro*, necroptosis (programmed necrosis) however was shown to be more prominent in the absence of MyD88. Necroptotic cell death is associated with aging/inflammaging and results in the release of DAMPs and therefore contributes to inflammation, as a measure of this process TNF-α release was detected by Harberts et al., and interestingly the release was increased in MyD88 KO cells (Harberts et al., 2014; Royce et al., 2019). The observations in the present study showed a similar increase of TNF-α in MyD88 KO mice, which could mean that necroptosis might be higher in these mice as well. But this hypothesis would require more detailed analysis to determine the exact cause. The elevated TNF-α expression moreover correlates to increased photocarcinogenesis, enhanced ear inflammation in CHS and also higher experimental scores of MyD88 KO mice in the experiment of photocarcinogenesis. Taken together, other effects that were observed in previous and the present work, like enhanced DNA damage (Opitz, 2016), less acanthosis and potentially slightly more immunosuppression can together with the more pronounced skin inflammation be considered as some of the main reason for increased tumor formation in MyD88 KO mice.

6. Summary

Excessive UV irradiation is a major risk factor for health. While chronic long-term UV exposure induces skin aging and suppression of the immune system, acute UV exposure leads to skin inflammation, also known as sunburn. In the long-term however, both forms of exposure can be detrimental and contribute to the development of skin cancer. UV-induced danger-associated molecular patterns (DAMPs) are thereby generated and mediate inflammation by signaling through toll-like receptors (TLRs) and IL-1 receptor family proteins, among which most receptors use MyD88 as an adaptor protein to transduce intracellular signaling. In chronic UVB irradiation, an important role for mast cell-specific MyD88 signaling was described which affected UV-induced mast cell accumulation.

In this thesis, it was shown that MyD88 is important for the activation and survival of *in vitro* generated mast cells and that especially IL-33 treatment of mast cells enhances these functions. *In vivo* blocking of the IL-33 receptor ST2 in chronic UVB irradiation of mice however did not change mast cell accumulation, but affected local skin immune cells, as well as keratinocytes and their proliferative potential, thus regulating acanthosis. Since IL-33 was not the cause for mast cell accumulation, next, the interaction between mast cells and DCs was studied because UV-induced indirect effects might also influence mast cell accumulation. It could be shown that in the skin, these two cell types are located in close proximity to each other and that DCs transfer MHCII molecules to mast cells. Moreover, MyD88 expression in mast cells elevated DC activation in mast cell-DC co-cultures, revealing that MyD88 in mast cells can regulate DC functions and potentially modulate T-cell responses. UVB exposure induced the expansion of Tregs, which are crucial in mediating immunosuppression. In the model of UV-induced immune suppression, UVB irradiation was able to reduce skin inflammation independent of MyD88. Interestingly, MyD88 deficiency led to increased inflammation due to a higher density of neutrophils, monocytes and moDCs in the skin. After long-term UVB irradiation, MyD88 KO mice showed accelerated tumor development compared to MyD88 proficient mice, which was partially rescued by mast cell specific MyD88 expression.

Overall, in this thesis, the importance of MyD88 for appropriate mast cell functions was highlighted and was shown to alter the immune responses in UV-induced diseases.

Zusammenfassung

Intensive UV-Strahlung stellt einen wesentlichen Risikofaktor für die Gesundheit dar. Chronische UV-Exposition führt zu vorzeitiger Hautalterung und trägt zur Immunsuppression bei, während akute UV-Exposition eine Entzündung der Haut auslöst, welche auch als Sonnenbrand bekannt ist. Beide Formen der UV-Exposition können langfristig zur Hautkrebsentstehung führen. Bei Bestrahlung der Haut mit UVB entstehen sterile Gefahrensignale (DAMPs), welche über *toll-like* Rezeptoren (TLRs) und über die IL-1 Rezeptorfamilie Entzündung vermitteln. Das Adaptorprotein MyD88 wird von den meisten dieser Rezeptoren für die intrazelluläre Signaltransduktion verwendet und spielt so eine zentrale Rolle im angeborenen Immunsystem. In früheren Arbeiten wurde der mastzellspezifischen MyD88 Signaltransduktion eine wichtige Rolle zugeschrieben, da sie die Mastzellakkumulation bei chronischer UVB Bestrahlung beeinflusste.

In der hier vorliegenden Arbeit konnte gezeigt werden, dass MyD88 wichtig für die Aktivierung und das Überleben *in vitro* generierter Mastzellen ist, wobei vor allem IL-33 Stimulation diese Funktionen besonders verstärkte. Die Blockierung des IL-33 Signalwegs bei chronischer UVB Bestrahlung zeigte *in vivo* jedoch keine Auswirkungen auf die Anzahl der Mastzellen in der Haut, verminderte jedoch die Proliferation von Keratinozyten und reduzierte die Eiwanderung inflammatorischer Immunzellen in die Haut. Zudem wurde die Interaktion zwischen Mastzellen und dendritischen Zellen (DC) untersucht, da neben direkten Auswirkungen, auch indirekt weitere Zellen nach UVB-Exposition die Mastzellakkumulation verursachen können. Mastzellen und DC konnten in der Haut in der Nähe zueinander lokalisiert werden, und in Co-Kulturen *in vitro* waren Mastzellen in der Lage die DC Aktivierung MyD88-abhängig leicht zu verstärken. Dies lässt vermuten, dass MyD88 auch bei diesen Interaktionen eine Rolle spielt und DC Aktivierung regulieren könnte und sich somit auf eine T-Zell Aktivierung auswirken könnte. UVB-Exposition erhöhte außerdem die Entstehung regulatorischer T-Zellen (Treg), welche eine Immunsuppression vermitteln. Im Modell der UV-induzierten Immunsuppression zeigte sich, dass MyD88 keine Rolle in der Entstehung einer solchen Immunsuppression zu spielen scheint. Interessanterweise zeigten MyD88 defiziente Mäuse aber eine generell verstärkte Entzündungsreaktion, welche sich auf eine erhöhte Infiltration von Neutrophilen und Monozyten zurückführen lässt. Im Modell der Photokarzinogenese zeigten MyD88 defiziente Mäuse außerdem eine früher einsetzende Entstehung und eine höhere Anzahl an Tumoren im Vergleich zu MyD88 profizienten Mäusen. Mäuse mit mastzellspezifischer MyD88

Expression waren hierbei jedoch wieder teilweise geschützt, was auf eine wichtige Rolle MyD88-abhängiger Signalwege bei der Tumorentstehung hindeutet. Zusammenfassend wurde die Relevanz MyD88-abhängiger Signalwege in Mastzellen beleuchtet und untersucht, wie diese bei UV-Exposition der Haut zur Immunsuppression und Tumorentstehung beitragen.

7. References

Abel, E. L., Angel, J. M., Kiguchi, K., & DiGiovanni, J. (2009). Multi-stage chemical carcinogenesis in mouse skin: Fundamentals and applications. *Nature Protocols*, *4*(9), 1350–1362.

Aberer, W., Romani, N., Elbe, A., & Stingl, G. (1986). Effects of physicochemical agents on murine epidermal Langerhans cells and Thy-1-positive dendritic epidermal cells. *The Journal of Immunology*, *136*(4), 1210–1216.

Agier, J., Pastwińska, J., & Brzezińska-Błaszczyk, E. (2018). An overview of mast cell pattern recognition receptors. *Inflammation Research*, *67*(9), 737–746.

Akira, S., Uematsu, S., & Takeuchi, O. (2006). Pathogen recognition and innate immunity. *Cell*, *124*(4), 783–801.

Alferink, J., Lieberam, I., Reindl, W., Behrens, A., Weiß, S., Hüser, N., Gerauer, K., Ross, R., Reske-Kunz, A. B., Ahmad-Nejad, P., Wagner, H., & Förster, I. (2003). Compartmentalized production of CCL17 in vivo: Strong inducibility in peripheral dendritic cells contrasts selective absence from the spleen. *Journal of Experimental Medicine*, *197*(5), 585–599.

Ali, N., Zirak, B., Rodriguez, R. S., Pauli, M. L., Truong, H. A., Lai, K., Ahn, R., Corbin, K., Lowe, M. M., Scharschmidt, T. C., Taravati, K., Tan, M. R., Ricardo-Gonzalez, R. R., Nosbaum, A., Bertolini, M., Liao, W., Nestle, F. O., Paus, R., Cotsarelis, G., … Rosenblum, M. D. (2017). Regulatory T Cells in Skin Facilitate Epithelial Stem Cell Differentiation. *Cell*, *169*(6), 1119–1129.

Amano, S. (2016). Characterization and mechanisms of photoageing-related changes in skin. Damages of basement membrane and dermal structures. *Experimental Dermatology*, *25*, 14–19.

Amôr, N. G., de Oliveira, C. E., Gasparoto, T. H., Boas, V. G. V., Perri, G., Kaneno, R., Lara, V. S., Garlet, G. P., Silva, J. S. da, Martins, G. A., Hogaboam, C., Cavassani, K. A., & Campanelli, A. P. (2018). ST2/IL-33 signaling promotes malignant development of experimental squamous cell carcinoma by decreasing NK cells cytotoxicity and modulating the intratumoral cell infiltrate. *Oncotarget*, *9*(56), 30894–30904.

Artru, F., Bou Saleh, M., Maggiotto, F., Lassailly, G., Ningarhari, M., Demaret, J., & Ntandja-Wandji, L.-C. (2020). IL-33/ST2 pathway regulates neutrophil migration and predicts outcome in patients with severe alcoholic hepatitis. To cite this version. *Journal of Hepatology*, *72*(6), 1052–1061.

Bachem, A., Güttler, S., Hartung, E., Ebstein, F., Schaefer, M., Tannert, A., Salama, A., Movassaghi, K., Opitz, C., Mages, H. W., Henn, V., Kloetzel, P. M., Gurka, S., & Kroczek, R. A. (2010). Superior antigen cross-presentation and XCR1 expression define human CD11c+CD141+ cells as homologues of mouse CD8+ dendritic cells. *Journal of Experimental Medicine*, *207*(6), 1273–1281.

Bech-Thomsen, N., & Wulf, H. C. (1995). Photoprotection due to pigmentation and epidermal thickness after repeated exposure to ultraviolet light and psoralen plus ultraviolet A therapy. *Photodermatology, Photoimmunology & Photomedicine*, *11*(5–6), 213–218.

Belkaid, Y., & Hand, T. W. (2014). Role of the microbiota in immunity and inflammation. *Cell*, *157*(1), 121–141.

Bernard, J. J., Gallo, R. L., & Krutmann, J. (2019). Photoimmunology: how ultraviolet radiation affects the immune system. *Nature Reviews Immunology*, *19*(11), 688–701.

Bosteels, C., Neyt, K., Vanheerswynghels, M., van Helden, M. J., Sichien, D., Debeuf, N., De Prijck, S., Bosteels, V., Vandamme, N., Martens, L., Saeys, Y., Louagie, E., Lesage, M., Williams, D. L., Tang, S. C., Mayer, J. U., Ronchese, F., Scott, C. L., Hammad, H., … Lambrecht, B. N. (2020). Inflammatory Type 2 cDCs Acquire Features of cDC1s and Macrophages to Orchestrate Immunity to Respiratory Virus Infection. *Immunity*, *52*(6), 1039–1056.

Bouladoux, N., Hennequin, C., Malosse, C., Malissen, B., Belkaid, Y., & Henri, S. (2017). Hapten-specific T cell-mediated skin inflammation: Flow cytometry analysis of mouse skin inflammatory infiltrate. *Methods in Molecular Biology*, *1559*, 21–36.

Byrne, S. N., Beaugie, C., O'Sullivan, C., Leighton, S., & Halliday, G. M. (2011). The immune-modulating cytokine and endogenous alarmin interleukin-33 is upregulated in skin exposed to inflammatory UVB radiation. *American Journal of Pathology*, *179*(1), 211–222.

Byrne, S. N., Hammond, K. J. L., Chan, C. Y. Y., Rogers, L. J., Beaugie, C., Rana, S., Marsh-Wakefield, F., Thurman, J. M., & Halliday, G. M. (2015). The alternative complement component factor B regulates UV-induced oedema, systemic suppression of contact and delayed hypersensitivity, and mast cell infiltration into the skin. *Photochemical and Photobiological Sciences*, *14*(4), 801–806.

Byrne, S. N., Limón-Flores, A. Y., & Ullrich, S. E. (2008). Mast Cell Migration from the Skin to the Draining Lymph Nodes upon Ultraviolet Irradiation Represents a Key Step in the Induction of Immune Suppression. *The Journal of Immunology*, *180*(7), 4648–4655.

Cadet, J., & Douki, T. (2018). Formation of UV-induced DNA damage contributing to skin cancer development. *Photochemical and Photobiological Sciences*, *17*(12), 1816–1841.

Carroll-Portillo, A., Cannon, J. L., te Riet, J., Holmes, A., Kawakami, Y., Kawakami, T., Cambi, A., & Lidke, D. S. (2015). Mast cells and dendritic cells form synapses that facilitate antigen transfer for T cell activation. *Journal of Cell Biology*, *210*(5), 851–864.

Castoldi, A., Andrade-Oliveira, V., Aguiar, C. F., Amano, M. T., Lee, J., Miyagi, M. T., Latância, M. T., Braga, T. T., da Silva, M. B., Ignácio, A., Carola Correia Lima, J. D., Loures, F. V., Albuquerque, J. A. T., Macêdo, M. B., Almeida, R. R., Gaiarsa, J. W., Luévano-Martínez, L. A., Belchior, T., Hiyane, M. I., … Câmara, N. O. S. (2017). Dectin-1 Activation Exacerbates Obesity and Insulin Resistance in the Absence of MyD88. *Cell Reports*, *19*(11), 2272–2288.

Castoldi, A., Braga, T. T., Correa-Costa, M., Aguiar, C. F., Bassi, Ê. J., Correa-Silva, R., Elias, R. M., Salvador, F., Moraes-Vieira, P. M., Cenedeze, M. A., Reis, M. A., Hiyane, M. I., Pacheco-Silva, Á., Gonçalves, G. M., & Câmara, N. O. S. (2012). TLR2, TLR4 and the Myd88 signaling pathway are crucial for neutrophil migration in acute kidney injury induced by sepsis. *PLoS ONE*, *7*(5), 1–14.

Cataisson, C., Salcedo, R., Hakim, S., Moffitt B. Andrea, A., Wright, L., Yi, M., Stephens, R., Dai, R. M., Lyakh, L., Schenten, D., Yuspa, H. S., & Trinchieri, G. (2012). IL-1R-MyD88 signaling in keratinocyte transformation and carcinogenesis. *Journal of Experimental Medicine*, *209*(9), 1689–1702.

Cavanagh, L. L., Barnetson, R. S., Basten, A., & Halliday, G. M. (1997). Dendritic epidermal T-cell involvement in induction of CD8+ T cell-mediated immunity against an ultraviolet radiation-induced skin tumor. *International Journal of Cancer*, *70*(1), 98–105.

Chacon-Salinas, R., Chen, L., Chavez-Blanco, A. D., Limon-Flores, A. Y., Ma, Y., & Ullrich, S. E. (2014). An essential role for platelet-activating factor in activating mast cell migration following ultraviolet irradiation. *Journal of Leukocyte Biology*, *95*(1), 139–148.

Chacón-Salinas, R., Limón-Flores, A. Y., Chávez-Blanco, A. D., Gonzalez-Estrada, A., & Ullrich, S. E. (2011). Mast Cell-Derived IL-10 Suppresses Germinal Center Formation by Affecting T Follicular Helper Cell Function. *The Journal of Immunology*, *186*(1), 25–31.

Chen, C. C., Grimbaldeston, M. A., Tsai, M., Weissman, I. L., & Galli, S. J. (2005). Identification of mast cell progenitors in adult mice. *Proceedings of the National Academy of Sciences of the United States of America*, *102*(32), 11408–11413.

Chen, W. Y., Tsai, T. H., Yang, J. L., & Li, L. C. (2018). Therapeutic Strategies for Targeting IL-33/ST2 Signalling for the Treatment of Inflammatory Diseases. *Cellular Physiology and Biochemistry*, *49*(1), 349–358.

Cheng, L. E., Hartmann, K., Roers, A., Krummel, M. F., & Locksley, R. M. (2013). Perivascular Mast Cells Dynamically Probe Cutaneous Blood Vessels to Capture Immunoglobulin E. *Immunity*, *38*(1), 166–175.

Choi, H. W., Suwanpradid, J., Kim, I. H., Staats, H. F., Haniffa, M., MacLeod, A. S., & Abraham, S. N. (2018). Perivascular dendritic cells elicit anaphylaxis by relaying allergens to mast cells via microvesicles. *Science*, *362*(6415), 1–11.

Choi, Y. S., Park, J. A., Kim, J., Rho, S. S., Park, H., Kim, Y. M., & Kwon, Y. G. (2012). Nuclear IL-33 is a transcriptional regulator of NF-κB p65 and induces endothelial cell activation. *Biochemical and Biophysical Research Communications*, *421*(2), 305–311.

Clausen, B. E., & Stoitzner, P. (2015). Functional specialization of skin dendritic cell subsets in regulating T cell responses. *Frontiers in Immunology*, *6*, 1–19.

Conrad, C., Meller, S., & Gilliet, M. (2009). Plasmacytoid dendritic cells in the skin: To sense or not to sense nucleic acids. *Seminars in Immunology*, *21*(3), 101–109.

Coussens, L. M., Raymond, W. W., Bergers, G., Laig-Webster, M., Behrendtsen, O., Werb, Z., Caughey, G. H., & Hanahan, D. (1999). Inflammatory mast cells up-regulate angiogenesis during squamous epithelial carcinogenesis. *Genes and Development*, *13*(11), 1382–1397.

Cumberbatch, M., & Kimber, I. (1992). Dermal tumour necrosis factor-alpha induces dendritic cell migration to draining lymph nodes, and possibly provides one stimulus for Langerhans' cell migration. *Immunology*, *75*(2), 257–263.

D'Orazio, J., Jarrett, S., Amaro-Ortiz, A., & Scott, T. (2013). UV radiation and the skin. *International Journal of Molecular Sciences*, *14*(6), 12222–12248.

Dagher, R., Copenhaver, A. M., Besnard, V., Berlin, A., Hamidi, F., Maret, M., Wang, J., Qu, X., Shrestha, Y., Wu, J., Gautier, G., Raja, R., Aubier, M., Kolbeck, R., Humbles, A. A., & Pretolani, M. (2020). IL-33-ST2 axis regulates myeloid cell differentiation and activation enabling effective club cell regeneration. *Nature Communications*, *11*(4786), 1–19.

Dahlin, J. S., Ding, Z., & Hallgren, J. (2015). Distinguishing Mast Cell Progenitors from Mature Mast Cells in Mice. *Stem Cells and Development*, *24*(14), 1703–1711.

Damiani, E., & Ullrich, S. E. (2016). Understanding the connection between platelet-activating factor, a UV-induced lipid mediator of inflammation, immune suppression and skin cancer. *Progress in Lipid Research*, *63*, 14–27.

Day, C. P., Marchalik, R., Merlino, G., & Michael, H. (2017). Mouse models of UV-induced melanoma: Genetics, pathology, and clinical relevance. *Laboratory Investigation*, *97*(6), 698–705.

Descotes, J., & Choquet-Kastylevsky, G. (2001). Gell and Coombs's classification: Is it still valid? *Toxicology*, *158*, 43–49.

Di Piazza, M., Nowell, C. S., Koch, U., Durham, A. D., & Radtke, F. (2012). Loss of Cutaneous TSLP-Dependent Immune Responses Skews the Balance of Inflammation from Tumor Protective to Tumor Promoting. *Cancer Cell*, *22*(4), 479–493.

Didovic, S., Opitz, F. V., Holzmann, B., Förster, I., & Weighardt, H. (2016). Requirement of MyD88 signaling in keratinocytes for Langerhans cell migration and initiation of atopic dermatitis-like symptoms in mice. *European Journal of Immunology*, *46*(4), 981–992.

Digiovanna, J. J., & Kraemer, K. H. (2012). Shining a light on xeroderma pigmentosum. *Journal of Investigative Dermatology*, *132*, 785–796.

Dinarello, C. A. (2018). Overview of the IL-1 family in innate inflammation and acquired immunity. *Immunological Reviews*, *281*(1), 8–27.

Dranoff, G. (2004). Cytokines in cancer pathogenesis and cancer therapy. *Nature Reviews Cancer*, *4*(1), 11–22.

Duault, C., Franchini, D. M., Familliades, J., Cayrol, C., Roga, S., Girard, J.-P., Fournié, J.-J., & Poupot, M. (2016). TCRVγ9 γδ T Cell Response to IL-33: A CD4 T Cell–Dependent Mechanism. *The Journal of Immunology*, *196*(1), 493–502.

Dudeck, A., Köberle, M., Goldmann, O., Meyer, N., Dudeck, J., Lemmens, S., Rohde, M., Roldán, N. G., Dietze-Schwonberg, K., Orinska, Z., Medina, E., Hendrix, S., Metz, M., Zenclussen, A. C., von Stebut, E., & Biedermann, T. (2019). Mast cells as protectors of health. *Journal of Allergy and Clinical Immunology*, *144*(4), 4–18.

Dudeck, A., Suender, C. A., Kostka, S. L., von Stebut, E., & Maurer, M. (2011). Mast cells promote Th1 and Th17 responses by modulating dendritic cell maturation and function. *European Journal of Immunology*, *41*(7), 1883–1893.

Dudeck, J., Froebel, J., Kotrba, J., Lehmann, C. H. K., Dudziak, D., Speier, S., Nedospasov, S. A., Schraven, B., & Dudeck, A. (2019). Engulfment of mast cell secretory granules on skin inflammation boosts dendritic cell migration and priming efficiency. *Journal of Allergy and Clinical Immunology*, *143*(5), 1849–1864.

Dudeck, J., Ghouse, S. M., Lehmann, C. H. K., Hoppe, A., Schubert, N., Nedospasov, S. A., Dudziak, D., & Dudeck, A. (2015). Mast-Cell-Derived TNF Amplifies CD8+ Dendritic Cell Functionality and CD8+ T Cell Priming. *Cell Reports*, *13*(2), 399–411.

Dudeck, J., Medyukhina, A., Fröbel, J., Svensson, C. M., Kotrba, J., Gerlach, M., Gradtke, A. C., Schröder, B., Speier, S., Figge, M. T., & Dudeck, A. (2017). Mast cells acquire MHC II from dendritic cells during skin inflammation. *Journal of Experimental Medicine*, *214*(12), 3791–3811.

Ehrlich, P. (1878). *Beiträge zur Theorie und Praxis der Histologischen Färbung*.

Eisen, H. N., Orris, L., & Belman, S. (1952). Elicitation of delayed allergic skin reactions with haptens; the dependence of elicitation on hapten combination with protein. *The Journal of Experimental Medicine*, *95*(5), 473–487.

Elbasiony, E., Mittal, S. K., Foulsham, W., Cho, W. K., & Chauhan, S. K. (2020). Epithelium-derived IL-33 activates mast cells to initiate neutrophil recruitment following corneal injury. *Ocular Surface*, *18*(4), 633–640.

Evans, H., Killoran, K. E., & Mitre, E. (2014). Measuring local anaphylaxis in mice. *Journal of Visualized Experiments*, *92*, 1–6.

Faurschou, A. (2010). Role of tumor necrosis factor-α in the regulation of keratinocyte cell cycle and DNA repair after ultraviolet-B radiation. *Danish Medical Bulletin*, *57*(10), 1–14.

Ferrer, I. R., West, H. C., Henderson, S., Ushakov, D. S., Sousa, P. S. E., Strid, J., Chakraverty, R., Yates, A. J., & Bennett, C. L. (2019). A wave of monocytes is recruited to replenish the long-term Langerhans cell network after immune injury. *Science Immunology*, *4*(38), 1–14.

Finlay, C. M., Cunningham, K. T., And, B. D., & Mills, K. H. G. (2020). IL-33–Stimulated Murine Mast Cells Polarize Alternatively Activated Macrophages, Which Suppress T Cells That Mediate Experimental Autoimmune Encephalomyelitis. *Journal of Imm*, *205*(7), 1909–1919.

Gais, P., Reim, D., Jusek, G., Rossmann-Bloeck, T., Weighardt, H., Pfeffer, K., Altmayr, F., Janssen, K.-P., & Holzmann, B. (2012). Cutting Edge: Divergent Cell-Specific Functions of MyD88 for Inflammatory Responses and Organ Injury in Septic Peritonitis. *The Journal of Immunology*, *188*(12), 5833–5837.

Galli, S. J., & Tsai, M. (2010). Mast cells in allergy and infection: Versatile effector and regulatory cells in innate and adaptive immunity. *European Journal of Immunology*, *40*(7), 1843–1851.

Galli, S. J., & Tsai, M. (2012). IgE and mast cells in allergic disease. *Nature Medicine*, *18*(5), 693–704.

Gallo, R. L., & Bernard, J. J. (2014). Innate immune sensors stimulate inflammatory and immunosuppressive responses to UVB radiation. *Journal of Investigative Dermatology*, *134*(6), 1508–1511.

Gantner, B. N., Simmons, R. M., Canavera, S. J., Akira, S., & Underhill, D. M. (2003). Collaborative induction of inflammatory responses by dectin-1 and toll-like receptor 2. *Journal of Experimental Medicine*, *197*(9), 1107–1117.

Gao, Y., Nish, S. A., Jiang, R., Hou, L., Licona-Limón, P., Weinstein, J. S., Zhao, H., & Medzhitov, R. (2013). Control of T helper 2 responses by transcription factor IRF4-dependent dendritic cells. *Immunity*, *39*(4), 722–732.

Gariboldi, S., Palazzo, M., Zanobbio, L., Selleri, S., Sommariva, M., Sfondrini, L., Cavicchini, S., Balsari, A., & Rumio, C. (2008). Low Molecular Weight Hyaluronic Acid Increases the Self-Defense of Skin Epithelium by Induction of β-Defensin 2 via TLR2 and TLR4. *The Journal of Immunology*, *181*(3), 2103–2110.

Gebhardt, T., Whitney, P. G., Zaid, A., MacKay, L. K., Brooks, A. G., Heath, W. R., Carbone, F. R., & Mueller, S. N. (2011). Different patterns of peripheral migration by memory CD4+ and CD8+ T cells. *Nature*, *477*(7363), 216–219.

Gell, P., & Coombs, R. (1963). *Clinical aspects of immunology*.

Gentek, R., Ghigo, C., Hoeffel, G., Bulle, M. J., Msallam, R., Gautier, G., Launay, P., Chen, J., Ginhoux, F., & Bajénoff, M. (2018). Hemogenic Endothelial Fate Mapping Reveals Dual Developmental Origin of Mast Cells. *Immunity*, *48*(6), 1160–1171.

Gibbs, N. K., Tye, J., & Norval, M. (2008). Recent advances in urocanic acid photochemistry, photobiology and photoimmunology. *Photochemical and Photobiological Sciences*, *7*(6), 655–667.

Gimenez-Rivera, V.-A., Siebenhaar, F., Zimmermann, C., Siiskonen, H., Metz, M., & Maurer, M. (2016). Mast Cells Limit the Exacerbation of Chronic Allergic Contact Dermatitis in Response to Repeated Allergen Exposure. *The Journal of Immunology*, *197*(11), 4240–4246.

Grimbaldeston, M.A., Simpson, A., Finlay-Jones, J. J., & Hart, P. H. (2003). The effect of ultraviolet radiation exposure on the prevalence of mast cells in human skin. *British Journal of Dermatology*, *148*(2), 300–306.

Grimbaldeston, Michele A., Chen, C. C., Piliponsky, A. M., Tsai, M., Tam, S. Y., & Galli, S. J. (2005). Mast cell-deficient W-sash c-kit mutant kitW-sh/W-sh mice as a model for investigating mast cell biology in vivo. *American Journal of Pathology*, *167*(3), 835–848.

Guhl, S., Stefaniak, R., Strathmann, M., Babina, M., Piazena, H., Henz, B. M., & Zuberbier, T. (2005). Bivalent effect of UV light on human skin mast cells - Low-level mediator release at baseline but potent suppression upon mast cell triggering. *Journal of Investigative Dermatology*, *124*(2), 453–456.

Haniffa, M., Shin, A., Bigley, V., McGovern, N., Teo, P., See, P., Wasan, P. S., Wang, X. N., Malinarich, F., Malleret, B., Larbi, A., Tan, P., Zhao, H., Poidinger, M., Pagan, S., Cookson, S., Dickinson, R., Dimmick, I., Jarrett, R. F., … Ginhoux, F. (2012). Human Tissues Contain CD141 hi Cross-Presenting Dendritic Cells with Functional Homology to Mouse CD103 + Nonlymphoid Dendritic Cells. *Immunity*, *37*(1), 60–73.

Harberts, E., Fishelevich, R., Liu, J., Atamas, S. P., & Gaspari, A. A. (2014). MyD88 mediates the decision to die by apoptosis or necroptosis after UV irradiation. *Innate Immunity*, *20*(5), 529–539.

Harberts, E., Zhou, H., Fishelevich, R., Liu, J., & Gaspari, A. A. (2015). Ultraviolet Radiation Signaling through TLR4/MyD88 Constrains DNA Repair and Plays a Role in Cutaneous Immunosuppression. *The Journal of Immunology*, *194*(7), 3127–3135.

Hart, P. H., Grimbaldeston, M. A., & Finlay-Jones, J. J. (2000). Mast cells in UV-B-induced immunosuppression. *Journal of Photochemistry and Photobiology B: Biology*, *55*, 81–87.

Hart, P. H., & Norval, M. (2018). Ultraviolet radiation-induced immunosuppression and its relevance for skin carcinogenesis. *Photochemical and Photobiological Sciences*, *17*(12), 1872–1884.

Hatanaka, K., Kitamura, Y., & Nishimune, Y. (1979). Local development of mast cells from bone marrow-derived precursors in the skin of mice. *Blood*, *53*(1), 142–147.

He, R., Yin, H., Yuan, B., Liu, T., Luo, L., Huang, P., Dai, L., & Zeng, K. (2017). IL-33 improves wound healing through enhanced M2 macrophage polarization in diabetic mice. *Molecular Immunology*, *90*, 42–49.

Hendrix, S., Kramer, P., Pehl, D., Warnke, K., Boato, F., Nelissen, S., Lemmens, E., Pejler, G., Metz, M., Siebenhaar, F., & Maurer, M. (2013). Mast cells protect from post-traumatic brain inflammation by the mast cell-specific chymase mouse mast cell protease-4. *FASEB Journal*, *27*(3), 920–929.

Henri, S., Poulin, L. F., Tamoutounour, S., Ardouin, L., Guilliams, M., De Bovis, B., Devilard, E., Viret, C., Azukizawa, H., Kissenpfennig, A., & Malissen, B. (2010). CD207+ CD103+ dermal dendritic cells cross-present keratinocyte-derived antigens irrespective of the presence of Langerhans cells. *Journal of Experimental Medicine*, *207*(1), 189–206.

Ho, L. H., Ohno, T., Oboki, K., Kajiwara, N., Suto, H., Iikura, M., Okayama, Y., Akira, S., Saito, H., Galli, S. J., & Nakae, S. (2007). IL-33 induces IL-13 production by mouse mast cells independently of IgE-Fc RI signals. *Journal of Leukocyte Biology*, *82*(6), 1481–1490.

Hoeffel, G., Wang, Y., Greter, M., See, P., Teo, P., Malleret, B., Leboeuf, M., Low, D., Oller, G., Almeida, F., Choy, S. H. Y., Grisotto, M., Renia, L., Conway, S. J., Stanley, E. R., Chan, J. K. Y., Ng, L. G., Samokhvalov, I. M., Merad, M., & Ginhoux, F. (2012). Adult Langerhans cells derive predominantly from embryonic fetal liver monocytes with a minor contribution of yolk sac-derived macrophages. *Journal of Experimental Medicine*, *209*(6), 1167–1181.

Hoff, S., Oyoshi, M. K., Hornick, J. L., & Geha, R. S. (2018). MyD88 signaling in T regulatory cells by endogenous ligands dampens skin inflammation in filaggrin deficient mice. *Clinical Immunology*, *195*, 88–92.

Honda, T., Egawa, G., Grabbe, S., & Kabashima, K. (2013). Update of immune events in the murine contact hypersensitivity model: Toward the understanding of allergic contact dermatitis. *Journal of Investigative Dermatology*, *133*(2), 303–315.

Hsu, C.-L., Neilsen, C. V., & Bryce, P. J. (2010). IL-33 Is Produced by Mast Cells and Regulates IgE-Dependent Inflammation. *PLoS ONE*, *5*(8), 1–9.

Hübner, M. P., Larson, D., Torrero, M. N., Mueller, E., Shi, Y., Killoran, K. E., & Mitre, E. (2011). Anti-FcεR1 antibody injections activate basophils and mast cells and delay Type 1 diabetes onset in NOD mice. *Clinical Immunology*, *141*(2), 205–217.

Iikura, M., Suto, H., Kajiwara, N., Oboki, K., Ohno, T., Okayama, Y., Saito, H., Galli, S. J., & Nakae, S. (2007). IL-33 can promote survival, adhesion and cytokine production in human mast cells. *Laboratory Investigation*, *87*(10), 971–978.

Jain, A., Kaczanowska, S., & Davila, E. (2014). IL-1 receptor-associated kinase signaling and its role in inflammation, cancer progression, and therapy resistance. *Frontiers in Immunology*, *5*, 1–8.

Jameson, J. M., Cauvi, G., Witherden, D. A., & Havran, W. L. (2004). A Keratinocyte-Responsive γδ TCR Is Necessary for Dendritic Epidermal T Cell Activation by Damaged Keratinocytes and Maintenance in the Epidermis. *The Journal of Immunology*, *172*(6), 3573–3579.

Jameson, S. C., & Masopust, D. (2018). Understanding Subset Diversity in T Cell Memory. *Immunity*, *48*(2), 214–226.

Jang, Y., Jeong, S. H., Park, Y. H., Bae, H. C., Lee, H., Ryu, W. I., Park, G. H., & Son, S. W. (2013). UVB induces HIF-1α-dependent TSLP expression via the JNK and ERK pathways. *Journal of Investigative Dermatology*, *133*(11), 2601–2608.

Jiang, X., Park, C. O., Sweeney, J. G., Yoo, M. J., Gaide, O., & Kupper, T. S. (2017). Dermal γδ T cells do not freely re-circulate out of skin and produce IL-17 to promote neutrophil infiltration during primary contact hypersensitivity. *PLoS ONE*, *12*(1), 1–20.

Joulia, R., L'Faqihi, F. E., Valitutti, S., & Espinosa, E. (2017). IL-33 fine tunes mast cell degranulation and chemokine production at the single-cell level. *Journal of Allergy and Clinical Immunology*, *140*(2), 497–509.

Jung, M.-Y., Smrž, D., Desai, A., Bandara, G., Ito, T., Iwaki, S., Kang, J.-H., Andrade, M. V., Hilderbrand, S. C., Brown, J. M., Beaven, M. A., Metcalfe, D. D., & Gilfillan, A. M. (2013). IL-33 Induces a Hyporesponsive Phenotype in Human and Mouse Mast Cells. *The Journal of Immunology*, *190*(2), 531–538.

Kaieda, S., Shin, K., Nigrovic, P. A., Seki, K., Lee, R. T., Stevens, R. L., & Lee, D. M. (2010). Synovial fibroblasts promote the expression and granule accumulation of tryptase via interleukin-33 and its receptor ST-2 (IL1RL1). *Journal of Biological Chemistry*, *285*(28), 21478–21486.

Kambayashi, T., Allenspach, E. J., Chang, J. T., Zou, T., Shoag, J. E., Reiner, S. L., Caton, A. J., & Koretzky, G. A. (2009). Inducible MHC Class II Expression by Mast Cells Supports Effector and Regulatory T Cell Activation. *The Journal of Immunology*, *182*(8), 4686–4695.

Kang, K., Hammerberg, C., Meunier, L., & Cooper, K. D. (1994). CD11b+ macrophages that infiltrate human epidermis after in vivo ultraviolet exposure potently produce IL-10 and represent the major secretory source of epidermal IL-10 protein. *The Journal of Immunology*, *153*(11), 5256–5264.

Kaplan, D. H., Igyártó, B. Z., & Gaspari, A. A. (2012). Early immune events in the induction of allergic contact dermatitis. *Nature Reviews Immunology*, *12*(2), 114–124.

Katsoulis-Dimitriou, K., Kotrba, J., Voss, M., Dudeck, J., & Dudeck, A. (2020). Mast Cell Functions Linking Innate Sensing to Adaptive Immunity. *Cells*, *9*(12), 1–19.

Kawai, T., & Akira, S. (2007). TLR signaling. *Seminars in Immunology*, *19*(1), 24–32.

Kawai, T., & Akira, S. (2011). Toll-like Receptors and Their Crosstalk with Other Innate Receptors in Infection and Immunity. *Immunity*, *34*(5), 637–650.

Kawai, T., Takeuchi, O., Fujita, T., Inoue, J., Mühlradt, P. F., Sato, S., Hoshino, K., & Akira, S. (2001). Lipopolysaccharide Stimulates the MyD88-Independent Pathway and Results in Activation of IFN-Regulatory Factor 3 and the Expression of a Subset of Lipopolysaccharide-Inducible Genes. *The Journal of Immunology*, *167*(10), 5887–5894.

Kett, W. C., Osmond, R. I. W., Moe, L., Skett, S. E., Kinnear, B. F., & Coombe, D. R. (2003). Avidin is a heparin-binding protein. Affinity, specificity and structural analysis. *Biochimica et Biophysica Acta - General Subjects*, *1620*, 225–234.

Kim, T. H., Ullrich, S. E., Ananthaswamy, H. N., Zimmerman, S., & Kripke, M. L. (1998). Suppression of Delayed and Contact Hypersensitivity Responses in Mice Have Different UV Dose Responses. *Photochemistry and Photobiology*, *68*(5), 738–744.

Kitajima, T., Iwashiro, M., Kuribayashi, K., & Imamura, S. (1995). Effect of parent genetic background on latency and antigenicity of UV-induced tumors originating in F1 hybrids. *Experimental Dermatology*, *4*(1), 42–45.

Kitamura, Y., Hatanaka, K., Murakami, M., & Shibata, H. (1979). Presence of mast cell precursors in peripheral blood of mice demonstrated by parabiosis. *Blood*, *53*(6), 1085–1088.

Kitamura, Y., Shimada, M., Hatanaka, K., & Miyano, Y. (1977). Development of mast cells from grafted bone marrow cells in irradiated mice. *Nature*, *268*(5619), 442–443.

Kitamura, Yukihiko, Matsuda, H., & Hatanaka, K. (1978). Clonal nature of mast-cell clusters formed in WI wv mice after bone marrow transplantation. *J. Biochem. Biophys. Acta*, *42*(9), 285–291.

Klekotka, P. A., Yang, L., & Yokoyama, W. M. (2010). Contrasting Roles of the IL-1 and IL-18 Receptors in MyD88-Dependent Contact Hypersensitivity. *Journal of Investigative Dermatology*, *130*(1), 184–191.

Kolter, J., Feuerstein, R., Zeis, P., Hagemeyer, N., Paterson, N., D'Errico, P., Baasch, S., Amann, L., Masuda, T., Lösslein, A., Gharun, K., Meyer-Luehmann, M., Waskow, C., Franzke, C. W., Grün, D., Lämmermann, T., Prinz, M., & Henneke, P. (2019). A Subset of Skin Macrophages Contributes to the Surveillance and Regeneration of Local Nerves. *Immunity*, *50*(6), 1482–1497.

Krebs in Deutschland für 2015/2016. (2019). Robert Koch-Institut, Gesellschaft der epidemiologischen Krebsregister in Deutschland e.V. www.krebsdaten.de. 2021-05-26

Kripke, M. L., Cox, P. A., Alas, L. G., & Yarosh, D. B. (1992). Pyrimidine dimers in DNA initiate systemic immunosuppression in UV- irradiated mice. *Proceedings of the National Academy of Sciences of the United States of America*, *89*(16), 7516–7520.

Kurimoto, I., & Streilein, J. W. (1992). cis-urocanic acid suppression of contact hypersensitivity induction is mediated via tumor necrosis factor-alpha. *The Journal of Immunology*, *148*(10), 3072–3078.

Kurow, O., Frey, B., Schuster, L., Schmitt, V., Adam, S., Hahn, M., Gilchrist, D., McInnes, I. B., Wirtz, S., Gaipl, U. S., Krönke, G., Schett, G., Frey, S., & Hueber, A. J. (2017). Full length interleukin 33 aggravates radiation-induced skin reaction. *Frontiers in Immunology*, *8*, 1–13.

Kurowska-Stolarska, M., Stolarski, B., Kewin, P., Murphy, G., Corrigan, C. J., Ying, S., Pitman, N., Mirchandani, A., Rana, B., van Rooijen, N., Shepherd, M., McSharry, C., McInnes, I. B., Xu, D., & Liew, F. Y. (2009). IL-33 Amplifies the Polarization of Alternatively Activated Macrophages That Contribute to Airway Inflammation. *The Journal of Immunology*, *183*(10), 6469–6477.

Lambrecht, B. N., & Hammad, H. (2017). The immunology of the allergy epidemic and the hygiene hypothesis. *Nature Immunology*, *18*(10), 1076–1083.

Lee, E. Y., Lee, M. W., & Wong, G. C. L. (2019). Modulation of toll-like receptor signaling by antimicrobial peptides. *Seminars in Cell and Developmental Biology*, *88*, 173–184.

Li, Y., Wu, J., Luo, G., & He, W. (2018). Functions of Vγ4 T cells and dendritic epidermal T cells on skin wound healing. *Frontiers in Immunology*, *9*, 1–9.

Li, Z., Liu, S., Xu, J., Zhang, X., Han, D., Liu, J., Xia, M., Yi, L., Shen, Q., Xu, S., Lu, L., & Cao, X. (2018). Adult Connective Tissue-Resident Mast Cells Originate from Late Erythro-Myeloid Progenitors. *Immunity*, *49*, 640–652.

Liew, F. Y., Girard, J. P., & Turnquist, H. R. (2016). Interleukin-33 in health and disease. *Nature Reviews Immunology*, *16*(11), 676–689.

Liu, X., Huang, H., Gao, H., Wu, X., Zhang, W., Yu, B., & Dou, X. (2018). Regulatory B cells induced by ultraviolet B through toll-like receptor 4 signalling contribute to the suppression of contact hypersensitivity responses in mice. *Contact Dermatitis*, *78*(2), 117–130.

Loser, K., Apelt, J., Voskort, M., Mohaupt, M., Balkow, S., Schwarz, T., Grabbe, S., & Beissert, S. (2007). IL-10 Controls Ultraviolet-Induced Carcinogenesis in Mice. *The Journal of Immunology*, *179*(1), 365–371.

MacLeod, A. S., Hemmers, S., Garijo, O., Chabod, M., Mowen, K., Witherden, D. A., & Havran, W. L. (2013). Dendritic epidermal T cells regulate skin antimicrobial barrier function. *Journal of Clinical Investigation*, *123*(10), 4364–4374.

MacLeod, A. S., Rudolph, R., Corriden, R., Ye, I., Garijo, O., & Havran, W. L. (2014). Skin-Resident T Cells Sense Ultraviolet Radiation–Induced Injury and Contribute to DNA Repair. *The Journal of Immunology*, *192*(12), 5695–5702.

Malissen, B., Tamoutounour, S., & Henri, S. (2014). The origins and functions of dendritic cells and macrophages in the skin. *Nature Reviews Immunology*, *14*(6), 417–428.

Mantri, C. K., & St. John, A. L. (2019). Immune synapses between mast cells and γδ T cells limit viral infection. *Journal of Clinical Investigation*, *129*(3), 1094–1108.

Martin, S. F., Dudda, J. C., Bachtanian, E., Lembo, A., Liller, S., Dürr, C., Heimesaat, M. M., Bereswill, S., Fejer, G., Vassileva, R., Jakob, T., Freudenberg, N., Termeer, C. C., Johner, C., Galanos, C., & Freudenberg, M. A. (2008). Toll-like receptor and IL-12 signaling control susceptibility to contact hypersensitivity. *Journal of Experimental Medicine*, *205*(9), 2151–2162.

Martin, S. F., Esser, P. R., Weber, F. C., Jakob, T., Freudenberg, M. A., Schmidt, M., & Goebeler, M. (2011). Mechanisms of chemical-induced innate immunity in allergic contact dermatitis. *Allergy: European Journal of Allergy and Clinical Immunology*, *66*(9), 1152–1163.

Mass, E., Ballesteros, I., Farlik, M., Halbritter, F., Günther, P., Crozet, L., Jacome-Galarza, C. E., Händler, K., Klughammer, J., Kobayashi, Y., Gomez-Perdiguero, E., Schultze, J. L., Beyer, M., Bock, C., & Geissmann, F. (2016). Specification of tissue-resident macrophages during organogenesis. *Science*, *353*(6304), 1–12.

Matsumura, Y., & Ananthaswamy, H. N. (2004). Toxic effects of ultraviolet radiation on the skin. *Toxicology and Applied Pharmacology*, *195*(3), 298–308.

Medzhitov, R., & Janeway, C. A. (1997). Innate immunity: The virtues of a nonclonal system of recognition. *Cell*, *91*(3), 295–298.

Megiovanni, A. M., Sanchez, F., Robledo-Sarmiento, M., Morel, C., Gluckman, J. C., & Boudaly, S. (2006). Polymorphonuclear neutrophils deliver activation signals and antigenic molecules to dendritic cells: a new link between leukocytes upstream of T lymphocytes. *Journal of Leukocyte Biology*, *79*(5), 977–988.

Mengoni, M., Tüting, T., & Gaffal, E. (2021). Photocarcinogenesis—molecular mechanisms and practical relevance. *Hautarzt*, *72*(1), 6–13.

Merad, M., Ginhoux, F., & Collin, M. (2008). Origin, homeostasis and function of Langerhans cells and other langerin-expressing dendritic cells. *Nature Reviews Immunology*, *8*(12), 935–947.

Michel, A., Schüler, A., Friedrich, P., Döner, F., Bopp, T., Radsak, M., Hoffmann, M., Relle, M., Distler, U., Kuharev, J., Tenzer, S., Feyerabend, T. B., Rodewald, H.-R., Schild, H., Schmitt, E., Becker, M., & Stassen, M. (2013). Mast Cell–deficient Kit W-sh "Sash" Mutant Mice Display Aberrant Myelopoiesis Leading to the Accumulation of Splenocytes That Act as Myeloid-Derived Suppressor Cells. *The Journal of Immunology*, *190*(11), 5534–5544.

Mikami, E., Kudo, M., Ohashi, R., Kawahara, K., Kawamoto, Y., Teduka, K., Fujii, T., Kitamura, T., Kure, S., Ishino, K., Sakatani, T., Wada, R., Saeki, H., & Naito, Z. (2019). Toll-like receptor 4 plays a tumor-suppressive role in cutaneous squamous cell carcinoma. *International Journal of Oncology*, *54*(6), 2179–2188.

Mittal, D., Saccheri, F., Vénéreau, E., Pusterla, T., Bianchi, M. E., & Rescigno, M. (2010). TLR4-mediated skin carcinogenesis is dependent on immune and radioresistant cells. *EMBO Journal*, *29*(13), 2242–2252.

Moon, T. C., Dean Befus, A., & Kulka, M. (2014). Mast cell mediators: Their differential release and the secretory pathways involved. *Frontiers in Immunology*, *5*, 1–18.

Moon, T. C., St Laurent, C. D., Morris, K. E., Marcet, C., Yoshimura, T., Sekar, Y., & Befus, A. D. (2010). Advances in mast cell biology: New understanding of heterogeneity and function. *Mucosal Immunology*, *3*(2), 111–128.

Moore, R. J., Owens, D. M., Stamp, G., Arnott, C., Burke, F., East, N., Holdsworth, H., Turner, L., Rollins, B., Pasparakis, M., Kollias, G., & Balkwill, F. (1999). Mice deficient in tumor necrosis factor-α are resistant to skin carcinogenesis. *Nature Medicine*, *5*(7), 828–831.

Mosteller, R. (1987). Simplified Calculation of Body-Surface Area. *New England Journal of Medicine*, *317*(17), 1098–1098.

Mueller, S. N., & Mackay, L. K. (2016). Tissue-resident memory T cells: Local specialists in immune defence. *Nature Reviews Immunology*, *16*(2), 79–89.

Mukai, K., Tsai, M., Starkl, P., Marichal, T., & Galli, S. J. (2016). IgE and mast cells in host defense against parasites and venoms. *Seminars in Immunopathology*, *38*(5), 581–603.

Murphy, K., & Weaver, C. (2017). *Janeway's Immunobiology*. Garland Science.

Nestle, F. O., Di Meglio, P., Qin, J. Z., & Nickoloff, B. J. (2009). Skin immune sentinels in health and disease. *Nature Reviews Immunology*, *9*(10), 679–691.

Netea, M. G., Domínguez-Andrés, J., Barreiro, L. B., Chavakis, T., Divangahi, M., Fuchs, E., Joosten, L. A. B., van der Meer, J. W. M., Mhlanga, M. M., Mulder, W. J. M., Riksen, N. P., Schlitzer, A., Schultze, J. L., Stabell Benn, C., Sun, J. C., Xavier, R. J., & Latz, E. (2020). Defining trained immunity and its role in health and disease. *Nature Reviews Immunology*, *20*(6), 375–388.

Nian, J. Bin, Zeng, M., Zheng, J., Zeng, L. Y., Fu, Z., Huang, Q. J., & Wei, X. (2020). Epithelial cells expressed IL-33 to promote degranulation of mast cells through inhibition on ST2/PI3K/mTOR-mediated autophagy in allergic rhinitis. *Cell Cycle*, *19*(10), 1132–1142.

Nielsen, M. M., Lovato, P., MacLeod, A. S., Witherden, D. A., Skov, L., Dyring-Andersen, B., Dabelsteen, S., Woetmann, A., Ødum, N., Havran, W. L., Geisler, C., & Bonefeld, C. M. (2014). IL-1β–Dependent Activation of Dendritic Epidermal T Cells in Contact Hypersensitivity. *The Journal of Immunology*, *192*(7), 2975–2983.

Nigrovic, P. A., Gray, D. H. D., Jones, T., Hallgren, J., Kuo, F. C., Chaletzky, B., Gurish, M., Mathis, D., Benoist, C., & Lee, D. M. (2008). Genetic inversion in mast cell-deficient Wsh mice interrupts corin and manifests as hematopoietic and cardiac aberrancy. *American Journal of Pathology*, *173*(6), 1693–1701.

Norman, M. U., Hwang, J., Hulliger, S., Bonder, C. S., Yamanouchi, J., Santamaria, P., & Kubes, P. (2008). Mast cells regulate the magnitude and the cytokine microenvironment of the contact hypersensitivity response. *American Journal of Pathology*, *172*(6), 1638–1649.

Norval, M., & Halliday, G. M. (2011). The consequences of UV-induced immunosuppression for human health. *Photochemistry and Photobiology*, *87*(5), 965–977.

Noske, K. (2018). Secreted immunoregulatory proteins in the skin. *Journal of Dermatological Science*, *89*(1), 3–10.

Opitz, F. V. (2016). *Rolle des Adaptermoleküls MyD88 im Mausmodell der Lichtalterung und Photokarzinogenese*.

Otsuka, A., Kubo, M., Honda, T., Egawa, G., Nakajima, S., Tanizaki, H., Kim, B., Matsuoka, S., Watanabe, T., Nakae, S., Miyachi, Y., & Kabashima, K. (2011). Requirement of Interaction between Mast Cells and Skin Dendritic Cells to Establish Contact Hypersensitivity. *PLoS ONE*, *6*(9), 1–10.

Parkin, J., & Cohen, B. (2001). An overview of the immune system. *Lancet*, *357*(9270), 1777–1789.

Pasman, L., & Kasper, D. L. (2017). Building conventions for unconventional lymphocytes. *Immunological Reviews*, *279*(1), 52–62.

Patra, V. K., Laoubi, L., Nicolas, J. F., Vocanson, M., & Wolf, P. (2018). A perspective on the interplay of ultraviolet-radiation, skin microbiome and skin resident memory TCRαβ+ cells. *Frontiers in Medicine*, *5*, 1–9.

Peng, B., Ming, Y., & Yang, C. (2018). Regulatory B cells: The cutting edge of immune tolerance in kidney transplantation review-Article. *Cell Death and Disease*, *9*(2), 1–13.

Penna, G., Amuchastegui, S., Giarratana, N., Daniel, K. C., Vulcano, M., Sozzani, S., & Adorini, L. (2007). 1,25-Dihydroxyvitamin D 3 Selectively Modulates Tolerogenic Properties in Myeloid but Not Plasmacytoid Dendritic Cells . *The Journal of Immunology*, *178*(1), 145–153.

Pilkington, S. M., Barron, M. J., Watson, R. E. B., Griffiths, C. E. M., & Bulfone-Paus, S. (2019). Aged human skin accumulates mast cells with altered functionality that localize to macrophages and vasoactive intestinal peptide-positive nerve fibres. *British Journal of Dermatology*, *180*(4), 849–858.

Piskin, G., Bos, J. D., & Teunissen, M. B. M. (2005). Neutrophils infiltrating ultraviolet B-irradiated normal human skin display high IL-10 expression. *Archives of Dermatological Research*, *296*(7), 339–342.

Prasad, R., & Katiyar, S. K. (2017). Crosstalk Among UV-Induced Inflammatory Mediators, DNA Damage and Epigenetic Regulators Facilitates Suppression of the Immune System. *Photochemistry and Photobiology*, *93*(4), 930–936.

Qiao, H., Andrade, M. V., Lisboa, F. A., Morgan, K., & Beaven, M. A. (2006). FcεR1 and toll-like receptors mediate synergistic signals to markedly augment production of inflammatory cytokines in murine mast cells. *Blood*, *107*(2), 610–618.

Qiu, C., Zhong, L., Huang, C., Long, J., Ye, X., Wu, J., Dai, W., Lv, W., Xie, C., & Zhang, J. (2020). Cell-bound IgE and plasma IgE as a combined clinical diagnostic indicator for allergic patients. *Scientific Reports*, *10*(1), 1–9.

Rana, S., Byrne, S. N., MacDonald, L. J., Chan, C. Y. Y., & Halliday, G. M. (2008). Ultraviolet B suppresses immunity by inhibiting effector and memory T cells. *American Journal of Pathology*, *172*(4), 993–1004.

Rastogi, R. P., Richa, Kumar, A., Tyagi, M. B., & Sinha, R. P. (2010). Molecular mechanisms of ultraviolet radiation-induced DNA damage and repair. *Journal of Nucleic Acids*, *2010*, 1–32.

Ravanat, J. L., Douki, T., & Cadet, J. (2001). Direct and indirect effects of UV radiation on DNA and its components. *Journal of Photochemistry and Photobiology B: Biology*, *63*, 88–102.

Reber, L. L., Sibilano, R., Starkl, P., Roers, A., Grimbaldeston, M. A., Tsai, M., Gaudenzio, N., & Galli, S. J. (2017). Imaging protective mast cells in living mice during severe contact hypersensitivity. *JCI Insight*, *2*(9), 1–13.

Ribot, J. C., Lopes, N., & Silva-Santos, B. (2021). γδ T cells in tissue physiology and surveillance. *Nature Reviews Immunology*, *21*(4), 221–232.

Riera Romo, M., Pérez-Martínez, D., & Castillo Ferrer, C. (2016). Innate immunity in vertebrates: An overview. *Immunology*, *148*(2), 125–139.

Rittié, L., & Fisher, G. J. (2015). Natural and sun-induced aging of human skin. *Cold Spring Harbor Perspectives in Medicine*, *5*, 1–14.

Royce, G. H., Brown-Borg, H. M., & Deepa, S. S. (2019). The potential role of necroptosis in inflammaging and aging. *GeroScience*, *41*(6), 795–811.

Sakaguchi, S., Wing, K., Onishi, Y., Prieto-Martin, P., & Yamaguchi, T. (2009). Regulatory T cells: How do they suppress immune responses? *International Immunology*, *21*(10), 1105–1111.

Saluja, R., Hawro, T., Eberle, J., Church, M. K., & Maurer, M. (2014). Interleukin-33 promotes the proliferation of mouse mast cells through St2/MyD88 and p38 MAPK-dependent and Kit-independent pathways. *Journal of Biological Regulators and Homeostatic Agents*, *28*(4), 575–585.

Sandig, H., & Bulfone-Paus, S. (2012). TLR signaling in mast cells: Common and unique features. *Frontiers in Immunology*, *3*, 1–13.

Sanford, J. A., & Gallo, R. L. (2013). Functions of the skin microbiota in health and disease. *Seminars in Immunology*, *25*(5), 370–377.

Sapudom, J., Alatoom, A., Mohamed, W. K. E., Garcia-Sabaté, A., McBain, I., Nasser, R. A., & Teo, J. C. M. (2020). Dendritic cell immune potency on 2D and in 3D collagen matrices. *Biomaterials Science*, *8*(18), 5106–5120.

Sasseville, D. (2008). Occupational Contact Dermatitis. *Allergy, Asthma & Clinical Immunology*, *4*(2), 59–65.

Schiering, C., Krausgruber, T., Chomka, A., Fröhlich, A., Adelmann, K., Wohlfert, E. A., Pott, J., Griseri, T., Bollrath, J., Hegazy, A. N., Harrison, O. J., Owens, B. M. J., Löhning, M., Belkaid, Y., Fallon, P. G., & Powrie, F. (2014). The alarmin IL-33 promotes regulatory T-cell function in the intestine. *Nature*, *513*(7519), 564–568.

Schlitzer, A., McGovern, N., Teo, P., Zelante, T., Atarashi, K., Low, D., Ho, A. W. S., See, P., Shin, A., Wasan, P. S., Hoeffel, G., Malleret, B., Heiseke, A., Chew, S., Jardine, L., Purvis, H. A., Hilkens, C. M. U., Tam, J., Poidinger, M., … Ginhoux, F. (2013). IRF4 Transcription Factor-Dependent CD11b+ Dendritic Cells in Human and Mouse Control Mucosal IL-17 Cytokine Responses. *Immunity*, *38*(5), 970–983.

Scholten, J., Hartmann, K., Gerbaulet, A., Krieg, T., Müller, W., Testa, G., & Roers, A. (2008). Mast cell-specific Cre/loxP-mediated recombination in vivo. *Transgenic Research*, *17*(2), 307–315.

Schwarz, A., Maeda, A., Kernebeck, K., Van Steeg, H., Beissert, S., & Schwarz, T. (2005). Prevention of UV radiation-induced immunosuppression by IL-12 is dependent on DNA repair. *Journal of Experimental Medicine*, *201*(2), 173–179.

Schwarz, A., Maeda, A., & Schwarz, T. (2007). Alteration of the Migratory Behavior of UV-Induced Regulatory T Cells by Tissue-Specific Dendritic Cells. *The Journal of Immunology*, *178*(2), 877–886.

Schwarz, A., Maeda, A., Wild, M. K., Kernebeck, K., Gross, N., Aragane, Y., Beissert, S., Vestweber, D., & Schwarz, T. (2004). Ultraviolet Radiation-Induced Regulatory T Cells Not Only Inhibit the Induction but Can Suppress the Effector Phase of Contact Hypersensitivity. *The Journal of Immunology*, *172*(2), 1036–1043.

Schwarz, A., Navid, F., Sparwasser, T., Clausen, B. E., & Schwarz, T. (2012). 1,25-Dihydroxyvitamin D exerts similar immunosuppressive effects as UVR but is dispensable for local UVR-induced immunosuppression. *Journal of Investigative Dermatology*, *132*(12), 2762–2769.

Schwarz, A., Noordegraaf, M., Maeda, A., Torii, K., Clausen, B. E., & Schwarz, T. (2010). Langerhans cells are required for UVR-induced immunosuppression. *Journal of Investigative Dermatology*, *130*(5), 1419–1427.

Schwarz, T. (2005). Mechanisms of UV-induced immunosuppression. *Keio J Med*, *54*(4), 165–171.

Schweintzger, N. A., Bambach, I., Reginato, E., Mayer, G., Limón-Flores, A. Y., Ullrich, S. E., Byrne, S. N., & Wolf, P. (2015). Mast cells are required for phototolerance induction and scratching abatement. *Experimental Dermatology*, *24*(7), 491–496.

Selander, C., Engblom, C., Nilsson, G., Scheynius, A., & Andersson, C. L. (2009). TLR2/MyD88-Dependent and -Independent Activation of Mast Cell IgE Responses by the Skin Commensal Yeast Malassezia sympodialis . *The Journal of Immunology*, *182*(7), 4208–4216.

Shelburne, C. P., Nakano, H., St. John, A. L., Chan, C., McLachlan, J. B., Gunn, M. D., Staats, H. F., & Abraham, S. N. (2009). Mast Cells Augment Adaptive Immunity by Orchestrating Dendritic Cell Trafficking through Infected Tissues. *Cell Host and Microbe*, *6*(4), 331–342.

Shen, H., Tesar, B. M., Walker, W. E., & Goldstein, D. R. (2008). Dual Signaling of MyD88 and TRIF Is Critical for Maximal TLR4-Induced Dendritic Cell Maturation. *The Journal of Immunology*, *181*(3), 1849–1858.

Siebenhaar, F., Metz, M., & Maurer, M. (2014). Mast cells protect from skin tumor development and limit tumor growth during cutaneous de novo carcinogenesis in a Kit-dependent mouse model. *Experimental Dermatology*, *23*(3), 159–164.

Simons, F. E. R. (2010). Anaphylaxis. *Journal of Allergy and Clinical Immunology*, *125*(2), 161–181.

Simpson, C. L., Patel, D. M., & Green, K. J. (2011). Deconstructing the skin: Cytoarchitectural determinants of epidermal morphogenesis. *Nature Reviews Molecular Cell Biology*, *12*(9), 565–580.

Soares, H., Waechter, H. N., Glaichenhaus, N., Mougneau, E., Yagita, H., Mizenina, O., Dudziak, D., Nussenzweig, M. C., & Steinman, R. M. (2007). A subset of dendritic cells induces CD4+ T cells to produce IFN-γ by an IL-12-independent but CD70-dependent mechanism in vivo. *Journal of Experimental Medicine*, *204*(5), 1095–1106.

Soucek, L., Lawlor, E. R., Soto, D., Shchors, K., Swigart, L. B., & Evan, G. I. (2007). Mast cells are required for angiogenesis and macroscopic expansion of Myc-induced pancreatic islet tumors. *Nature Medicine*, *13*(10), 1211–1218.

Sreevidya, C. S., Fukunaga, A., Khaskhely, N. M., Masaki, T., Ono, R., Nishigori, C., & Ullrich, S. E. (2010). Agents that reverse UV-induced immune suppression and photocarcinogenesis affect DNA repair. *Journal of Investigative Dermatology*, *130*(5), 1428–1437.

Srinivas, S., Watanabe, T., Lin, C. S., William, C. M., Tanabe, Y., Jessell, T. M., & Costantini, F. (2001). Cre reporter strains produced by targeted insertion of EYFP and ECFP into the ROSA26 locus. *BMC Developmental Biology*, *1*, 1–8.

Stanojević, M., Stanojević, Z., Jovanović, D., & Stojiljković, M. (2004). Ultraviolet radiation and melanogenesis. *Archive of Oncology*, *12*(4), 203–205.

Strom, K., Schönfeld, M., Nagy, P., & Raab, W. (2015). A new occupational disease nr. 5103: A case report presenting details. *Trauma Und Berufskrankheit*, *17*(4), 207–210.

Suhng, E., Kim, B. H., Choi, Y. W., Choi, H. Y., Cho, H., & Byun, J. Y. (2018). Increased expression of IL-33 in rosacea skin and UVB-irradiated and LL-37-treated HaCaT cells. *Experimental Dermatology*, *27*(9), 1023–1029.

Sumpter, T. L., Balmert, S. C., & Kaplan, D. H. (2019). Cutaneous immune responses mediated by dendritic cells and mast cells. *JCI Insight*, *4*(1), 1–13.

Supajatura, V., Ushio, H., Nakao, A., Akira, S., Okumura, K., Ra, C., & Ogawa, H. (2002). Differential responses of mast cell Toll-like receptors 2 and 4 in allergy and innate immunity. *Journal of Clinical Investigation*, *109*(10), 1351–1359.

Suto, H., Nakae, S., Kakurai, M., Sedgwick, J. D., Tsai, M., & Galli, S. J. (2006). Mast Cell-Associated TNF Promotes Dendritic Cell Migration. *The Journal of Immunology*, *176*(7), 4102–4112.

Szczepanik, M., Majewska-Szczepanik, M., Wong, F. S., Kowalczyk, P., Pasare, C., & Wen, L. (2018). Regulation of contact sensitivity in non-obese diabetic (NOD) mice by innate immunity. *Contact Dermatitis*, *79*(4), 197–207.

Takatori, H., Makita, S., Ito, T., Matsuki, A., & Nakajima, H. (2018). Regulatory mechanisms of IL-33-ST2-mediated allergic inflammation. *Frontiers in Immunology*, *9*, 1–7.

Takeuchi, O., & Akira, S. (2010). Pattern Recognition Receptors and Inflammation. *Cell*, *140*(6), 805–820.

Tamoutounour, S., Guilliams, M., MontananaSanchis, F., Liu, H., Terhorst, D., Malosse, C., Pollet, E., Ardouin, L., Luche, H., Sanchez, C., Dalod, M., Malissen, B., & Henri, S. (2013). Origins and functional specialization of macrophages and of conventional and monocyte-derived dendritic cells in mouse skin. *Immunity*, *39*(5), 925–938.

Tang, X. Z., Jung, J. B., & Allen, C. D. C. (2019). A case of mistaken identity: The MAR-1 antibody to mouse FcεRIα cross-reacts with FcγRI and FcγRIV. *Journal of Allergy and Clinical Immunology*, *143*(4), 1643–1646.

Tarlinton, D., & Good-Jacobson, K. (2013). Diversity among memory B cells: Origin, consequences, and utility. *Science*, *341*(6151), 1205–1211.

Tharp, M. D., Seelig, L. L., Tigelaar, R. E., & Bergstresser, P. R. (1985). Conjugated avidin binds to mast cell granules. *Journal of Histochemistry & Cytochemistry*, *33*(1), 27–32.

Thomanek, V. (2020). *Cellular mechanisms of UV-induced immunosuppression*.

Toichi, E., Lu, K. Q., Swick, A. R., McCormick, T. S., & Cooper, K. D. (2008). Skin-infiltrating monocytes/macrophages migrate to draining lymph nodes and produce IL-10 after contact sensitizer exposure to UV-irradiated skin. *Journal of Investigative Dermatology*, *128*(11), 2705–2715.

Tomura, M., Honda, T., Tanizaki, H., Otsuka, A., Egawa, G., Tokura, Y., Waldmann, H., Hori, S., Cyster, J. G., Watanabe, T., Miyachi, Y., Kanagawa, O., & Kabashima, K. (2010). Activated regulatory T cells are the major T cell type emigrating from the skin during a cutaneous immune response in mice. *Journal of Clinical Investigation*, *120*(3), 883–893.

Tong, P. L., Roediger, B., Kolesnikoff, N., Biro, M., Tay, S. S., Jain, R., Shaw, L. E., Grimbaldeston, M. A., & Weninger, W. (2015). The skin immune atlas: Three-dimensional analysis of cutaneous leukocyte subsets by multiphoton microscopy. *Journal of Investigative Dermatology*, *135*(1), 84–93.

Tussiwand, R., Everts, B., Grajales-Reyes, G. E., Kretzer, N. M., Iwata, A., Bagaitkar, J., Wu, X., Wong, R., Anderson, D. A., Murphy, T. L., Pearce, E. J., & Murphy, K. M. (2015). Klf4 Expression in Conventional Dendritic Cells Is Required for T Helper 2 Cell Responses. *Immunity*, *42*(5), 916–928.

Valent, P., Akin, C., Hartmann, K., Nilsson, G., Reiter, A., Hermine, O., Sotlar, K., Sperr, W. R., Escribano, L., George, T. I., Kluin-Nelemans, H. C., Ustun, C., Triggiani, M., Brockow, K., Gotlib, J., Orfao, A., Kovanen, P. T., Hadzijusufovic, E., Sadovnik, I., … Galli, S. J. (2020). Mast cells as a unique hematopoietic lineage and cell system: From Paul Ehrlich's visions to precision medicine concepts. *Theranostics*, *10*(23), 10743–10768.

Van Der Aar, A. M. G., Sibiryak, D. S., Bakdash, G., Van Capel, T. M. M., Van Der Kleij, H. P. M., Opstelten, D. J. E., Teunissen, M. B. M., Kapsenberg, M. L., & De Jong, E. C. (2011). Vitamin D3 targets epidermal and dermal dendritic cells for induction of distinct regulatory T cells. *Journal of Allergy and Clinical Immunology*, *127*(6), 1532–1540.

Vasanthakumar, A., Moro, K., Xin, A., Liao, Y., Gloury, R., Kawamoto, S., Fagarasan, S., Mielke, L. A., Afshar-Sterle, S., Masters, S. L., Nakae, S., Saito, H., Wentworth, J. M., Li, P., Liao, W., Leonard, W. J., Smyth, G. K., Shi, W., Nutt, S. L., … Kallies, A. (2015). The transcriptional regulators IRF4, BATF and IL-33 orchestrate development and maintenance of adipose tissue-resident regulatory T cells. *Nature Immunology*, *16*(3), 276–285.

Wang, B., Fujisawa, H., Zhuang, L., Freed, I., Howell, B. G., Shahid, S., Shivji, G. M., Mak, T. W., & Sauder, D. N. (2000). CD4 + Th1 and CD8 + Type 1 Cytotoxic T Cells Both Play a Crucial Role in the Full Development of Contact Hypersensitivity . *The Journal of Immunology*, *165*(12), 6783–6790.

Wang, J. X., Kaieda, S., Ameri, S., Fishgal, N., Dwyer, D., Dellinger, A., Kepley, C. L., Gurish, M. F., & Nigrovic, P. A. (2014). IL-33/ST2 axis promotes mast cell survival via BCLXL. *Proceedings of the National Academy of Sciences of the United States of America*, *111*(28), 10281–10286.

Wang, K., Tao, L., Su, J., Zhang, Y., Zou, B., Wang, Y., Zou, M., Chen, N., Lei, L., & Li, X. (2017). TLR4 supports the expansion of FasL+CD5+CD1dhi regulatory B cells, which decreases in contact hypersensitivity. *Molecular Immunology*, *87*, 188–199.

Waskow, C., Liu, K., Darrasse-Jèze, G., Guermonprez, P., Ginhoux, F., Merad, M., Shengelia, T., Yao, K., & Nussenzweig, M. (2008). The receptor tyrosine kinase Flt3 is required for dendritic cell development in peripheral lymphoid tissues. *Nature Immunology*, *9*(6), 676–683.

Weitzmann, A., Naumann, R., Dudeck, A., Zerjatke, T., Gerbaulet, A., & Roers, A. (2020). Mast Cells Occupy Stable Clonal Territories in Adult Steady-State Skin. *Journal of Investigative Dermatology*, *140*(12), 2433–2441.

Whibley, N., Tucci, A., & Powrie, F. (2019). Regulatory T cell adaptation in the intestine and skin. *Nature Immunology*, *20*(4), 386–396.

Wong, Y., Nakamizo, S., Tan, K. J., & Kabashima, K. (2019). An update on the role of adipose tissues in psoriasis. *Frontiers in Immunology*, *10*, 1–7.

Yamamoto, M., Sato, S., Mori, K., Hoshino, K., Takeuchi, O., Takeda, K., & Akira, S. (2002). Cutting Edge: A Novel Toll/IL-1 Receptor Domain-Containing Adapter That Preferentially Activates the IFN-β Promoter in the Toll-Like Receptor Signaling. *The Journal of Immunology*, *169*(12), 6668–6672.

Yao, C., Oh, J. H., Lee, D. H., Bae, J. S., Jin, C. L., Park, C. H., & Chung, J. H. (2015). Toll-like receptor family members in skin fibroblasts are functional and have a higher expression compared to skin keratinocytes. *International Journal of Molecular Medicine*, *35*(5), 1443–1450.

Yu, Y., Blokhuis, B. R., Garssen, J., & Redegeld, F. A. (2015). Non-IgE mediated mast cell activation. *European Journal of Pharmacology*, *778*, 33–43.

Zeng, F., Chen, H., Chen, L., Mao, J., Cai, S., Xiao, Y., Li, J., Shi, J., Li, B., Xu, Y., Tan, Z., Gong, F., Li, B., Qian, Y., Dong, L., & Zheng, F. (2021). An Autocrine Circuit of IL-33 in Keratinocytes Is Involved in the Progression of Psoriasis. *Journal of Investigative Dermatology*, *141*(3), 596–606.

Zhang, L.-J., Chen, S. X., Guerrero-Juarez, C. F., Zheng, Y., Plikus, M. V, Gallo Correspondence, R. L., Li, F., Tong, Y., Liang, Y., Liggins, M., Chen, X., Chen, H., Li, M., Hata, T., & Gallo, R. L. (2019). Age-Related Loss of Innate Immune Antimicrobial Function of Dermal Fat Is Mediated by Transforming Growth Factor Beta Article Age-Related Loss of Innate Immune Antimicrobial Function of Dermal Fat Is Mediated by Transforming Growth Factor Beta. *Immunity*, *50*, 121–136.

Zhang, L.-J., Guerrero-Juarez, C. F., Hata, T., Bapat, S. P., Ramos, R., Plikus, M. V., & Gallo, R. L. (2015). Dermal adipocytes protect against invasive Staphylococcus aureus skin infection. *Science*, *347*(6217), 67–71.

Zhang, Y., Leung, D. Y. M., Richers, B. N., Liu, Y., Remigio, L. K., Riches, D. W., & Goleva, E. (2012). Vitamin D Inhibits Monocyte/Macrophage Proinflammatory Cytokine Production by Targeting MAPK Phosphatase-1. *The Journal of Immunology*, *188*(5), 2127–2135.

Zhou, L., Chong, M. M. W., & Littman, D. R. (2009). Plasticity of CD4+ T Cell Lineage Differentiation. *Immunity*, *30*(5), 646–655.

Ziegler, S. F. (2012). Thymic stromal lymphopoietin and allergic disease. *Journal of Allergy and Clinical Immunology*, *130*(4), 845–852.

Publications

Oliver Schanz, Rieka Chijiiwa, Sevgi Can Cengiz, Yasmin Majlesain, Heike Weighardt, Haruko Takeyama, Irmgard Förster. Dietary AhR Ligands Regulate AhRR Expression in Intestinal Immune Cells and Intestinal Microbiota Composition. Int J Mol Sci. 2020 Apr 30;21(9):3189. doi: 10.3390/ijms21093189.

Jacqueline Taylor, Julia Sellin, Lars Kuerschner, Lennart Krähl, Yasmin Majlesain, Irmgard Förster, Christoph Thiele, Heike Weighardt, Elvira Weber. Generation of immune cell containing adipose organoids for in vitro analysis of immune metabolism. Sci Rep. 2020 Dec 3;10(1):21104. doi: 10.1038/s41598-020-78015-9.

Nadine Herrmann, Tim J Nümm, Kazumasa Iwamoto, Nicole Leib, Susanne Koch, Yasmin Majlesain, Laura Maintz, Helene Kirins, Sylvia Schnautz, Thomas Bieber. Vitamin D 3-Induced Promotor Dissociation of PU.1 and YY1 Results in FcεRI Reduction on Dendritic Cells in Atopic Dermatitis. J Immunol. 2021 Feb 1;206(3):531-539. doi: 10.4049/jimmunol.2000667

Acknowledgements

I would like to use the opportunity here to sincerely thank all the persons who supported and helped me in the past years, in one or the other way, making this thesis possible.

First of all, I would like to thank PD Dr. Heike Weighardt and Prof. Dr. Irmgard Förster for their support and for giving me the opportunity to conduct my PhD project on this interesting topic, as well as the Jürgen Manchot Foundation for my doctoral scholarship (Nov. 2017- Oct. 2020). Furthermore, I would like to thank Prof. Dr. Eva Kiermaier for agreeing to be the second examiner of my thesis.

A big thank you to all the members, past and present, of the AG Förster/AG Weighardt for the nice work atmosphere and help in the lab. I appreciated all the discussions about scientific and private things and I am thankful for having such great colleagues. Here, I would like to again highlight Heike, who as my supervisor and mentor let me work and develop independently, gave scientific advice and guided the way whenever I needed it. Also, I would like to thank Viktoria Thomanek for her assistance with establishing the UV-induced immunosuppression experiments.

Moreover, I am very grateful for the constant encouragement of my family, especially my parents, who taught me to be persistent and to face the future optimistically. Thank you for all your love and support that have brought me so far.

Lastly, I would like to thank my friends who supported and motivated me during my whole studies and helped me clear my head in stressful phases. A special thanks goes to Tobias for always being patient and understanding, and just for all the good times we spend together. Thank you for always being there for me.